UNIVERSIDADE FEDERAL DO RIO GRANDE DO SUL

INSTITUTO DE CIÊNCIAS BÁSICAS E DA SAÚDE

PROGRAMA DE PÓS-GRADUAÇÃO EM CIÊNCIAS BIOLÓGICAS:
BIOQUÍMICA

Rafael Dai Prá da Luz

Thermoregulatory control by Agrp neurons during postnatal development in mice

Controle termorregulatório pelos neurônios Agrp durante o desenvolvimento pós-natal em camundongos

PORTO ALEGRE
2019

Rafael Dai Prá da Luz

Thermoregulatory control by Agrp neurons during postnatal development in mice

Controle termorregulatório pelos neurônios Agrp durante o desenvolvimento pós-natal em camundongos

Dissertation submitted to the Graduate Program in Biological Sciences: Biochemistry, in partial fulfillment of the requirements for the degree of Master of Sciences in Biochemistry.

Dissertação apresentada ao Programa de Pós-Graduação em Ciências Biológicas: Bioquímica do Instituto de Ciências Básicas da Saúde da Universidade Federal do Rio Grande do Sul como requisito parcial para a obtenção do título de mestre em Bioquímica.

Orientador (Advisor): Prof. Dr. Marcelo de Oliveira Dietrich (Universidade de Yale, New Haven, Estados Unidos)

Porto Alegre

2019

"You don't learn to walk by following rules. You learn by doing, and by falling over."
Richard Branson

Acknowledgements

Here, I would like to take the opportunity to thank all of those who supported me during my time as a master student at Universidade Federal do Rio Grande do Sul and Yale University.

Professor Marcelo Dietrich: Thank you for letting me become part of an incredible laboratory. Also, I would like to thank you for teaching and guiding me during these special years. Your help, insights and support were essential in those challenging moments of disbelief and failure. Additionally, the opportunities you have given me to present the projects in seminars really helped me to prepare for the next step in my career as a scientist. I truly hope I can share all of the knowledge and examples I learned from you. Thank you so much.

Marcelo Zimmer: Having the opportunity to work with you has immensely added to my dissertation. Your enthusiasm, ethics, willingness to help and drive to do science were essential to motivate me to overcome the challenges that crossed my way. It has been a wonderful experience to share my thoughts, ideas and to be part of your projects. Thanks for all your support, guidance and friendship.

Professor Diogo Souza: I would like to thank you for all your support throughout my master studies. Your passion for science and teaching is unique. Thanks professor!

Dietrich Lab: Jeremy: It was wonderful to have you around to discuss the most different topics related to science. I admire you, J! Thanks for all the support. **Onur:** Merhaba arkadaş! Thanks for all the support in the thermal experiments and surgeries. It was also great having you to give me Turkish lessons and to share Turkish coffee during our scientific discussions. Thank you so much, man. **Lucas and Juliana:** Thank you so much for all your help with brain slicing and behavioral experiments. I am sure you will succeed in your future careers. **Gabriela:** Thanks a lot for the support in the lab. I can't forget to thank you for the innumerable scientific discussions, alternative hypotheses, and laughs, thanks. **Delva**: Your support and friendship in those challenging moments were essential.

It is always a pleasure to hear your criticisms and ideas, I admire you, Del, thanks. **Antonio:** Thanks for all the discussions and insights during the vocalization experiments and USV analyses. Your mathematical and statistical insights during discussions were inspiring. **Gustavo:** I wasn't expecting to meet someone as cool as you, Gustavo. Thanks for the insights, discussions and life advises during my time at Yale. I really admire you for always favoring efficiency. **Arthur:** Your critical approach to everything that comes your way is very inspiring. Seeing you take on your project motivates me a lot. Every day is a new knowledge from you. It does not matter if it is on data visualization, paper discussions or programming skills. I really admire you, and I am sure you will achieve everything you plan to. Thanks for all the late-night discussions, Slack calls and messages. **Mahdieh:** Your enthusiasm and insights motivated me a lot during the writing process. Your feedback on the writing aspects of this dissertation contributed a lot to strengthen and clarify my ideas. Thanks for all your time and support!

I would like to thank all of those friends I made at Yale who made my stay in New Haven better.

Dietrich seedLab: Leticia: I thank you for your feedback in the dissertation, help in the hospital and in the seedLab group. **Andre:** Thanks for your help and support in the seedLab group, I am sure you will have a great future in Europe, best of luck on your new journey. **Gabriel:** Thanks for your help and support in the seedLab group. Best of luck in Canada!

Mom, Lu, Sté and nini: You were always there when I needed the most, even for the simplest things. I have no words to describe your importance throughout the period I was in Brazil and when I was at Yale. I love you with all my heart.

PREAMBLE

Presentation

This dissertation (written in English) is organized in three parts, in accordance with local rules of the *Graduate Program in Biological Sciences: Biochemistry* (UFRGS):

Part I: Introduction and Aims.
Part II: Material and Methods and Results.
Part III: Discussion, Conclusion, Future Perspectives and References (+Annexes).

Scientific contributions in the form of co-authored research articles that are not part of the main body of this dissertation can be found in the item Annexes.

The experiments described here were performed in the Comparative Medicine Department - Yale School of Medicine, Yale University (New Haven, CT, USA) under supervision of Prof. Dr. Marcelo de Oliveira Dietrich as part of the CAPES International Cooperative Program (PGCI) project between Prof. Dr. Marcelo de Oliveira Dietrich (Yale University) and Prof. Diogo Onofre Gomes de Souza, Department of Biochemistry - Universidade Federal do Rio Grande do Sul (Porto Alegre, RS, Brazil).

PREÂMBULO

Apresentação

Esta dissertação de mestrado (escrita em inglês) será organizada em três partes, de acordo com as normas do Programa de Pós-Graduação em Ciências Biológicas: Bioquímica (UFRGS):

Parte I: Introdução e Objetivos.

Parte II: Materiais e Métodos e Resultados

Parte III: Discussão, Conclusão, Perspectivas Futuras e Referências (+ Anexos).

Contribuições científicas sob forma de co-autoria em artigos científicos que não foram incluídos no corpo principal desta dissertação serão adicionadas no item Anexos.

Os experimentos descritos nesta dissertação de mestrado foram realizados no Departamento de Medicina Comparativa – Escola de Medicina da Universidade de Yale (New Haven, CT, EUA) sob supervisão do Prof. Dr. Marcelo de Oliveira Dietrich como parte do Programa Geral de Cooperação Internacional (PGCI) da CAPES entre o Prof. Dr. Marcelo de Oliveira Dietrich (Universidade de Yale) e Prof. Dr. Diogo Onofre Gomes de Souza, Departamento de Bioquímica – Universidade Federal do Rio Grande do Sul (Porto Alegre, RS, Brasil).

Abstract

Thermoregulation is a physiological process that is important for the survival of mammals during the early postnatal development. Despite the importance of thermoregulation in early development, the neuronal substrates that modulate this process are not well understood. In this dissertation, I studied the contribution of the Agouti-Related protein (Agrp) neurons to the control of thermoregulation during postnatal development in mice. I found that Agrp neurons were activated once animals were isolated at room temperature ($\approx$23 ºC) from the nursing nest. Warm temperatures ($\approx$35 ºC) blunted this effect. Also, using *in vivo* fiber photometry, Agrp neuronal activity presented rapid dynamics when isolated P16-P17 pups were submitted to changes in the surface floor temperature of the apparatus. To better comprehend the role of Agrp neurons in thermoregulation we used chemogenetic and pharmacological approaches. Chemogenetic activation of these neurons led to a rapid decrease in skin temperature. This decrease in skin temperature was blunted in P10 mice deficient for neuropeptide Y (NPY). Additionally, ghrelin, a gut-hormone that activates the Agrp neurons, also decreased skin temperature in P10 mice, an effect that was blunted in Y_1R^{KO} mice. These results suggest that Agrp neurons modulate thermoregulation in neonatal mice via NPY and, likely, Y_1R. Our findings highlight the importance of the Agrp neurons in the control of thermoregulation in mice during postnatal development.

Keywords: Thermoregulation. Body temperature. Postnatal development. Hypothalamus. Agrp neurons.

Resumo

A termorregulação é um processo fisiológico crítico para a sobrevivência dos mamíferos durante o período de desenvolvimento pós-natal. Apesar da importância da termorregulação durante o período do desenvolvimento pós-natal, os mecanismos neuronais que modulam a termorregulação não são bem elucidados. Nesta dissertação, eu avaliei a contribuição dos neurônios que expressam a proteína relacionada ao agouti (AGRP) para o controle da termorregulação em camundongos durante o desenvolvimento pós-natal. Observei que os neurônios Agrp tornaram-se ativos quando os camundongos foram isolados do ninho à temperatura ambiente ($\approx$23 ºC). Porém, quando os animais foram isolados com um suporte térmico que mimetiza temperaturas encontradas no ninho ($\approx$35 ºC), a ativação desses neurônios foi atenuada. Além disso, utilizando fotometria por fibra óptica *in vivo*, verificamos que a atividade dos neurônios Agrp apresentou uma rápida dinâmica quando animais no dia pós-natal 16-17 (DPN16-17) foram isolados e submetidos à variações na superfície do chão do aparato. Além disso, a fim de compreender o papel dos neurônios Agrp na termorregulação, utilizamos abordagens quimiogenéticas e farmacológicas. A ativação específica desses neurônios por meio de estratégia quimiogenética promoveu uma rápida queda na temperatura da pele dos animais. Essa queda na temperatura foi suprimida em camundongos DPN10 nocautes para expressão do neuropeptídeo Y (NPY). Adicionalmente, grelina, um hormônio derivado do estômago que ativa os neurônios Agrp, também promoveu queda na temperatura da pele dos animais, um efeito que foi diminuído em camundongos nocaute para o receptor de NPY Y_1 (Y_1R). Esses resultados sugerem que os neurônios Agrp controlam a termorregulação via mecanismos dependentes de NPY e, possivelmente, Y_1R. Nossos achados demonstram a importância dos neurônios Agrp no controle da termorregulação em camundongos durante o desenvolvimento pós-natal.

Palavras-chave: Termorregulação. Temperatura corporal. Desenvolvimento pós-natal. Hipotálamo. Neurônios Agrp.

List of abbreviations

Agrp	Agouti-related protein
ARC	Arcuate nucleus of the hypothalamus
BAT	Brown adipose tissue
3V	Third ventricle
NPY	Neuropeptide Y
GABA	Gamma-aminobutyric acid
MC3R	Melanocortin 3 receptor
MC4R	Melanocortin 4 receptor
ICV	Intracerebroventricular
cAMP	Cyclic adenine monophosphate
SNS	Sympathetic nervous system
GhSR	Growth hormone secretagogue receptor
P10	Postnatal day 10
UCP1	Uncoupling protein 1
FFAs	Free fatty acids
SC	Subcutaneous
Bp	Base pairs
IEGs	Immediate early genes
AAV	Adeno-associated virus
NA	Numeric aperture
CNO	Clozapine-N-oxide
Fps	Frames per second
hM3Dq	Human muscarinic M3 receptor
hM4Di	Human muscarinic M4 receptor
Trpv1	Transient receptor potential vanilloid 1
GPCRs	G-protein coupled-receptors
DMH	Dorsomedial hypothalamus
PVH	Paraventricular nucleus of the hypothalamus
LH	Lateral hypothalamus
POA	Preoptic area
shRNA	Short hairpin RNA

Table of contents

PART I

In this part introduction and general aims of the dissertation will be described.

1. INTRODUCTION

1.1 Agrp neurons and energy balance

Agouti-related protein (Agrp) neurons are a neuronal population that is located in the arcuate nucleus (ARC) of the hypothalamus (**Figure 1**). The portion of the ARC where Agrp neurons are located is in close proximity to the third ventricle. In this area, the capillaries that form the blood-brain barrier are fenestrated (Rinne, 1966), thus allowing circulating factors to interact directly with the Agrp neurons (Cansell et al., 2012).
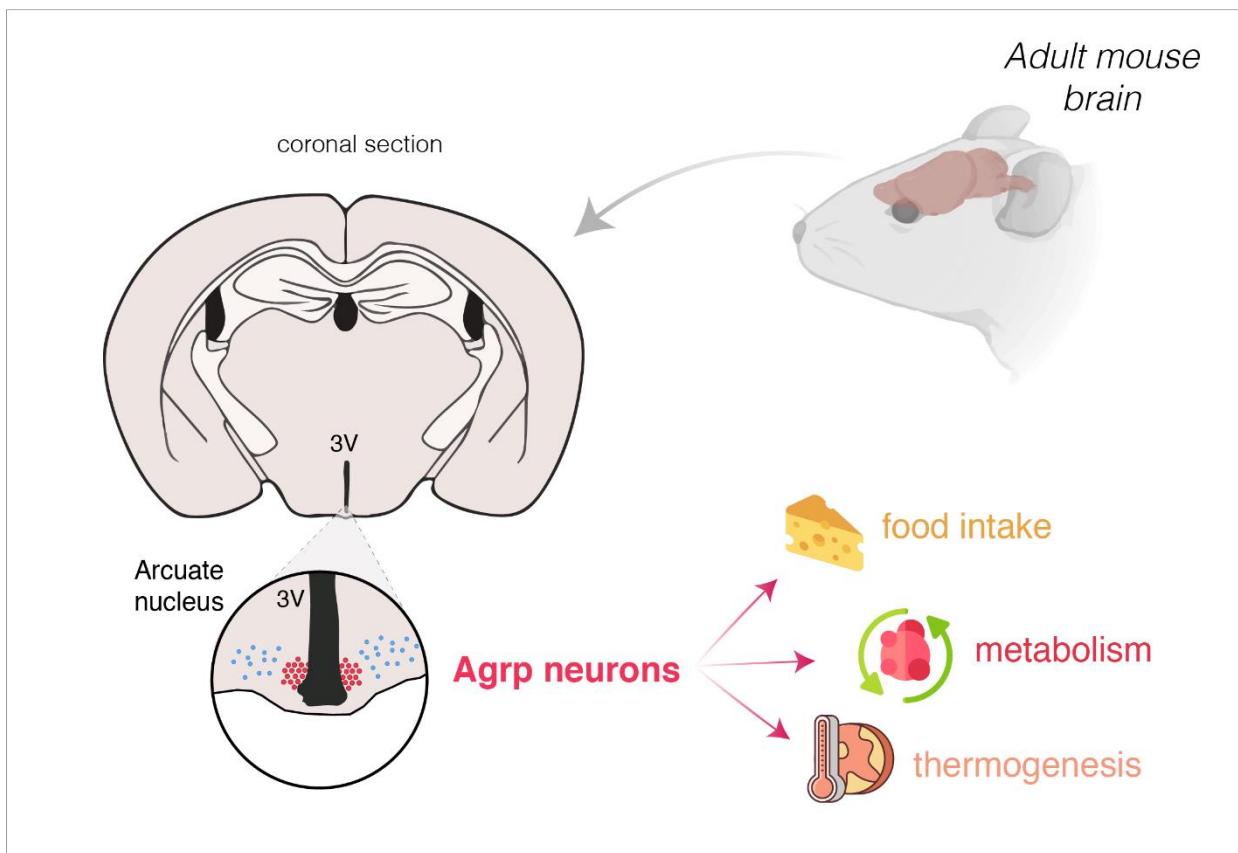
Figure 1. Illustration of the location of Agrp neurons and their function in adult mice. Agrp neurons are located in the more medial region of the arcuate nucleus of the hypothalamus. Agrp neurons modulate food intake, metabolism and also thermogenesis in adult mice. Agrp, agouti-related protein; 3V, third ventricle.

Agrp neurons have been shown to control food intake and food related-behaviors in mice (**Figure 1**). Initially, food-deprived mice showed increased levels of AGRP in the brain (Cone, 2005; Mizuno and Mobbs, 1999). Subsequently, ablation of Agrp neurons in adult mice reduced food intake, leading to aphagia and, consequential, death (Gropp et

al., 2005; Luquet et al., 2005). Additionally, chemogenetic[1] and optogenetic[2] activation of the Agrp neurons drove a robust increase in food intake (Aponte et al., 2011; Dietrich et al., 2015; Krashes et al., 2011). This body of work supports the importance of the Agrp neurons as key orchestrators of food intake in mammals.

In addition to food intake, Agrp neurons also affect whole-body lipid metabolism and brown adipose tissue (BAT) thermogenesis (**Figure 1**) (Burke et al., 2017; Cavalcanti-de-Albuquerque et al., 2019; Joly-Amado et al., 2012; Steculorum et al., 2016). More specifically, Agrp neuron activation promotes a reduction in energy expenditure with a concomitant reduction in BAT thermogenesis (Burke et al., 2017; Ruan et al., 2014; Steculorum et al., 2016; Yasuda et al., 2004).

Agrp neurons release agouti-related protein (AGRP), neuropeptide Y (NPY) and GABA (γ-aminobutyric acid) (Clark et al., 1984; Hahn et al., 1998; Horvath et al., 1997) (**Figure 2**). AGRP is a 132-amino acid peptide that was originally described to evoke food intake when injected into the brain of adult mice (Rossi et al., 1998; Yasuda et al., 2004). AGRP exerts its effects through antagonism of the melanocortin-3 receptor (MC3R) and melanocortin-4 receptor (MC4R) (Morton and Schwartz, 2001; Sobrino Crespo et al., 2014), which are broadly expressed in the brain.

NPY is a 36-amino acid peptide with potent orexigenic[3] properties (Loh et al., 2015). NPY acts through G-protein-coupled receptors (GPCRs), of which five have been identified in rodents - Y_1, Y_2, Y_4, Y_5 and Y_6 (Lin et al., 2004; Loh et al., 2015). Y receptors are associated with $G_{i/o}$ G proteins to inhibit target cells, decreasing cAMP levels (Kassis et al., 1987). In adult mice, NPY also induces feeding behavior and suppresses BAT thermogenesis. For example, injections of NPY into the brain robustly stimulate feeding in rodents and other mammals (Clark et al., 1984; Larsen et al., 1999; Miner et al., 1989). Furthermore, repeated injections of NPY in the brain for several days lead to sustained hyperphagia, body weight gain and fat accumulation (Stanley et al., 1986). Therefore, similar to AGRP, NPY increases food intake and decreases energy expenditure.

---

[1] Chemogenetic: a technique which uses modified receptors that are selectively activated by synthetic small drugs to manipulate neuronal activity (for more details, see **Box 3** in the material and methods section).
[2] Optogenetic: a technique which uses modified receptors that are activated by light to manipulate neuronal activity.
[3] Orexigenic molecules are molecules that elicit food intake.

In addition to AGRP and NPY, Agrp neurons also release the classic inhibitory neurotransmitter GABA that is also important to maintain normal energy homeostasis. Inactivation of GABA biosynthesis in the ARC or selectively in the AGRP neurons leads to anorexia (Wu et al., 2009). Additionally, mice lacking GABA release by the Agrp neurons present higher energy expenditure (Tong et al., 2008; Wu et al., 2009). Together, these findings show that Agrp neurons control energy balance via their three transmitters, AGRP, NPY, and GABA.

Agrp neurons are responsive to several hormones released in the circulation. A key modulator of Agrp neuronal activity is the hormone ghrelin, which is released during food deprivation (**Figure 2**). Ghrelin is a 28-amino acid protein derived from the X/A-like cells in the gastric oxyntic glands of the stomach (Date et al., 2000; Hayashida et al., 2002). Similar to modulation of Agrp neuron activity or injection of AGRP and NPY in the brain, ghrelin administration induces food intake, body weight gain and decreases energy expenditure (Kamegai et al., 2001; Nakazato et al., 2001; Tschop et al., 2000; Wren et al., 2001). The effects of ghrelin on metabolism depend on Agrp neurons as ablation of these neurons or knock-down of ghrelin receptors in Agrp neurons blunt the effects of ghrelin on energy homeostasis (Chen et al., 2017; Luquet et al., 2005; Wang et al., 2014)
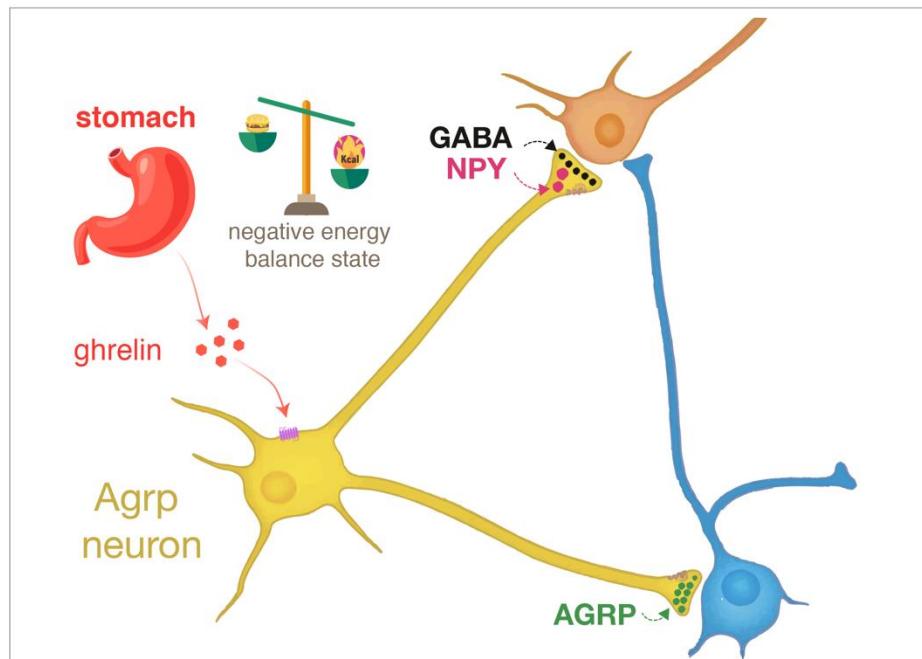
Figure 2. Illustration showing the factors that activate the Agrp neurons and the transmitters they release upon activation. The peripheral hormone ghrelin activates the Agrp neurons (shown in yellow) since they densely express the ghrelin receptor (GHSR, shown in pink). Additionally, a negative energy balance state also activates the Agrp neurons. A negative energy balance state occurs when energy expenditure is higher than energy intake. AGRP, agouti-related protein; NPY, neuropeptide Y; GABA, γ-aminobutyric acid.

1.2. Thermoregulation

Thermoregulation is the process by which animals tightly regulate body temperature (Romanovsky, 2018; Tan and Knight, 2018). Most of the existent knowledge of the thermoregulation in mammals was developed in rodents (Meyer et al., 2017; Romanovsky, 2018). To maintain the thermoregulation at homeostatic levels, adult and neonate rodents utilize behavioral and physiological mechanisms to protect against thermal stressors (**Figure 3**). Behavioral mechanisms are a significant strategy to maintain body temperature because they are less energy demanding (behavioral mechanisms will be further explain in the following section) (Tan and Knight, 2018). For instance, rodents build nests to conserve heat and also huddle altogether in order to conserve energy (Romanovsky, 2018). In contrast, physiological mechanisms are involuntary and are mostly mediated via autonomic responses that can generate or dissipate heat (Tan and Knight, 2018). Physiological mechanisms include shivering thermogenesis, which occurs in skeleton muscles, non-shivering thermogenesis mediated by BAT (more details are found in **Box 1**) and vasoconstriction and vasodilation. Shivering thermogenesis, non-shivering thermogenesis, and vasoconstriction occur upon cold exposure to generate or conserve heat. On the other hand, vasodilation occurs in response to increases in temperature, leading to heat dissipation that prevents increases in body temperature.
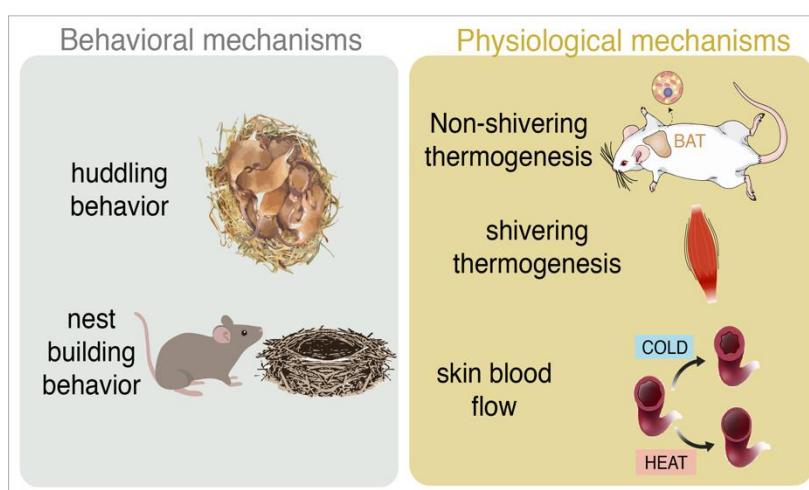
Figure 3. Thermoregulation in rodents. Behavioral mechanisms are goal-oriented and include huddling and nest-building behaviors to conserve heat or reduce heat loss. Physiological mechanisms are involuntary and mostly autonomic responses that can generate or dissipate heat. They include non-shivering thermogenesis, skeleton muscle shivering thermogenesis and modulation of the skin blood flow, constriction or dilation of blood vessels.

Box 1 | Brown adipose tissue thermogenesis

Brown adipose tissue converts chemical energy from triglycerides into heat (Cannon and Nedergaard, 2004). This conversion is possible due to the activation of the sympathetic nervous system in response to environmental cold exposure (Kawate et al., 1994; Meywirth et al., 1991).

The generation of heat by brown adipocytes can be described as BAT thermogenesis, cold-induced thermogenesis, non-shivering thermogenesis or adaptive-thermogenesis. Brown adipocytes generate heat and contribute to the maintenance of body temperature due to the high number of mitochondria. These mitochondria highly express a protein named uncoupling protein 1 (UCP1) (Nedergaard and Cannon, 2018). UCP1 is capable of uncoupling mitochondrial respiration from ATP regeneration, and thus converts the energy stored as triglycerides into heat. The activation of the β_3-adrenergic receptors, which are on the surface of brown adipocytes, drives lipolysis of the intracellular triglyceride stores and drives the release of free fatty acids (FFAs). The release of FFAs enhances the activity of the respiratory chain and the conductance of protons through UCP1, thus uncoupling the respiratory chain from ATP regeneration (Cannon and Nedergaard, 2004).

At birth, mice already have brown adipose tissue, however, the brown adipocytes are small and contain little fat. However, there is a rapid growth of BAT in the first days of life (2-5 days), which is accompanied by a dramatic increase of brown adipocyte dimensions, number of mitochondria, fat lipid size and cold-induced thermogenesis (Vinter et al., 1982). The increase in cold-induced thermogenesis suggests that the innervation of the sympathetic nervous system is already functional in these very early ages.

Additional mechanisms to generate heat are immature and not well developed in neonatal mice. In contrast, since brown adipocytes seem to be functional and ready to generate heat, BAT thermogenesis is the main physiological process neonates use to maintain body temperature (Leon, 1986; Vinter et al., 1982).

1.2.1 Thermoregulation in neonates

Animals at different ages present different energetic and thermoregulatory demands that can be illustrated by the development of thermoregulation in rodents (**Figure 4**). In mice and rats, the first stage in the development of thermoregulation - from postnatal day 0 to postnatal day 7 - is considered a period of ectothermy[4] in which neonates have a very limited capacity of thermoregulation and their body temperature fluctuates with ambient temperature.

During this period, neonates are furless, prone to rapidly lose heat due to their small size and large surface-to-volume ratio. During the first days of life, the dam is

---

[4] Ectothermy: form of controlling body temperature in ectotherms. Body temperature of ectotherms fluctuates according to environmental temperature. Additionally, these animals cannot generate internal heat.

responsible for keeping the offspring warm (Lagerspetz, 1966). Within the nest, there is a direct heat transfer from the dam to the offspring during contact bouts. These contact bouts keep the temperature of the offspring within a 33-35°C range (Leon et al., 1978). Accordingly, dams remain in the nursing nest in contact with the offspring for 75-90% of the time during the first week of life (Leon et al., 1978). As the neonates grow, develop fur, fat deposits, and increase thermoregulatory capacity, the dam gradually reduces the time spent in the nursing nest.

In the second stage (from postnatal day 7 to postnatal day 13), mice and rats exhibit improved thermoregulatory capacity. They already utilize BAT thermogenesis to control body temperature, however, still with limited capacity to maintain body temperature. Finally, in the third stage (ages closer to the weaning period - 21 days old), mice and rats display similar thermoregulatory capacity as observed in adults. For example, mice at this stage have a dense layer of fur that helps preventing heat loss and have abundant fat deposits (Lagerspetz, 1966).
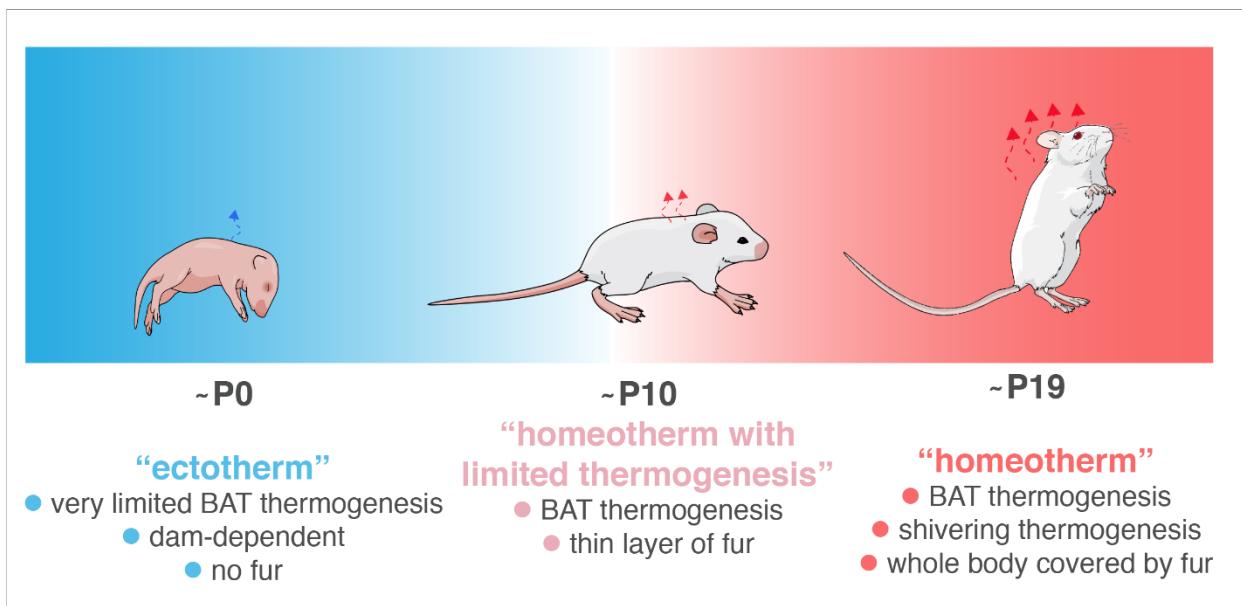
Figure 4. **Development of thermoregulation in mice.** After birth, mice are considered ectotherms since their body temperature fluctuates according to the ambient temperature. Additionally, at this age, pups do not efficiently recruit BAT thermogenesis, have no fur and are fully dependent on the dam to control body temperature. Around postnatal day 10 (P10), pups rely on BAT thermogenesis. At this age, they have a thin layer of fur and small fat deposits. Closer to the weaning period, animals already achieved maximum thermoregulatory capacity. They can rely on shivering and BAT thermogenesis, have a dense layer of fur and abundant fat deposits to face abrupt ambient temperature variations.

In addition to the physiological development of thermogenesis, a robust thermoregulatory behavior in neonatal mice and rats is huddling. Huddling is characterized by the social aggregation with other nestmates, in which neonates move on top of each other in order to conserve heat (Gilbert et al., 2010). Huddling allows the neonates to maximize energy savings by decreasing their cold-exposed body surface area, by reducing their heat loss through warming of ambient temperatures surrounding the group (Gilbert et al., 2010).

The development of these physiological and behavioral mechanisms to control body temperature is critical for the survival of mice. However, our understanding of development of functional regulatory mechanisms in the control of early life thermoregulation is still limited (**Figure 5**). Considering postnatal day 10 mice use brown adipose tissue thermogenesis to control body temperature upon isolation and there is evidence that Agrp neurons modulate thermogenesis in adult mice, in this dissertation, to start bridging this gap in our knowledge, I aimed to study the capability of Agrp neurons in the mammalian hypothalamus to control thermogenesis during the early postnatal development of mice.
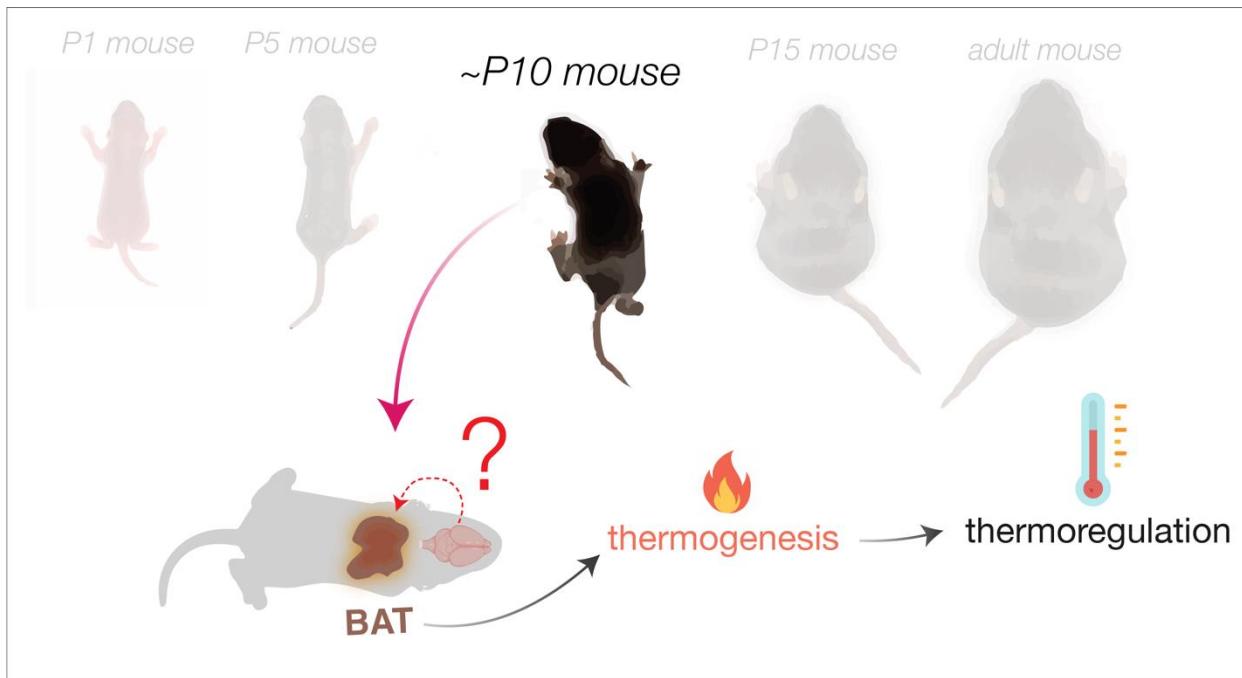
Figure 5. The control of thermogenesis and thermoregulation is not well understood during early postnatal development in mice. BAT thermogenesis is an important physiological mechanism that contributes to the thermoregulation in mice during postnatal development. Agrp neurons modulate BAT thermogenesis in adult mice. However, the role of the Agrp neurons in thermoregulation is not known in mice during early postnatal development.

2. AIM

To understand the contribution of Agrp neurons in the thermoregulatory mechanisms of mice during postnatal development.

PART II

In this part, material and methods and results sections will be described.

3. MATERIAL AND METHODS

3.1 Animals

Experimental procedures were conducted in the Department of Comparative Medicine at Yale University (New Haven, CT, USA). Mice from both genders were used in all of the experiments. All preweaning mice were 09-17 days old. Dams were 3 - 8 months. The following mouse lines were used in this study: C57BL/6J (stock number 000664, Jax); $Gt(ROSA)26^{Sortm1(Trpv1,ECFP)Mde/J}$ (stock number 008513, Jax); $Trpv1^{tm1Jul/J}$ (stock number 003770, Jax); $Slc32a1^{tm1Lowl}$ ($Vgat^{fl/fl}$, stock number 012897, Jax); B6N.129-$Rpl22^{tm1.1Psam/J}$ (Rpl22^{LSL-HA}, stock number 011029, Jax); $Agrp^{tm1(Cre)Lowl/J}$ (stock number 012899, Jax); B6.129-$Ucp1^{tm1Kz/J}$ (stock number 003124, Jax), $Y_1R^{<tm1.1Wpg>/WEHIAusb}$, $Y_2R^{<tm1.1Hhz>/Ausb}$, $PPYR(Y_4R)^{1<tm1.1Hhz>/WEHIAusb}$ (kindly donated by Herbert Herzog); Agrp$^{Ires-Cre}$;R26$^{fl-hM3D(Gq)}$;$Npy^{KO/KO}$ (kindly donated by Jens Brüning).

$Agrp^{Trpv1}$ mice: $Agrp^{Cre/+}$;Trpv1$^{KO/KO}$;$R26^{LSL-Trpv1}$; control animals were described as $Trpv1^{KO/KO}$; $R26^{LSL-Trpv1}$ (for further details about the Cre-Lox system and transgenic mouse models, see **Box 2**). $Agrp^{Cre}$ and $R26^{LSL-Trpv1}$ mice were backcrossed to $Trpv1^{KO/KO}$ mice to avoid the side effects of capsaicin when injected systemically to activate the Agrp neurons (for further details about the Trpv1 model, see **Box 3**) (Arenkiel et al., 2008; Dietrich et al., 2015; Guler et al., 2012; Ruan et al., 2014), as previously characterized (Dietrich et al., 2015; Zimmer et al., 2019).

$Agrp^{VgatKO}$ were $Agrp^{Cre/+}$;Trpv1$^{KO/KO}$;$R26^{LSL-Trpv1}$;$Vgat^{fl/fl}$; control animals were described as $Trpv1^{KO/KO}$;$R26^{LSL-Trpv1}$;$Vgat^{fl/fl}$. $Agrp^{HA}$ mice were generated by crossing $Agrp^{Cre}$ and Rpl22^{LSL-HA} mice. Analysis of ectopic expression of *Cre* recombinase was performed by using a specific set of primers against the excised conditional allele, as characterized previously (Dietrich et al., 2015). Mice with ectopic expression of the excised allele were excluded from the studies.

$Agrp^{Cre}$;R26$^{fl-hM3D(Gq)}$;$Npy^{KO/KO}$ (Agrp^{hM3Dq};Npy^{KO}) animals were generated by crossing hM3Dq$^{fl/fl}$;$Npy^{KO/+}$ to $Agrp^{Cre/+}$;hM3Dq$^{fl/fl}$;$Npy^{KO/+}$ animals. hM3Dq$^{fl/fl}$;$Npy^{KO/KO}$ and $Agrp^{Cre/+}$;hM3Dq$^{fl/fl}$;$Npy^{KO/+}$ were used as controls (for further details about the DREADDs technology, see **Box 3**).

Box 2 | Transgenic mice and the *Cre*-Lox system

The *Cre*-Lox system is a widely used tool in mouse experiments to selectively express or knockout genes of interest in a cell-specific manner (Song and Palmiter, 2018). This system involves two components, a *Cre* recombinase, and its recognition sites, the LoxP sites. LoxP sites are directional 34 bp sequences composed by two (2) 13 bp recognition sites separated by an 8 bp spacer region and were originally described in the genome of P1 bacteriophage.

Cre recombinases recognize the loxP sites. Depending on the orientation of these sites, three outcomes can result from the recombination: (1) if both loxP sites are in the same orientation, recombination will result in the excision of the sequence, deleting from its original locus; (2) if both LoxP sites are in opposite orientations, recombination will result in the inversion of the sequence (inactivation or activation depending on the orientation of the DNA sequence of the region of interest that is between the LoxP sites); (3) if both loxP sites are in separate fragments of DNA, recombination will result in translocation.

In this dissertation, this system was used to generate genetic mouse models to selectively activate the Agrp neurons. For that, we performed several crosses. One of them involved crossing a mouse line that expressed the Transient receptor potential vanilloid 1 (Trpv1) in the Rosa26 locus (R26$^{\text{LoxP-Stop-LoxP-Trpv1}}$) with another mouse line that expressed the recombinase *Cre* in the Agrp neurons (*Agrp^{Cre}*). Combining the *Cre* recombinase and a stop codon flanked by LoxP sites in the same orientation will result in the excision of the stop codon and expression of the Trpv1 only in the cells that express the *Cre* recombinase, or in other words the Agrp neurons.

The other model involved crossing a mouse line that expressed the *Cre* recombinase in the Agrp neurons with another mouse lines that expressed the human muscarinic M3 receptor (hM3Dq) in the Rosa26 locus (*R26$^{\text{LoxP-Stop-LoxP-hM3Dq}}$*). Thus, the action of the *Cre*-Lox system allows the selective expression of these receptors in the Agrp neurons.

Additionally, knockout animals (Ucp1^{KO}; Y$_1$R^{KO}; Y$_2$R^{KO}; Y$_4$R^{KO}) were generated by crossing heterozygotes of the same strain. Additionally, we used *Agrp^{Cre}*;Y$_1$R^{KO}; *Agrp^{Cre}*;Y$_2$R^{KO} and *Agrp^{Cre}*;Y$_4$R^{KO}; which were generated by crossing *Agrp^{Cre}*;Y$_1$R$^{KO/+}$; *Agrp^{Cre}*;Y$_2$R$^{KO/+}$ and *Agrp^{Cre}*;Y$_4$R$^{KO/+}$ to concomitant Y receptor knockout animals.

All animals used in this study were kept in temperature and humidity-controlled rooms, in a 12/12 h light/dark cycle, with lights on from 7:00 AM to 7:00 PM. Food and water were provided *ad libitum*. All procedures were approved by Institutional Animal Care and Use Committee (Yale University), IACUC # 2015-20042.

Box 3 | Chemogenetic manipulation of neurons

With the advances in molecular biology and genetics, researchers developed strategies to selectively modulate the activity of neurons in animal models. One model that was used in this dissertation was the Trpv1 model. Trpv1 is a non-selective cation channel that, upon activation, depolarizes cells and rapidly induces action potentials in neurons (Caterina et al., 1997). Capsaicin, a component of hot chili peppers, is a selective agonist of Trpv1 (Caterina et al., 1997). However, the Trpv1 receptor is widely expressed in the peripheral nervous system. To circumvent the problem of injecting capsaicin and activating off-target receptors, researchers developed a mouse line knockout for the Trpv1, with specific expression in a genetically defined neuronal population (Dietrich et al., 2015; Guler et al., 2012). Injecting capsaicin will open the Trpv1 receptor in the neuronal population of interest. Capsaicin binding to the Trpv1 receptor will cause Ca^{+2} and Na^+ to get into the cell making the neuron depolarize. This method provides a rapid and robust activation of neurons.

Researchers also modified G-protein coupled receptors (GPCRs), preserving the natural function of the receptors while altering specific properties such as agonist binding and kinetics. Designer receptors exclusively activated by designer drugs (DREADDs) are genetically engineered GPCRs that are activated by synthetic small molecules (designer drugs) considered physiologically inert (Armbruster et al., 2007). With this technology is possible to remotely control selected neuronal populations and circuits as well (Roth, 2016). Muscarinic receptors were modified to be able to solely bind to a synthetic drug. Clozapine-N-oxide (CNO) was selected as the designer ligand activate the modified GPCR. The three main types of signaling pathways for muscarinic-based DREADDs are G_q, G_i and G_s. G_q DREADD increases neuronal firing by stimulating phospholipase C, releasing intracellular calcium stores. One example is the human muscarinic receptor M3 (hM3Dq) (Conklin et al., 2008). G_s DREADDs are less commonly used, stimulating cAMP production (Conklin et al., 2008). In contrast, Gi DREADDs inhibit cAMP production, provoking inhibition of the neuron (Urban and Roth, 2015). One example is the human muscarinic receptor M4 (hM4Di). These methods are intertwined with the use of the *Cre*-Lox system (**Box 2**). Usually, these receptors (Trpv1 and hM3Dq or hM4Di) are expressed in a *Cre*-dependent manner.

3.2 Drugs

The following drugs were used in these studies: capsaicin (10 mg/kg, s.c. dissolved in 3.33% Tween-80 in PBS from Sigma, cat. #M2028-1G); Clozapine-N-Oxide, CNO (1 mg/kg, s.c., dissolved in saline, from TOCRIS cat. #4936 and from Cayman Chemical cat. #16882); and human ghrelin (0.5, 1 and 2 mg/kg, s.c, dissolved in saline from Prospecbio, cat. #HOR-297).

3.3 Fos labeling as a marker of Agrp neuron activation

When a neuron is active and depolarizes, the transient rise of intracellular Ca^{+2} and activation of downstream pathways drive the expression of immediate early genes (IEGs) within minutes of neuronal activation (Sheng and Greenberg, 1990). Among the IEGs, Fos is one of the best-characterized IEGs. Hence, Fos has been widely used as a marker of neuronal activity in response to sensory stimuli or in different behaviors (Barros et al., 2015; Morgan and Curran, 1989). Therefore, we took advantage of Fos to evaluate the Agrp neuronal activity in response to different stimuli.

3.3.1 Isolation of P10 mice from dam and siblings

At postnatal day 10, pups were separated from the dam for 90 minutes and thermal support was provided using a heating pad set at ≈35°C. This device was placed underneath the apparatus in which the pups were separated. The thermal condition was monitored using a calibrated thermometer. For this experiment, pups were divided into the following conditions: kept with dam and siblings in the homecage (nest); isolated for 90 minutes with thermal support; and isolated for 90 min without thermal support (room temperature, ≈23ºC). After 90 minutes, pups were perfused, and brains were collected for Fos analysis. Immunohistochemistry was performed as described in 3.7.

3.3.2 Isolation of P10 mice raised at thermoneutrality [5]

Two weeks prior delivery, a pregnant female was placed in a humidity and temperature-controlled climate chamber set to 70-80% of humidity, ≈35°C (Sables Systems), considered thermoneutral condition (Blumberg and Alberts, 1990; Blumberg et al., 1992). Temperature and humidity in the climate chamber were monitored twice a day until the experimental day. At postnatal day 10, pups were divided into the following conditions: kept with dam and siblings in the homecage (nest); isolated for 90 minutes at thermoneutral condition (70-80% of humidity, ≈35°C) and isolated for 90 minutes at room

---

[5] Thermoneutrality is condition in which there is a thermal balance between the animal and the environment. In thermoneutrality or thermoneutral conditions animals do not use any thermoregulatory mechanism.

temperature (≈23ºC). After 90 minutes, pups were perfused, and brains were collected for Fos analysis. Immunohistochemistry was performed as described in 3.7.

3.4 Fiber Photometry in P16-P17 mice

$Agrp^{Cre/Cre}$ mouse newborns (P0-P1) were first cryoanesthetized. Briefly, newborns were placed on ice, covered with aluminum foil to prevent direct contact. After 10 minutes, mice were removed from the ice and placed onto a chilled rat/mouse neonatal frame (Stoelting Co., cat. #51625). Next, a *Cre*-dependent adeno-associated virus (AAV) encoding the calcium sensor jGCaMP7s (AAV8-CAG-Flex-jGCaMP7s-SV40, Penn Vector Core) was injected into the arcuate nucleus of the $Agrp^{Cre/Cre}$ mice using a Hamilton syringe unilaterally at a volume of 300 nL using following coordinates from lambda: AP = +0.98mm; ML = -0.3mm, DV = -4.1mm. Utilization of fiber photometry system in neonatal mice is still a challenge. Due to unsuccessful surgeries and recordings in younger ages (P10-P12), animals were submitted to a surgical procedure on postnatal days 15 or 16, where a fiber optic cannula (NA = 0.48, core diameter = 400 µm, Doric Lenses) was placed over the arcuate nucleus of the hypothalamus using the following coordinates using bregma as reference: AP = -1.38 mm, ML = -0.3mm, DV= -5.8 mm. One day after placing the fiber optic cannula, experimental mice were placed in a hot/cold plate (Ugo Basile, cat. #35150) with controlled surface floor temperature. Mice were first acclimated to the environment for 15 min at 20°C. Next, mice were connected to the fiber photometry setup for an additional 15 min, then calcium transients from the Agrp neurons were recorded and the surface floor temperature was altered from 20°C to 35°C (at a rate of 1°C every 10s), and the animals were kept in this new temperature for 10 min. Subsequently, the surface floor temperature was altered from 35°C to 20°C (at a rate of 1°C every 25s), and the Agrp neuronal response was recorded.

The fiber photometry system consisted of two different sets of LEDs: a 405 nm LED sinusoidally modulated at 211 Hz and a 460 nm LED sinusoidally modulated at 333 Hz. Both light streams were merged into an optical fiber patch using a mini cube (Doric Systems, model FMC4_AE(405)_E(460-490)_F(500-550)). The fiber optic patch was connected to the cannula in the mouse. Fluorescence emitted by jGCaMP7s in response to light excitation was collected with the same fiber patch cord and focused into a

photodetector (Newport, model 2151). The signal collected at the photodetector was collected in a digital fiber photometry processor (Tucker-Davis Technologies, RZ5P). Signal was processed and pre-analyzed using the Synapse Software Suite (Tucker-Davis Technologies). The data was exported to MATLAB for post-processing. First, the isosbestic channel (405 nm excitation) was fitted to the calcium-dependent channel (460 nm excitation, denoted as F) using first order polynomial fitting (F_0 denotes the fitted isosbestic). The calcium fluorescence activity was calculated as $(F - F_0)/F$. High-frequency components of the fluorescence activity were filtered out by a low pass filter of 0.5 Hz. Next, we downsampled the signal by averaging it in non-overlapping windows of 0.1s. Finally, the Z-score was calculated considering the first 10 min at room temperature as the baseline. Animals with poor jGCaMP7s expression or misplacement of the fiber optic cannula were discarded from the study.

3.5 Activation of Agrp neurons followed by skin temperature measurements

At postnatal days 09, 10 or 11, pups ($Agrp^{Trpv1}$; $Agrp^{VgatKO}$; $Agrp^{hM3Dq}$;Npy^{KO}; and C57BL/6J) were initially isolated from the dam and siblings at room temperatures ($\approx23^{o}C$) and placed into an apparatus (5 cm x 16.5 cm x 7 cm) composed of 8 eight small chambers (2.5 cm x 4.125 cm x 7 cm). All animals were placed individually in one of the chambers and the skin temperature was video recorded using an infrared thermal camera (T460, FLIR) which was placed 1 m distant from the apparatus. First, animals were initially isolated for 20 min in order to evaluate their skin temperature prior injection. Next, mice were injected subcutaneously with 10 mg/kg capsaicin ($Agrp^{Trpv1}$ and $Agrp^{VgatKO}$ pups), 1 mg/kg CNO ($Agrp^{hM3Dq}$;Npy^{KO} pups), or 0.5, 1 or 2 mg/kg ghrelin (C57BL/6J pups) and skin temperature was recorded for 60 min after injection. After the experiment was over, pups returned to the homecage. Data were collected using the software FLIR Tools[+] (FLIR). Data collection was set to 7.5 frames per second (fps). Data from mice that rapidly decreased the skin temperature during the initial 20-min were not used in the analysis. Data were processed and analyzed in MATLAB (2018a or above). Using a custom-made script, the number of measurements per minute was calculated and the mean of the skin temperature per 5 minutes was calculated.
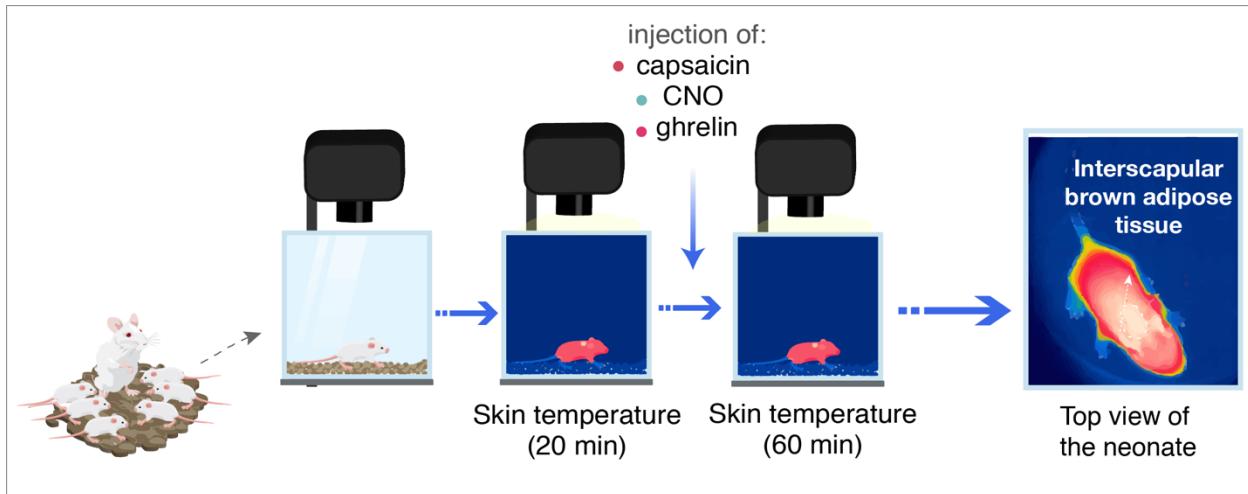
Figure 6. Protocol used to evaluate skin temperature of P9-P11 mice. We measured the skin temperature of P9-P11 mice using thermal imaging. In order to do that, animals were first isolated for twenty minutes (baseline). Next, animals were injected with capsaicin, CNO or ghrelin and skin temperature was recorded for 60 min. We collected the maximum temperature measurements of the skin. Usually, the maximum temperature points detected referred to the area on top of the interscapular brown adipose tissue.

3.6 Analysis of skin temperature in different mouse lines upon isolation

At postnatal days 9 to 11 (P9-P11), pups were isolated from the dams and siblings at room temperatures ($\approx$23ºC) and placed into a small chamber (8.5 cm x 8 cm x 10.5 cm). One animal was isolated at a time. Pups were isolated for 90 minutes and skin temperature was video recorded using an infrared thermal camera (T460, FLIR). For this set of experiments, thirty seconds of the maximum temperature measurements of skin temperature were collected every five minutes. Next, the number of measurements per thirty seconds every five minutes was counted and the mean of skin temperature per five minutes was calculated using Microsoft Excel (v.1625).

3.7 Immunohistochemistry

3.7.1 Fos and HA

P10-P11 mice were deeply anesthetized and perfused with freshly prepared fixative solution (paraformaldehyde 4%, in PBS 1x [pH = 7.4]). Brains were post-fixed

overnight in paraformaldehyde 4% and sectioned on a vibratome (Leica Vibratome 1200S). Coronal brain sections (50 µm) were washed in PBS 1x (pH = 7.4) and pre-incubated with Triton X-100 (0.3% in PBS 1x) for 30 min. Next, sections were incubated in a blocking solution (Triton 0.3%, Donkey Serum 10%, Glycine 0.3M in PBS 1x) for two hours. Sections were then incubated with rabbit polyclonal anti-c-Fos (1:200; Santa Cruz Biotechnologies, cat. #sc-52,) or rabbit monoclonal anti-c-Fos (1:1000; Cell Signaling Technology, cat. #2250) and mouse polyclonal anti-HA (1:1000; Biolegend, cat. #1612B,) for 16 hrs. After, sections were extensively washed in 0.3% Triton in PBS and incubated with secondary fluorescent Alexa antibodies (1:500). Sections were mounted and visualized by a Leica TCS SP5 Spectral Confocal Microscope (Center for Cellular e Molecular Imaging, Yale University). During the entire procedure, experimenters were blinded to the experimental groups. The ImageJ analysis software (version 1.51h, NIH, USA) was utilized to count the number of HA-positive ($Agrp^{HA}$ neurons) and Fos-positive (active) neurons manually.

3.7.2 GFP (jGCaMP7s)

After the experiments, mice were deeply anesthetized and perfused with freshly prepared fixative solution (paraformaldehyde 4%, in PBS 1x [pH = 7.4]). Brains were post-fixed overnight in paraformaldehyde 4% and sectioned on a vibratome (Leica Vibratome 1200S). Coronal brain sections (100 µm) were washed in PBS 1x (pH = 7.4) and pre-incubated with Triton X-100 (0.3% in PBS 1x) for 30 min. Next, sections were incubated in a blocking solution (Triton 0.3%, Donkey Serum 10%, Glycine 0.3M in PBS 1x) for two hours. Sections were then incubated with chicken anti-GFP polyclonal (1:2000; Abcam, cat. #AB13970) for 16 hrs. After, sections were extensively washed in 0.3% Triton in PBS and incubated with secondary fluorescent Alexa antibodies (1:1000). Sections were mounted and visualized by a Keyence All-in-One Fluorescence Microscope BZ-X800 (Department of Comparative Medicine, Yale University). Viral infection and cannula placement were analyzed.

3.8 Statistical analysis and data plotting

MATLAB (2018a or above) and GraphPad Prism 8.1 were used to analyze the data and plot the figures. Figures were further edited in Adobe Illustrator CC. Illustrations were designed by Mind the Graph (MindtheGraph.com), BioRender (bioRENDER.com) and Freepik (flaticon.com). Data were first subjected to the Shapiro-Wilk normality test. If a parametric distribution was assumed, parametric tests were utilized. When comparing two groups, Student's t-test was used. However, when standard deviations were not equal, Welch t-test was used. When comparing multiple groups, analysis of variance (ANOVA) was used followed by Bonferroni multiple comparison test. If a nonparametric distribution was assumed, when comparing two groups, the Mann-Whitney U test was used. When comparing multiple groups, Kruskal-Wallis nonparametric ANOVA was used with Dunn correction. A two-way repeated measures (RM) ANOVA between groups was used to evaluate time and genotype as dependent variables followed by Bonferroni's multiple comparison test. Statistical data are provided in the figures. $P < 0.05$ was considered statistically significant.

4. RESULTS

4.1 Isolation of P10 mice at room temperature induces activation of Agrp neurons, while isolation with thermal support blunts this activation

In order to assess whether exposure of neonates (P10) to room temperature ($\approx 23°C$), in contrast to the nest temperature ($\approx 35°C$), would activate the Agrp neurons, we generated a mouse model ($Agrp^{HA}$) in which we could selectively label the Agrp neurons (**Figure 7A**) (Sanz et al., 2009). Using Fos as a proxy for neuronal activity together with hemagglutinin (HA) staining, we determined the percentage of activated Agrp neurons in P10 mice (**Figure 7B**). Since a ninety-minute period allows maximum Fos expression (Barros et al., 2015), we exposed the isolated neonates to different ambient temperatures for ninety-minutes in these studies (**Figure 7C**).

We found that P10 mice isolated at room temperature showed increased percentage of activated Agrp neurons (**Figure 7D**) compared to pups kept with dam and siblings. Furthermore, P10 mice isolated with thermal support presented reduced percentage of activated Agrp neurons (nest: 1.03 ± 0.30 %, n = 6; Isolated $_{RT}$: 24.36 ± 2.59 %, n = 7; Isolated $_{TS}$: 2.75 ± 0.52 %, n = 8 [Mean $\pm$ SEM], $F_{2,18} = 70.46$, p < 0.0001, one-way ANOVA followed by Bonferroni's multiple comparison test, **Figure 7D**).

During the lactation period, dams leave the nursing nest to obtain food. This behavior of the dams presumably creates windows in which environmental temperature decreases in the nest. With that in mind, we tested whether these episodes of drops in environmental temperature would influence the activation of Agrp neurons during isolation. To exclude these events of ambient temperature drop, we raised mice in thermoneutral conditions (**Figure 7E**). At postnatal day 10 (P10), mice were either isolated at room temperature or isolated at thermoneutral conditions. Again, mice raised at thermoneutral conditions showed higher activation of the Agrp neurons upon isolation at room temperatures but not at thermoneutral conditions (nest: 0.63 ± 0.34 %, n = 2; isolated $_{RT}$: 27.94 ± 3.14 %, n = 3; isolated $_{TN}$: 6.17 ± 1.54 %, n = 3 [Mean $\pm$ SEM], $F_{2,5} = 37.91$, p = 0.001, one-way ANOVA followed by Bonferroni's multiple comparison test, **Figure 7F**).

Overall, these findings indicate that the activation of Agrp neurons in P10 mice is triggered by the lack of thermal insulation provided by dam and siblings. This effect is not influenced by previous episodes of decreased environmental temperature.
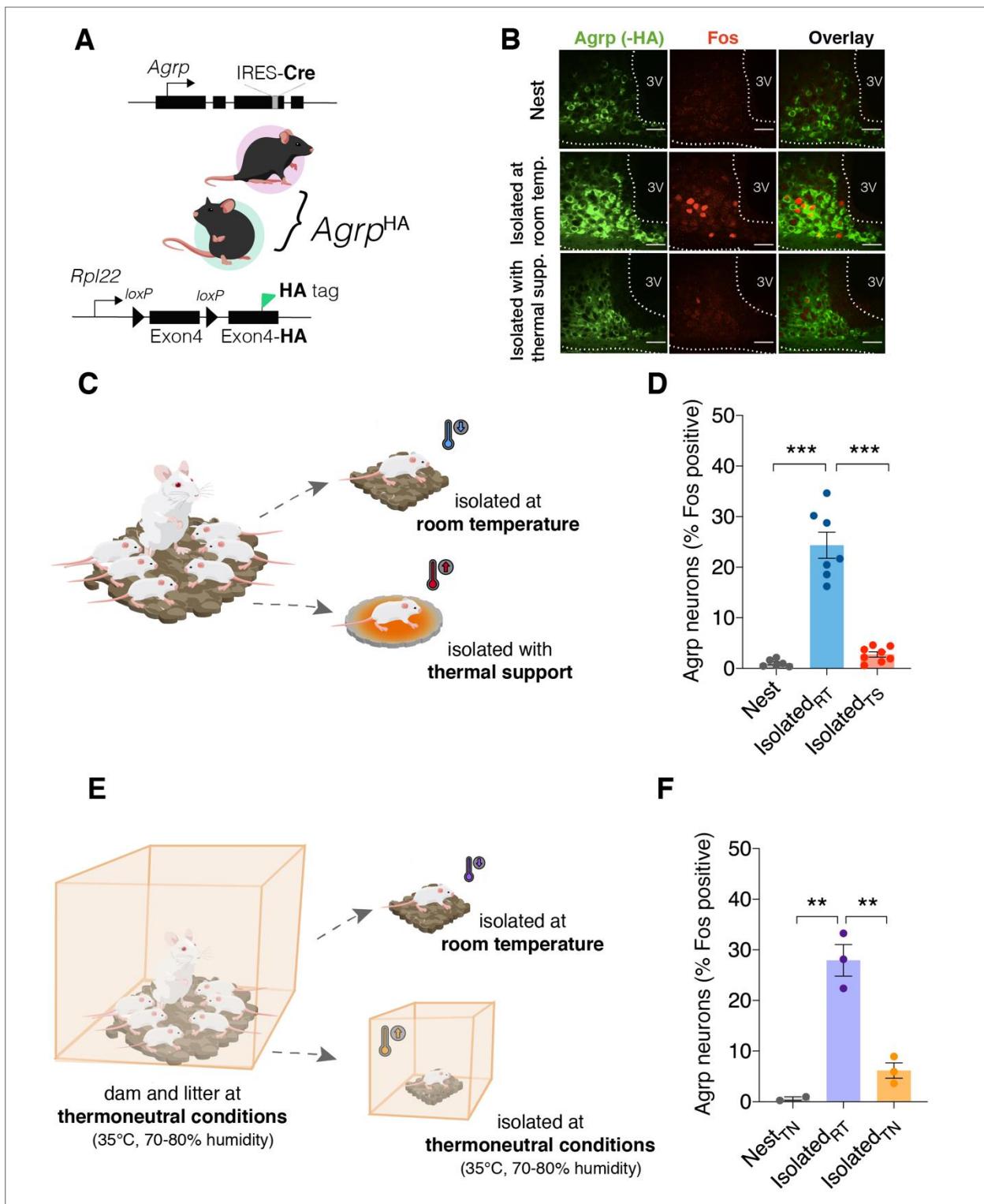
Figure 7. Isolation of P10 mice from dam and siblings at room temperature induces activation of Agrp neurons while isolation with thermal support blunts this effect. A Illustration describing the generation of the animal model *Agrp*[HA].

4.2 Agrp neuronal activity is rapidly modulated by changes in floor temperature

Fos experiments do not provide temporal dynamics of physiological activation of Agrp neurons. To better comprehend the neuronal activity dynamics of Agrp neurons, we injected a *Cre*-dependent virus encoding jGCaMP7s in *Agrp*[Cre/Cre] virus in mouse pups (Dana et al., 2018) (**Figure 8A**). Then, we used fiber photometry to measure neuronal activity from Agrp neurons in P16-P17 mice while we manipulated the floor temperature in the recording apparatus (**Figure 8B**). Initially, animals were on top of a floor temperature at $\approx$20°C, then floor temperature was altered to $\approx$35°C and decreased it back to $\approx$20°C (**Figure 8C**).

After successfully targeting the arcuate nucleus and infecting the Agrp neurons in P16-P17 mice (**Figure 8D**), we measured the calcium transients from the Agrp neurons. We observed that an increase in floor temperature to $\approx$35°C progressively reduced Agrp neuron activity, an effect that began within seconds of the change in floor temperature and prolonged for more than a minute after floor temperature reached $\approx$35°C (**Figure 8E**). The decreased activity of Agrp neurons at $\approx$35°C persisted during the remaining period of exposure (**Figure 8E**). Once floor temperature returned to temperatures $\approx$20°C, Agrp neuron activity rapidly increased to baseline levels (**Figure 8E**). Interestingly, this resetting of Agrp neuronal activity was much faster than the suppression in neuronal activity during the increase in floor temperature (**Figure 8E**). Taken together, these results show that Agrp neurons rapidly respond to changes in temperature. The rapid dynamics of Agrp neuronal activity and the fact that we tested the response of mice by changing the temperature in the floor of the apparatus indicate that somatosensorial detection of ambient temperatures can modulate the activity of Agrp neurons.

_____

B Representative images of immunohistochemistry for HA (green, labels Agrp neurons in *Agrp*[HA] mice), Fos (red), and overlay. Scale bars represent 50 μm. **C** Illustration describing the experimental design to evaluate Agrp neuron activity using Fos as a marker for neuronal activity. **D** Percentage of Fos positive Agrp neurons in three different conditions, nest (n = 6), isolated $_{RT}$ (n = 7), isolated $_{TS}$ (n = 8). **E** Illustration describing the experimental conditions. **F** Percentage of Fos positive Agrp neurons of animals raised in thermoneutrality, nest (n = 2), Isolated $_{RT}$ (n = 3), Isolated $_{TN}$ (n = 3). Bars represent mean $\pm$ SEM. * represents $p < 0.05$; ** represents $p < 0.01$; *** represents $p < 0.001$; **** represents $p < 0.0001$. RT, room temperature; TS, thermal support; TN, thermoneutral conditions.
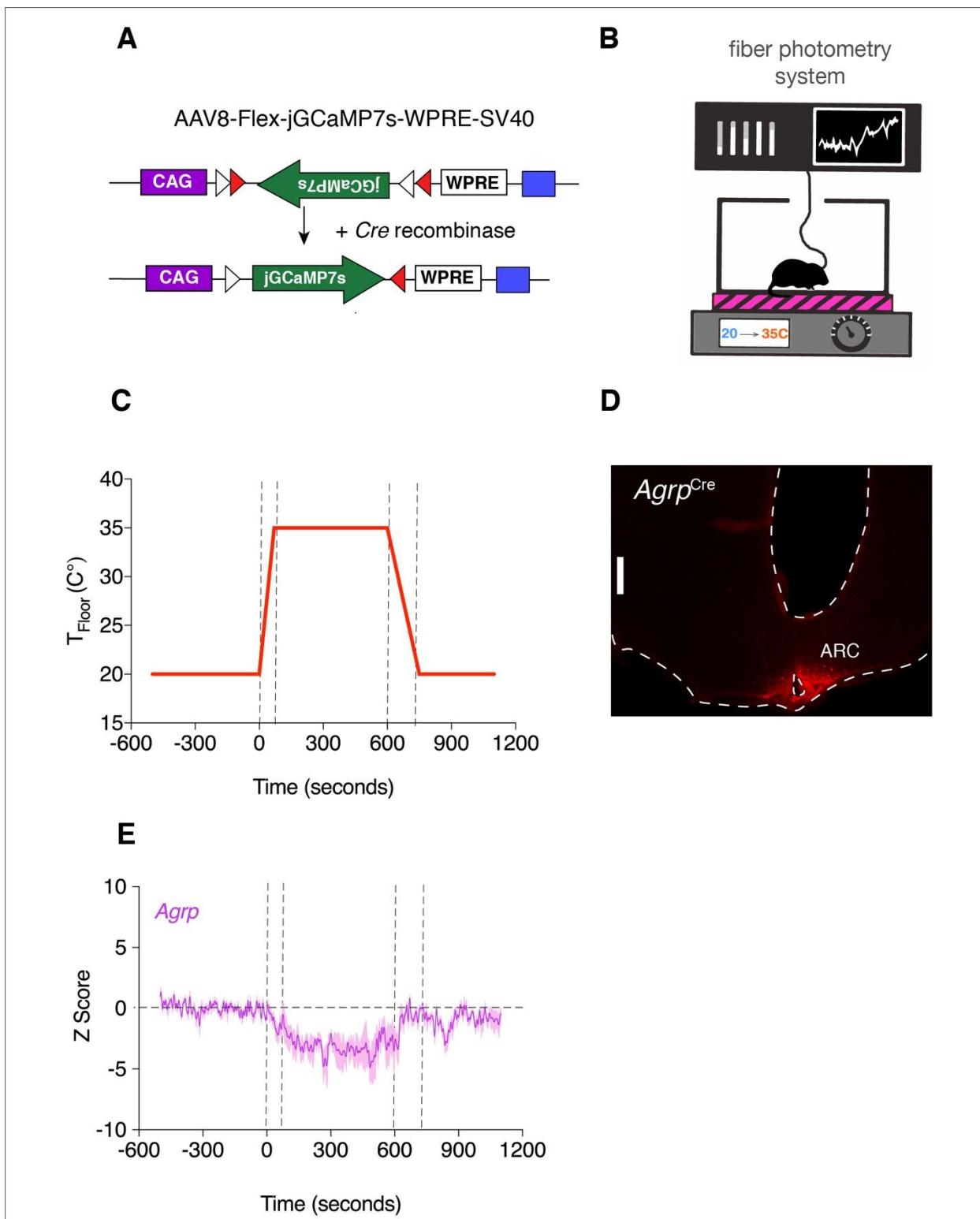
**Figure 8. Agrp neuronal activity is rapidly modulated by changes in floor temperature. A** Illustration of the viral vector jGCaMP7s. **B** Illustration describing the experimental setup. **C** Experimental design describing how we manipulated the floor temperature (20 °C – 35 °C – 20 °C). **D** Immunohistochemistry showing viral infection (*j*GCaMP7s) in the Agrp neurons (scale 100 µm).

(legend continues on the next page)

4.3 Skin temperature can be used as a readout of brown adipose tissue thermogenesis

Next, we aimed to tested whether manipulating the activity of Agrp neurons could modulate BAT thermogenesis in P10-P11 pups. First, we sought to determine a reliable method to infer BAT temperatures and activity in these young mice with minimal interference to their physiology (i.e., avoiding use of catheters and surgically inserted probes). We first assessed whether skin temperature could be used as a readout of brown adipose tissue thermogenesis using thermal imaging. For that, we utilized pups that cannot use BAT thermogenesis ($Ucp1^{KO}$) during isolation for ninety minutes.

As expected, upon isolation at room temperature, we detected that $Ucp1^{KO}$ pups rapidly reduced the skin temperature (interaction: $F_{6,114} = 44.24$, p < 0.0001; time: $F_{1.477,28.07} = 212.3$, p < 0.0001; genotype: $F_{1,19} = 96.72$, p < 0.0001, two-way ANOVA with repeated measures, followed by Bonferroni's multiple comparison test, **Figure 9A**). Furthermore, pups lacking UCP1 presented decreased skin temperature nadir (minimum skin temperature measurement detected during isolation; control: 32.02 ± 0.40 °C, n = 14; $Ucp1^{KO}$: 26.21 ± 0.40 °C, n = 7 [Mean ± SEM], t = 10.17; df = 16.45; p < 0.0001, two-tailed Welch's T-test, **Figure 9B**). Also, we calculated the difference between nadir and initial skin temperature (delta skin temperature). $Ucp1^{KO}$ pups presented higher delta skin temperature (control: - 2.79 ± 0.36 °C, n = 14; $Ucp1^{KO}$: - 7.11 ± 0.43 °C, n = 7 [Mean ± SEM], t = 7.68; df = 15.98; p < 0.0001, two-tailed Welch's T-test, **Figure 9C**). Altogether, these results indicate that thermal imaging is a suitable method to infer BAT thermogenesis based on skin temperature in P10-P11 mice.

_____

E Agrp neuronal response to changes in floor temperature (n = 5). Lines represent mean ± SEM. In **C** and **E** vertical dashed lines represent the start and end of the temperature changes. ARC, arcuate nucleus of the hypothalamus.
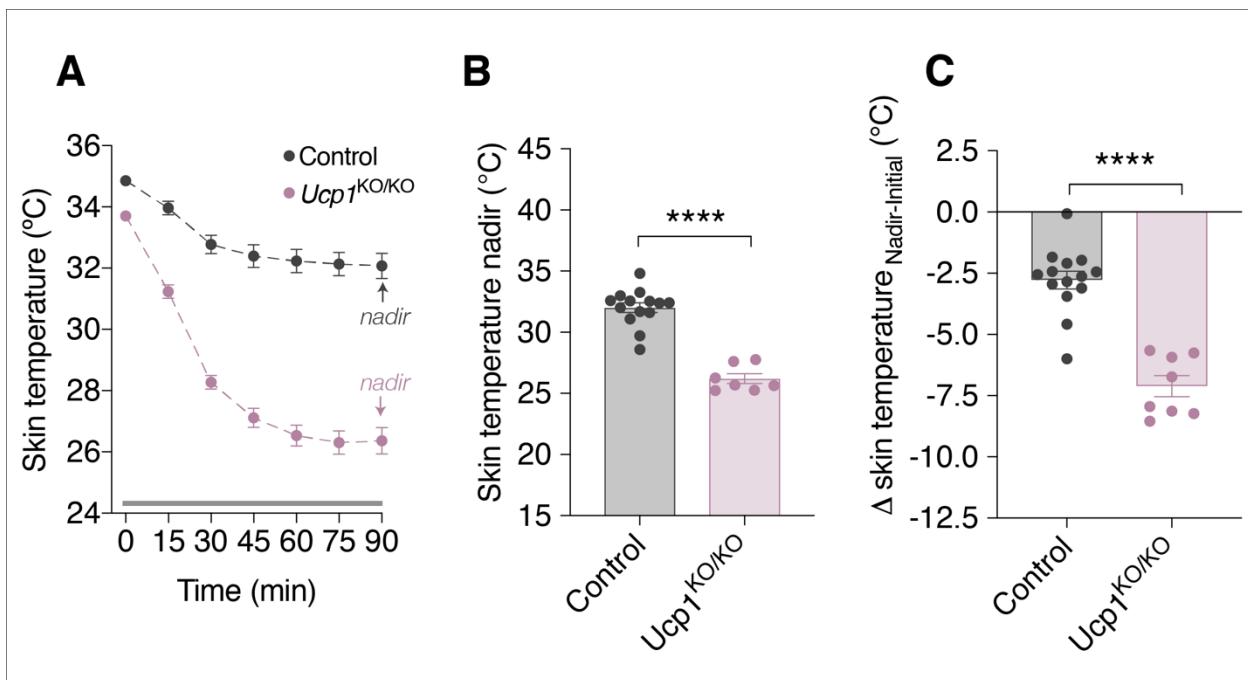
Figure 9. Skin temperature can be used as a readout of brown adipose tissue thermogenesis. **A** Skin temperature measurement in 15-min bins; controls (n = 14), $Ucp1^{KO}$ (n = 7). **B** Skin temperature nadir (minimum skin temperature measurements detected during isolation). **C** Delta skin temperature calculated by the difference between skin temperature nadir and initial skin temperature during isolation. In figure **A,** symbols represent mean ± SEM; horizontal grey bar represents time points with significant differences (p < 0.05); and arrows indicate the nadir. In **B-C,** bar plots show mean ± SEM. * represents p < 0.05; ** represents p < 0.01; *** represents p < 0.001. **** represents p < 0.0001.

4.4 Chemogenetic activation of Agrp neurons reduces skin temperature in P10 mice

We investigated whether chemogenetic activation of Agrp neurons in P10 pups could affect thermoregulation using $Agrp^{Trpv1}$ mice (**Figure 10A**) (Dietrich et al., 2015; Ruan et al., 2014; Zimmer et al., 2019). Mice were first isolated for twenty minutes for evaluation of baseline temperature. Next, mice were injected with 10 mg/kg capsaicin and skin temperature was assessed for sixty minutes (**Figure 10B**). Mice that expressed the Trpv1 receptor in the Agrp neurons ($Agrp^{Trpv1}$) rapidly reduced skin temperature after capsaicin administration when compared to control animals (interaction: $F_{15,60} = 34.71$, p < 0.0001; genotype: $F_{1,4} = 130.6$, p = 0.0003; time: $F_{15,60} = 44.03$, p < 0.0001, two-way ANOVA with repeated measures followed by Bonferroni's multiple comparison test, **Figure 10C**). Additionally, after capsaicin administration, $Agrp^{Trpv1}$ mice also presented decreased skin temperature nadir compared to control animals (control: 33.51 ± 0.41 °C, n = 5; $Agrp^{Trpv1}$: 29.94 ± 0.33 °C, n = 5 [Mean ± SEM], t = 6.80; df = 7.63; p = 0.0002, two-

tailed Welch's T-test, **Figure 10D**). Furthermore, we calculated the difference between nadir and initial skin temperature (delta skin temperature). $Agrp^{Trpv1}$ pups presented higher delta skin temperature than control mice (control: - 0.85 $\pm$ 0.36 °C, n = 5; $Agrp^{Trpv1}$: - 4.35 $\pm$ 0.36 °C, n = 5 [Mean $\pm$ SEM], t = 6.91; df = 8.00; p = 0.0001, two-tailed Welch's T-test, **Figure 10E**). Overall, these findings demonstrate that Agrp neurons modulate skin temperature in P10 mice, suggesting that these neurons control BAT thermogenesis at these young ages.
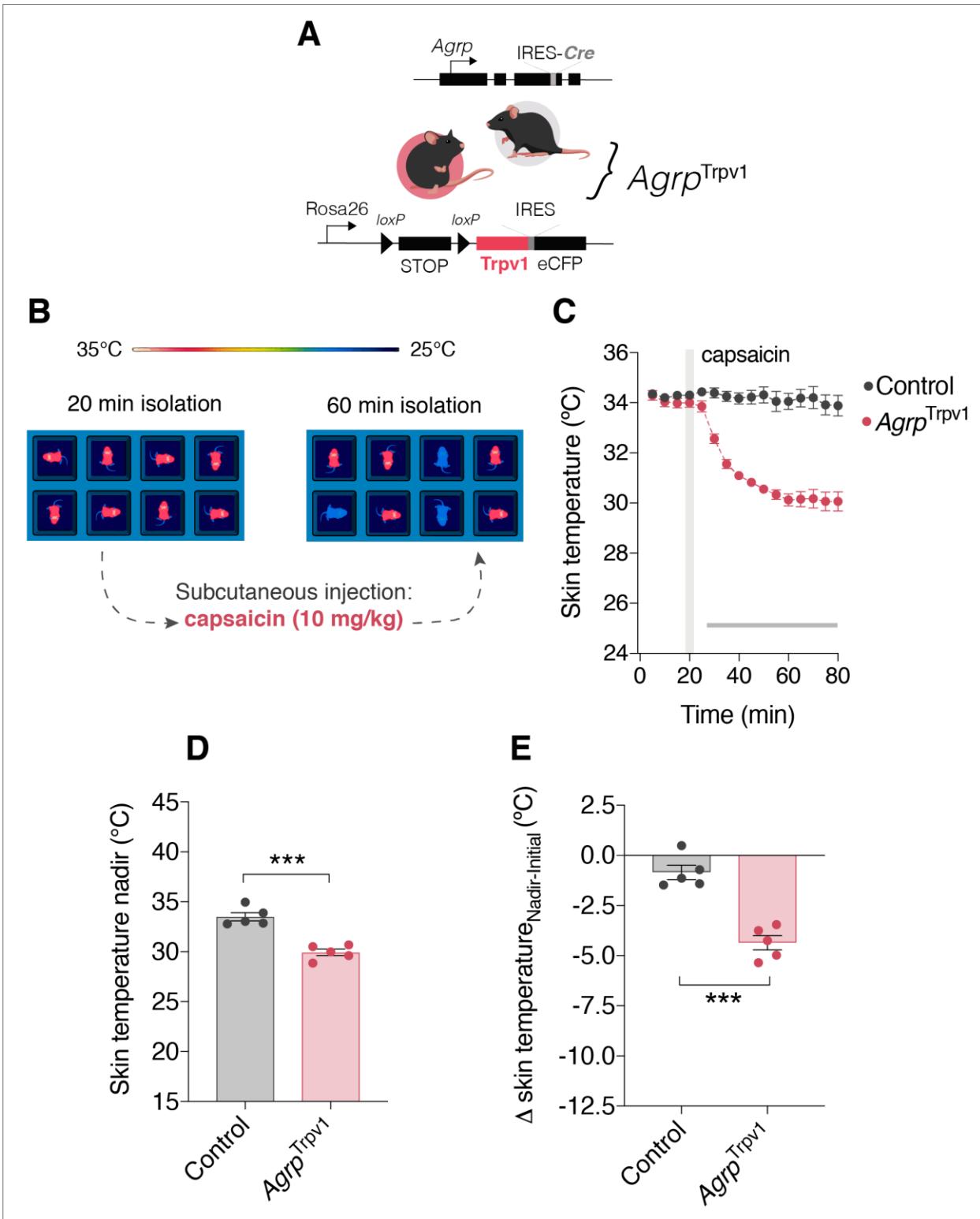
**Figure 10. Chemogenetic Agrp activation reduces skin temperature in P10 mice. A** Illustration describing the generation of the animal model *Agrp*Trpv1. **B** Illustration describing the experimental design. **C** Skin temperature measurements in 5-min bins upon initial isolation and Agrp activation using capsaicin, controls (n = 5), *Agrp*Trpv1 (n = 5).

(legend continues on the next page)

4.5 Reduction in skin temperature after Agrp activation requires NPY but not GABA

Agrp neurons release AGRP, NPY and GABA (Aponte et al., 2011; Hahn et al., 1998; Krashes et al., 2013; Tong et al., 2008). To evaluate the transmitters by which Agrp neurons modulate skin temperature of P9-P10 mice, we tested animals lacking GABA and NPY. First, mice were isolated for twenty minutes for evaluation of baseline temperature. Next, we chemogenetically activated the Agrp neurons using 10 mg/kg capsaicin and recorded the skin temperature in $Agrp^{VgatKO}$ mice (**Figure 11A**) upon isolation (**Figure 11B**). Animals lacking GABA release by Agrp neurons also exhibited a reduction in skin temperature upon chemogenetic Agrp activation (interaction: $F_{15,75}$ = 97.96, p < 0.0001; time: $F_{2.158,10.79}$ = 74.11, p < 0.0001; genotype: $F_{1,5}$ = 110.1, p = 0.0001; two-way ANOVA with repeated measured followed by Bonferroni's multiple comparison test, **Figure 11C**). $Agrp^{VgatKO}$ mice presented decreased skin temperature nadir compared to control mice (control: 32.82 ± 0.14 °C, n = 4; $Agrp^{VgatKO}$: 28.06 ± 0.24 °C, n = 3 [Mean ± SEM], t = 16.99; df = 3.32; p = 0.0002, two-tailed Welch's T-test, **Figure 11D**). Also, we calculated the difference between nadir and initial skin temperature (delta skin temperature). $Agrp^{VgatKO}$ pups presented higher delta skin temperature values than control mice (control: - 1.36 ± 0.18 °C, n = 3; $Agrp^{VgatKO}$: - 5.76 ± 0.15 °C, n = 3 [Mean ± SEM], t = 19.05; df = 5.00; p < 0.0001, two-tailed Welch's T-test, **Figure 11E**). These results suggest that the reduction in skin temperature is not mediated by GABA release by the Agrp neurons.

_____

D Skin temperature nadir (minimum skin temperature measurements detected), controls (n = 5), $Agrp^{Trpv1}$ (n = 5). **E** Delta skin temperature calculated by the difference between skin temperature nadir and initial skin temperature, controls (n = 5), $Agrp^{Trpv1}$ (n = 5). In figure **C** lines represent mean ± SEM; horizontal grey bar represents time points with significant differences (p < 0.05). In **D-E** bar plot shows mean ± SEM. * represents p < 0.05; ** represents p < 0.01; *** represents p < 0.001. **** represents p < 0.0001.
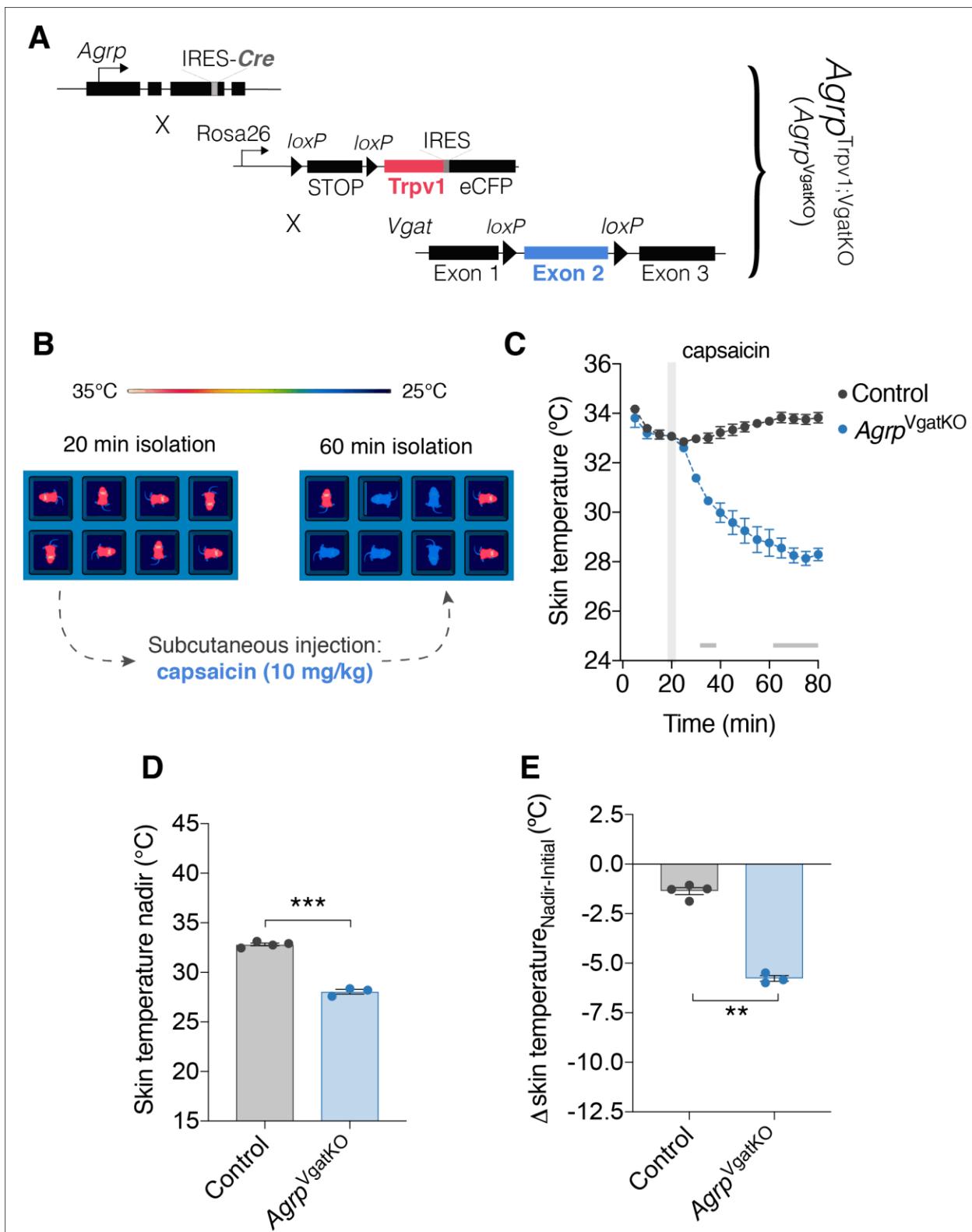
**Figure 11. Chemogenetic Agrp activation reduces skin temperature in P9-P10 mice lacking GABA release by the Agrp neurons**. **A** Illustration describing the mouse model *Agrp*[VgatKO]. **B** Illustration describing the experimental design.

(legend continues on the next page)

Next, we chemogenetically activated the Agrp neurons in control P10-P11 mice and in P10-P11 mice lacking NPY using excitatory DREADDS (designer receptors exclusively activated by designer drugs) technology (**Figure 12A**) (Armbruster et al., 2007). First, we isolated mice at room temperature for twenty minutes (**Figure 12B**). After, mice were injected with 1 mg/kg CNO and skin temperature was assessed for the next one hour. Mice that expressed the hM3Dq receptor in the Agrp neurons and were heterozygotes for NPY (*Agrp*^{hM3Dq};*Npy*$^{KO/+}$), exhibited a reduction in skin temperature after CNO injection. In comparison, mice which expressed the hM3Dq but lacked NPY (*Agrp*^{hM3Dq};*Npy*$^{KO/KO}$) did not display this reduction in skin temperature (interaction: $F_{30,210}$ = 13.44, p < 0.0001; time: $F_{1.703,23.85}$ = 11.97, p = 0.0004; genotype: $F_{2,14}$ = 13.25, p = 0.0006, two-way ANOVA with repeated measures followed by Bonferroni's multiple comparison test, **Figure 12C**). Additionally, *Agrp*^{hM3Dq};*Npy*$^{KO/+}$ mice presented decreased skin temperature nadir. This reduced skin temperature nadir did not occur in *Agrp*^{hM3Dq};*Npy*$^{KO/KO}$ mice (*Npy*^{KO}: 34.92 ± 0.30 °C, n = 7; *Agrp*^{hM3Dq};*Npy*$^{KO/+}$: 30.90 ± 0.56 °C, n = 7; *Agrp*^{hM3Dq};*Npy*$^{KO/KO}$: 35.47 ± 0.20 °C [Mean ± SEM], $F_{2,14}$ = 30.22; p < 0.0001, one-way ANOVA followed by Bonferroni's multiple comparison test, **Figure 12D**). We also calculated the difference between skin temperature nadir and initial skin temperature (delta skin temperature). We observed that P10-P11 mice expressing the hM3Dq receptor but lacking NPY showed decreased delta skin temperature (*Npy*^{KO}, n = 7 animals; *Agrp*^{hM3Dq};*Npy*$^{KO/+}$, n = 7 animals; *Agrp*^{hM3Dq};*Npy*$^{KO/KO}$, n = 3 animals, p = 0.0003, Kruskal-Wallis test followed by Dunn's multiple comparison test, **Figure 12E**). Overall, these findings indicate that the reduction in skin temperature upon chemogenetic activation of Agrp neurons in P10 mice requires NPY.

_____

C Skin temperature measurements in 5-min bins upon initial isolation and Agrp activation using capsaicin; controls (n = 4), *Agrp*^{VgatKO} (n = 3). **D** Skin temperature nadir (minimum skin temperature measurements detected), controls (n = 4), *Agrp*^{VgatKO} (n = 3). **E** Delta skin temperature calculated by the difference between skin temperature nadir and initial skin temperature, controls (n = 4), *Agrp*^{VgatKO} (n = 3). In figure **C** lines represent mean ± SEM; horizontal grey bar represents time points with significant differences (p < 0.05). In **D-E** bar plot shows mean ± SEM. * represents p < 0.05; ** represents p < 0.01; *** represents p < 0.001. **** represents p < 0.0001.
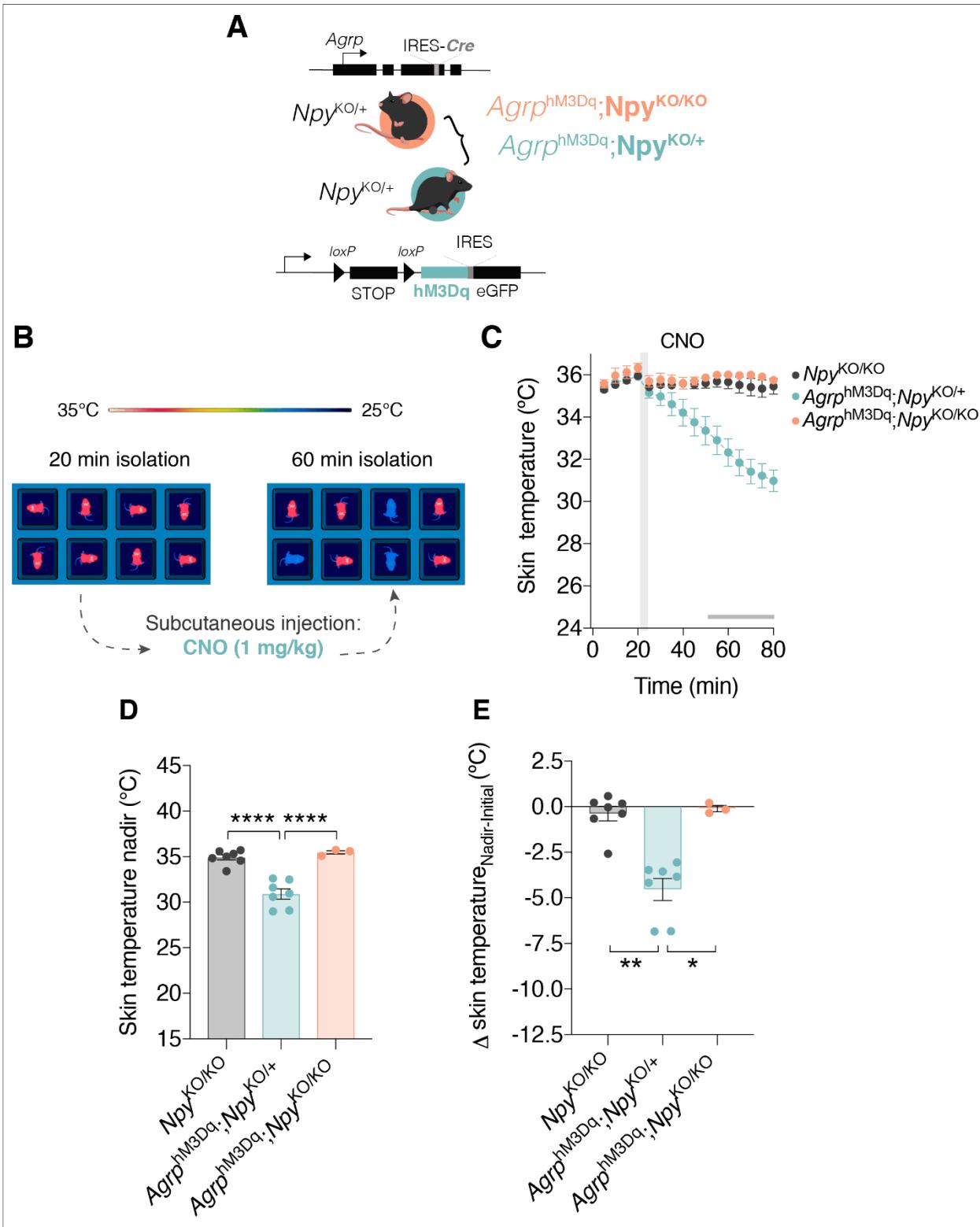
Figure 12. Chemogenetic activation of Agrp neurons do not reduce skin temperature in P10-P11 mice lacking NPY. **A** Illustration describing the generation of the mouse lines $Agrp^{hM3Dq};Npy^{KO/+}$ and $Agrp^{hM3Dq};Npy^{KO}$/KO. **B** Illustration describing the experimental conditions.

(legend continues on the next page)

4.6 Ghrelin reduces skin temperature in P10-P11 mice

Agrp neurons are activated by ghrelin (Andrews et al., 2008; Cowley et al., 2003; Steculorum et al., 2015). In order to evaluate whether ghrelin would reduce the skin temperature in P10-P11 mice, we submitted wild-type (C57BL/6J) P10-P11 mice to exogenous ghrelin injections. P10-P11 mice were initially isolated for twenty minutes and their skin temperature was recorded (**Figure 13A**). Next, pups were injected with different doses of ghrelin [0.5, 1 or 2 mg/kg (s.c)] and skin temperature was assessed for one hour. All ghrelin doses promoted a rapid reduction in skin temperature (interaction: $F_{30,255}$ = 1.691, p = 0.0167; time: $F_{1.352,22.98}$ = 100.2, p < 0.0001; ghrelin dose: $F_{2,17}$ = 0.823, p = 0.454, two-way ANOVA with repeated measures followed by Bonferroni's multiple comparison test, **Figure 13B**). Skin temperature nadir differences were similar between groups (2 mg/kg: 30.78 $\pm$ 0.39 °C, n = 11; 1 mg/kg: 30.84 $\pm$ 0.65 °C, n = 5; 0.5 mg/kg: 31.55 $\pm$ 0.68 °C, n = 4 [Mean $\pm$ SEM], $F_{2,17}$ = 0.512 p = 0.61, one-way ANOVA followed by Bonferroni's multiple comparison test, **Figure 13C**). Also, we found that all groups displayed decreased skin temperature (2 mg/kg: - 4.071 $\pm$ 0.402 °C, n = 11; 1 mg/kg: - 4.42 $\pm$ 0.53 °C, n = 5; 0.5 mg/kg: - 3.67 $\pm$ 0.72 °C, n = 4 [Mean $\pm$ SEM], $F_{2,17}$ = 0.36, p = 0.70, one-way ANOVA followed by Bonferroni's multiple comparison test, **Figure 13D**). Since ghrelin also promoted a decrease in skin temperature, similarly to Agrp neuron activation using chemogenetic tools, we decided to use exogenous ghrelin injections to explore the role of the downstream targets of NPY signaling in thermoregulation.

_____

C Skin temperature measurements in 5-min bins upon chemogenetic activation of Agrp neurons before and after CNO administration, *Npy*[KO] (n = 7), *Agrp*[hM3Dq];*Npy*[KO/+] (n = 7), *Agrp*[hM3Dq];*Npy*[KO/KO] (n = 3). **C** Skin temperature nadir (minimum skin temperature measurements detected), Npy[KO] (n = 7), *Agrp*[hM3Dq];*Npy*[KO/+] (n = 7), *Agrp*[hM3Dq];*Npy*[KO/KO] (n = 3). **D** Delta skin temperature calculated by the difference between skin temperature nadir and initial skin temperature after CNO administration, *Npy*[KO] (n = 7), *Agrp*[hM3Dq];*Npy*[KO/+] (n = 7), *Agrp*[hM3Dq];*Npy*[KO/KO] (n = 3). In figure **C** lines represent mean $\pm$ SEM; horizontal grey bar represents time points with significant differences (p < 0.05). In **D-E**, bar plot shows mean $\pm$ SEM. * represents p < 0.05; ** represents p < 0.01; *** represents p < 0.001. **** represents p < 0.0001.
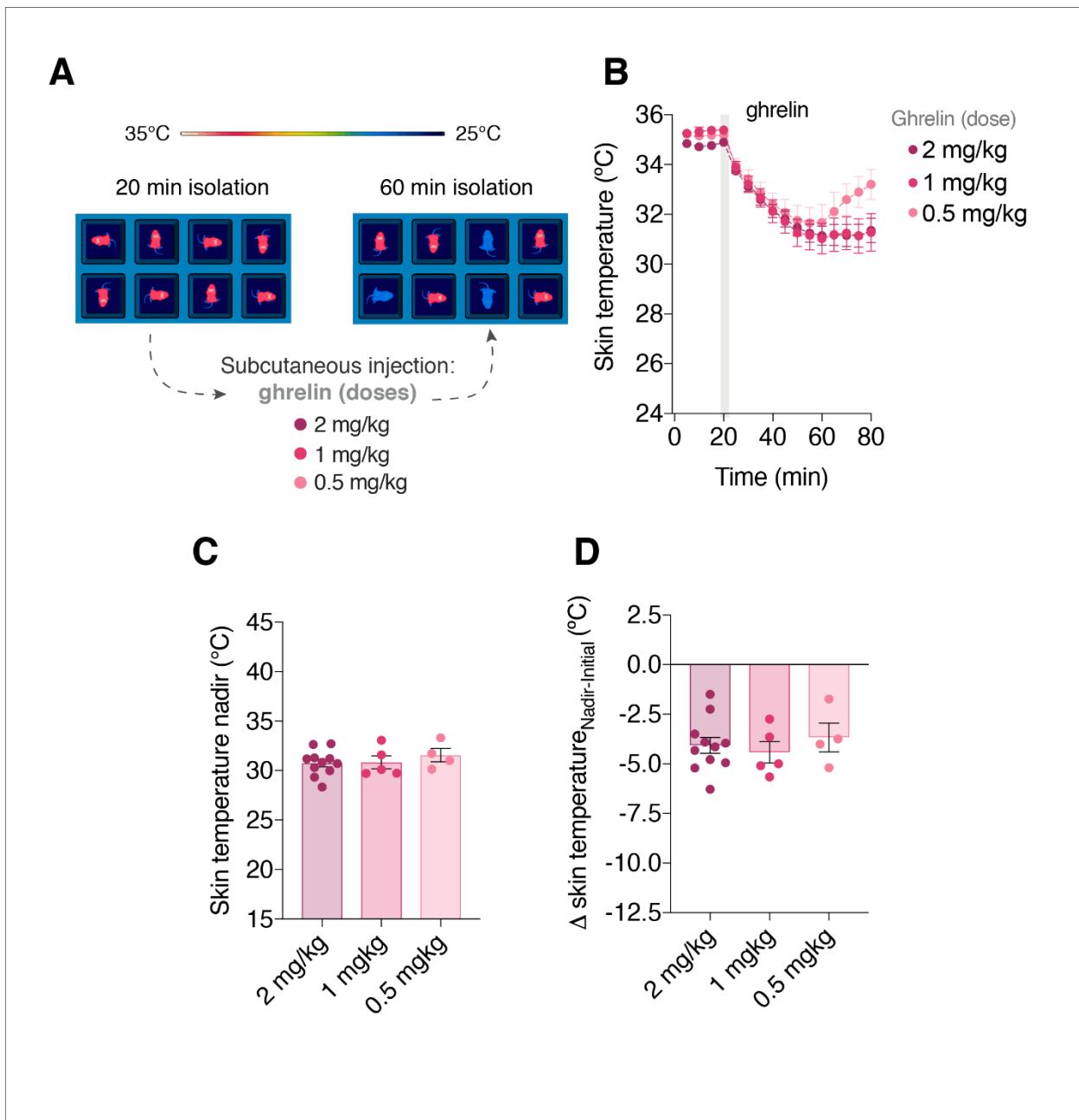
Figure 13. Exogenous ghrelin injections reduce skin temperature of neonatal mice. **A** Illustration describing the experimental conditions. **B** Skin temperature measurements before (baseline, 20 min) and after ghrelin injection (60 min) in 5-min bins, 2 mg/kg (n = 11), 1 mg/kg (n = 5), 0.5 mg/kg (n = 4). **C** Skin temperature nadir (minimum skin temperature measurements detected), 2 mg/kg (n = 11), 1 mg/kg (n = 5), 0.5 mg/kg (n = 4). **D** Delta skin temperature calculated by the difference between initial and minimum skin temperature, 2 mg/kg (n = 11), 1 mg/kg (n = 5), 0.5 mg/kg (n = 4). In **B**, lines represent mean $\pm$ SEM. In **C-D**, bar plot shows mean $\pm$ SEM. * represents $p < 0.05$; ** represents $p < 0.01$; *** represents $p < 0.001$. **** represents $p < 0.0001$.

4.7 Neuropeptide Y receptors Y₁ and Y₂ affect thermoregulation in P10-P11 mice

We previously found that Agrp neuronal activation requires NPY to reduce the skin temperature in P10 mice. However, different Y receptors could be mediating these effects (Y_1R, Y_2R, Y_4R or Y_5R). Hence, we first evaluated the skin temperature of P10-P11 mice lacking the NPY receptors Y_1R, Y_2R and Y_4R upon ninety-minute isolation utilizing thermal imaging. We found that Y_1R^{KO} pups presented higher skin temperature than control littermates upon isolation (interaction: $F_{6,144} = 3.14$, $p = 0.0064$; time: $F_{6,144} = 3.18$, $p = 0.0058$; genotype: $F_{1,24} = 5.57$, $p = 0.027$, two-way ANOVA with repeated measures followed by Bonferroni's multiple comparison test, **Figure 14A**). Analyzing skin temperature nadir we found that Y_1R^{KO} presented higher skin temperature nadir than control mice (control: 33.21 ± 0.32 °C, n = 16; Y_1R^{KO}: 34.26 ± 0.28 °C, n = 10 [Mean ± SEM]; t = 2.27; df = 24; p = 0.033, two-tailed Welch's T-test, **Figure 14B**). However, no differences were observed between the groups for delta skin temperature (control = 16 animals, Y_1R^{KO} = 10 animals; U = 44.50; p = 0.06, Mann-Whitney U test, **Figure 14C**). These findings show that mice lacking Y_1R present higher skin temperature upon isolation, and could, therefore be a potential target of NPY signaling to suppress BAT thermogenesis in young mouse pups.
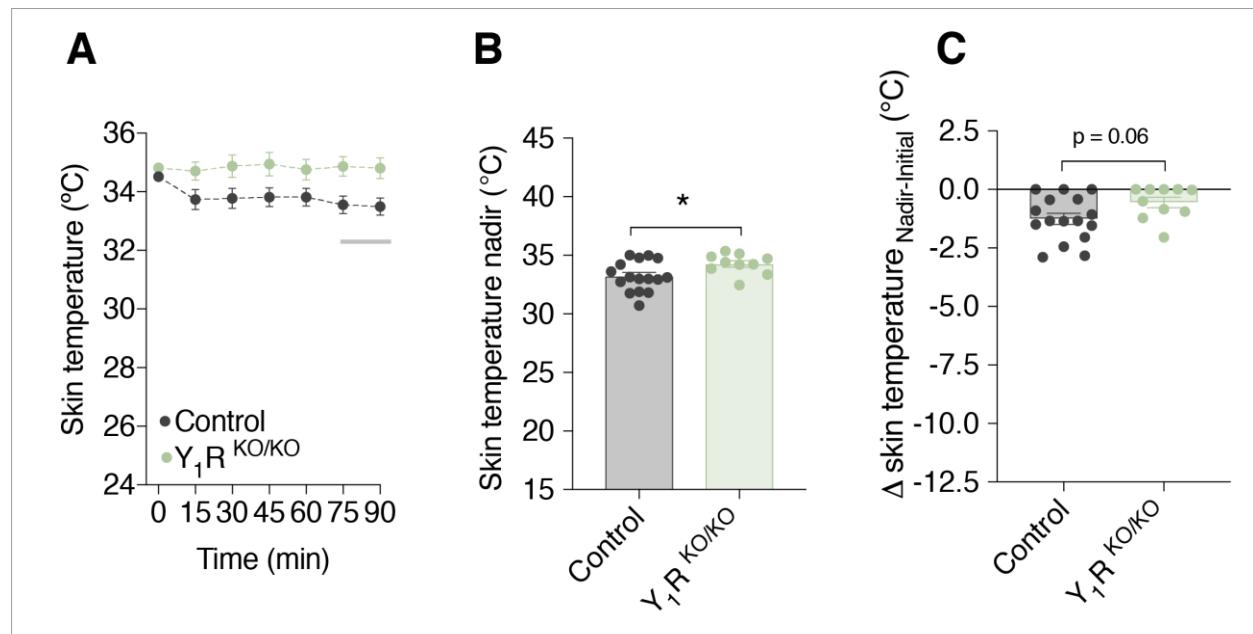

Figure 14. Y_1R^{KO} P10-P11 mice displays higher skin temperature. **A** Skin temperature measurements in 15-min bins, control (n = 16), Y_1R^{KO} (n = 10).

(legend continues on the next page)

We also found that Y_2R^{KO} pups presented a rapid decrease in skin temperature when isolated at room temperature (interaction: $F_{6,105} = 0.64$; $p = 0.80$; time: $F_{6,105} = 4.60$; $p = 0.0004$; genotype: $F_{1,105} = 22.79$; $p < 0.0001$, two-way ANOVA with repeated measures followed by Bonferroni's multiple comparison test, **Figure 15A**). Furthermore, we observed a decrease in skin temperature nadir (control: 33.69 ± 0.26 °C, n = 5; Y_2R^{KO}: 32.62 ± 0.31 °C, n = 12 [Mean $\pm$ SEM], t = 2.66; df = 13.38; p = 0.0193, two-tailed Welch's T-test, **Figure 15B**). We also found that Y_2R^{KO} pups showed increased delta skin temperature (control: - 0.97 ± 0.27 °C, n = 5; Y_2R^{KO}: - 2.04 ± 0.29 °C, n = 12 [Mean $\pm$ SEM], t = 2.20; df = 15; p = 0.04, two-tailed Welch's T-test, **Figure 15C**). Overall, these results suggest that the lack of Y_2R also affects thermoregulation in P10-P11 mice. However, mice lacking Y_2R had increased drop in skin temperature, which would suggest, that these receptors are not involved in the decrease in skin temperature upon NPY signaling in neonates.

_____

B Skin temperature nadir (minimum skin temperature measurements detected), control (n = 16), Y_1R^{KO} (n = 10). **C** Delta skin temperature calculated by the difference between skin temperature nadir and initial skin temperature, control (n = 16), Y_1R^{KO} (n = 10). In **A**, lines represent mean $\pm$ SEM. Horizontal grey bar represents time points in which p < 0.05. In **B-C,** bar plots show mean $\pm$ SEM. * represents p < 0.05; ** represents p < 0.01; *** represents p < 0.001. **** represents p < 0.0001.
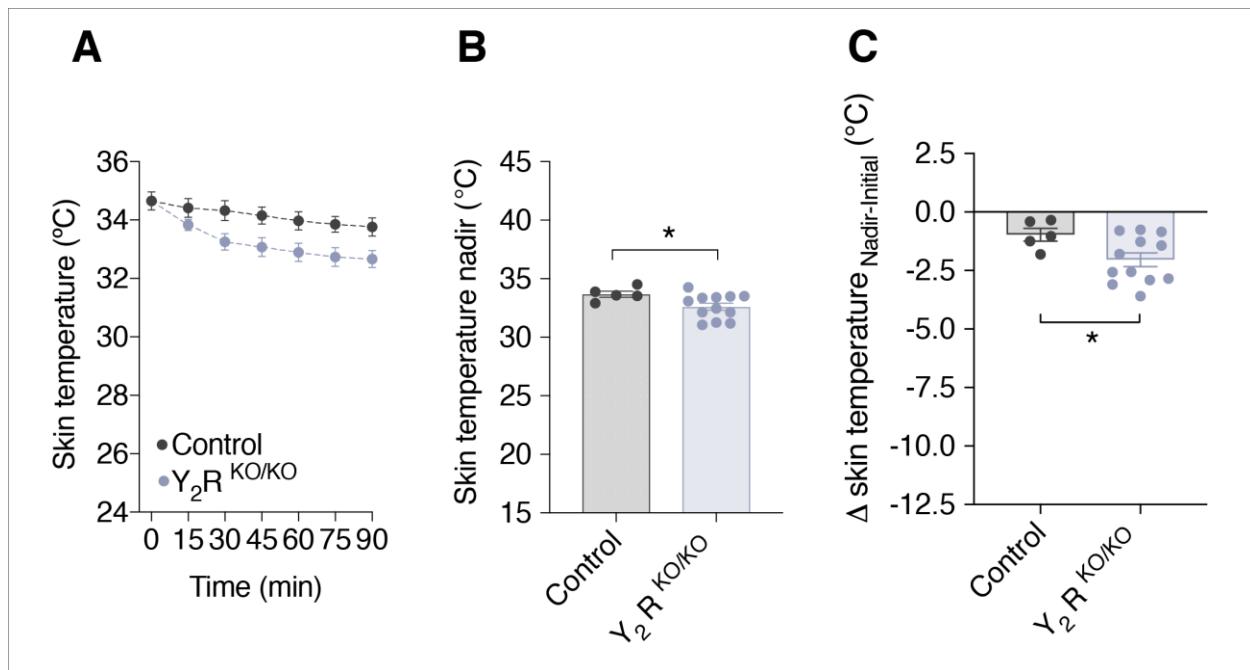
Figure 15. *Y₂Rᴷᴼ* **P10-P11 mice rapidly decreases skin temperature upon isolation**. **A** Skin temperature measurements in 15-min bins, control (n = 5), Y_2R^{KO} (n = 12). **B** Skin temperature nadir (minimum skin temperature measurements detected), control (n = 5), Y_2R^{KO} (n = 12). **C** Delta skin temperature calculated by the difference between skin temperature nadir and initial skin temperature, control (n = 5), Y_2R^{KO} (n = 12). In **A**, lines represent mean ± SEM. In **B-C,** bar plots show mean ± SEM. * represents $p < 0.05$; ** represents $p < 0.01$; *** represents $p < 0.001$. **** represents $p < 0.0001$.

Finally, we also assessed skin temperature dynamics in P10-P11 Y_4R^{KO} mice. Upon isolation, skin temperature dropped similarly in both groups (interaction: $F_{6,160}$ = 0.075, p = 0.99; time: $F_{6,160}$ = 3.21, p = 0.0053; genotype: $F_{1,160}$ = 0.35, p = 0.55, two-way ANOVA followed by Bonferroni's multiple comparison, **Figure 16A**). Furthermore, Y_4R^{KO} and control mice did not show any significant difference in skin temperature nadir (control: 33.33 ± 0.33 °C, n = 12; Y_4R^{KO}: 33.15 ± 0.43 °C, n = 13 [Mean ± SEM], t = 0.33; df = 22.03; p = 0.75, two-tailed Welch's T-test, **Figure 16B**). Also, we detected no differences between groups in the delta skin temperature (control: - 1.52 ± 1.07 °C, n = 12; Y_4R^{KO}: - 1.64 ± 1.26 °C, n = 13; t = 0.25; df = 22.85; p = 0.80, two-tailed Welch's T-test, **Figure 16C**). Taken together, these results indicate that neuropeptide Y₄R does not affect thermoregulation in neonatal mice.
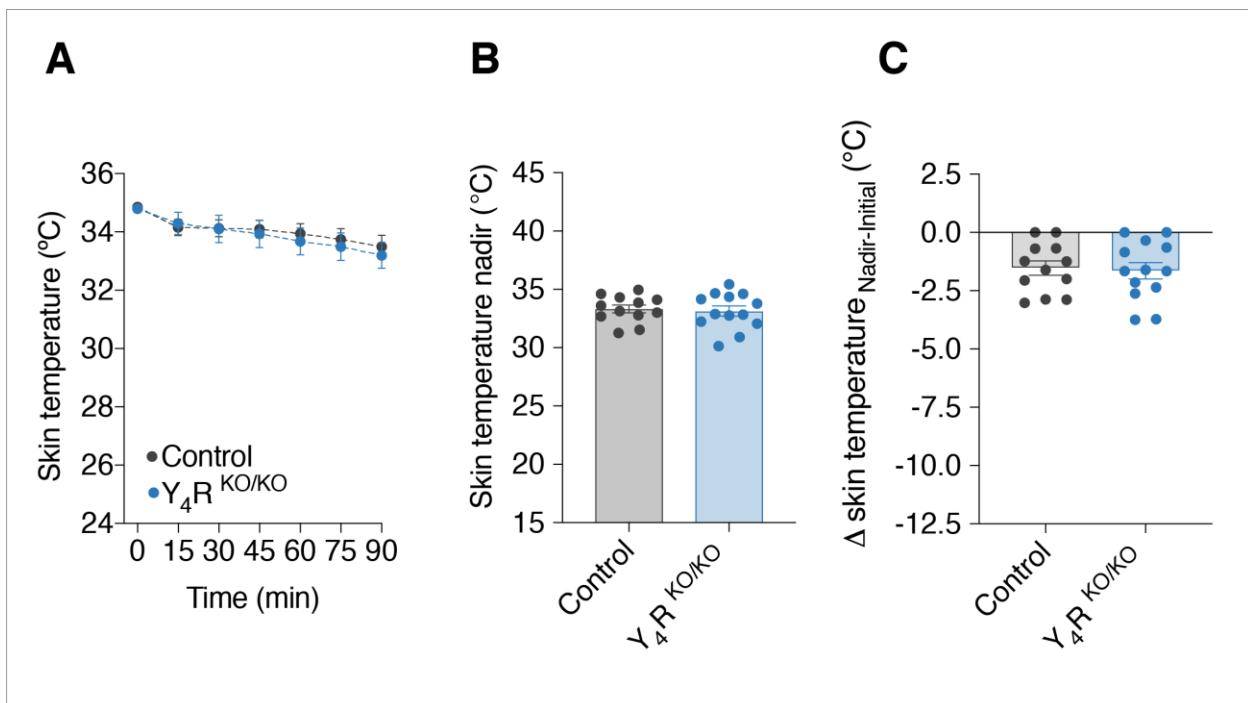
Figure 16. *Y_4R^{KO}* **P10 mice do not have altered skin temperature dynamics and characteristics**. **A** Skin temperature measurements in 15-min bins, control (n = 12), *Y_4R^{KO}* (n = 13). **B** Skin temperature nadir (minimum skin temperature measurements detected), control (n = 12), *Y_4R^{KO}* (n = 13). **C** Delta skin temperature calculated by the difference between skin temperature nadir and initial skin temperature, control (n = 12), *Y_4R^{KO}* (n = 13). In **A**, lines represent mean $\pm$ SEM. In **B-C** bar plots show mean $\pm$ SEM. * represents $p < 0.05$; ** represents $p < 0.01$; *** represents $p < 0.001$. **** represents $p < 0.0001$.

4.8 Y_1R possibly mediates the reduction in skin temperature upon exogenous ghrelin injections

Ghrelin injections reduced the skin temperature of neonatal mice (**Figure 13B**). Also, we previously found that Y_1R and Y_2R seem to be important for thermoregulation in P10 mice. To further elucidate which Y receptor is involved in reducing skin temperature upon ghrelin signaling, we injected either saline or ghrelin (1 mg/kg) in P10-P11 mice (**Figure 17A**) lacking Y_1R and Y_2R (**Figure 17B**).
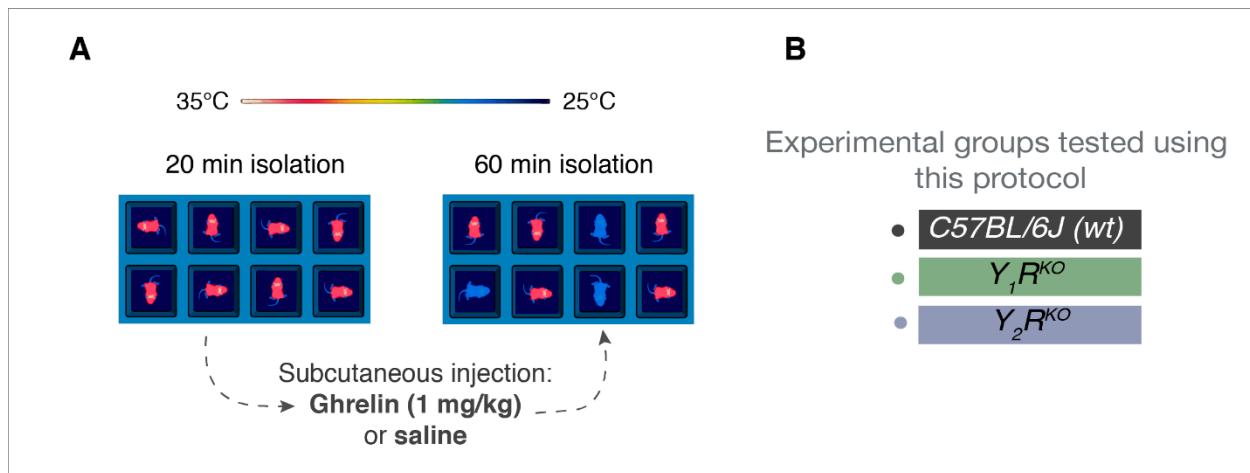
Figure 17. Experimental design used to assess the role of different Y receptors in thermoregulation. **A** Experimental setup utilized for these experiments. **B** Experimental groups tested.

For this experiment, we first isolated the pups for twenty minutes. Next, mice were either injected subcutaneously with 1 mg/kg ghrelin or saline and the skin temperature of the pups was measured for one hour. We found that C57BL/6J mice injected with ghrelin reduced skin temperature compared to the animals injected with saline, an effect that was not seen for the other groups (interaction: $F_{45,1575} = 24.23$, $p < 0.0001$; time: $F_{1.540,161.7} = 12.88$, $p < 0.0001$; group: $F_{3,105} = 23.05$, $p < 0.0001$, two-way ANOVA with repeated measures followed by Bonferroni's multiple comparison test, **Figure 18A**; $F_{45,1170} = 10.64$, $p < 0.0001$; time: $F_{1.281,99.90} = 24.37$, $p < 0.0001$; group: $F_{3,78} = 6.836$, $p = 0.0004$, two-way ANOVA with repeated measures followed by Bonferroni's multiple comparison test, **Figure 18B**). Also, pups lacking Y_1R did not reduce the skin temperature upon ghrelin injection (C57BL/6J - saline = 31 animals; C57BL/6J - ghrelin: = 30; U = 10.5; p < 0.0001, Mann-Whitney U test; Y_1R^{KO} - saline = 25 animals; Y_1R^{KO} - ghrelin = 25; U = 243; p = 0.181, Mann-Whitney U test; Y_2R^{KO} - saline = 11 animals; Y_2R^{KO} - ghrelin = 12 animals; U = 30; p = 0.0270, Mann-Whitney U test; Multiple Mann-Whitney U test, **Figure 18C**). Calculating delta skin temperature, only pups lacking Y_1R injected with ghrelin did not exhibit a decrease in skin temperature when compared to pups injected with saline (C57BL/6J - saline = 31 animals; C57BL/6J - ghrelin: = 30; U = 118; p < 0.0001, Mann-Whitney U test; Y_1R^{KO} - saline = 25 animals; Y_1R^{KO} - ghrelin = 25; U = 251; p = 0.2369, Mann-Whitney U test; Y_2R^{KO} - saline = 11 animals; Y_2R^{KO} - ghrelin = 12 animals; U = 23; p = 0.0070, Mann-Whitney U test;, **Figure 18D**). Altogether, these results possibly

suggest that Y_1R modulates the reduction of the skin temperature in P10-P11 mice, followed by ghrelin treatment.
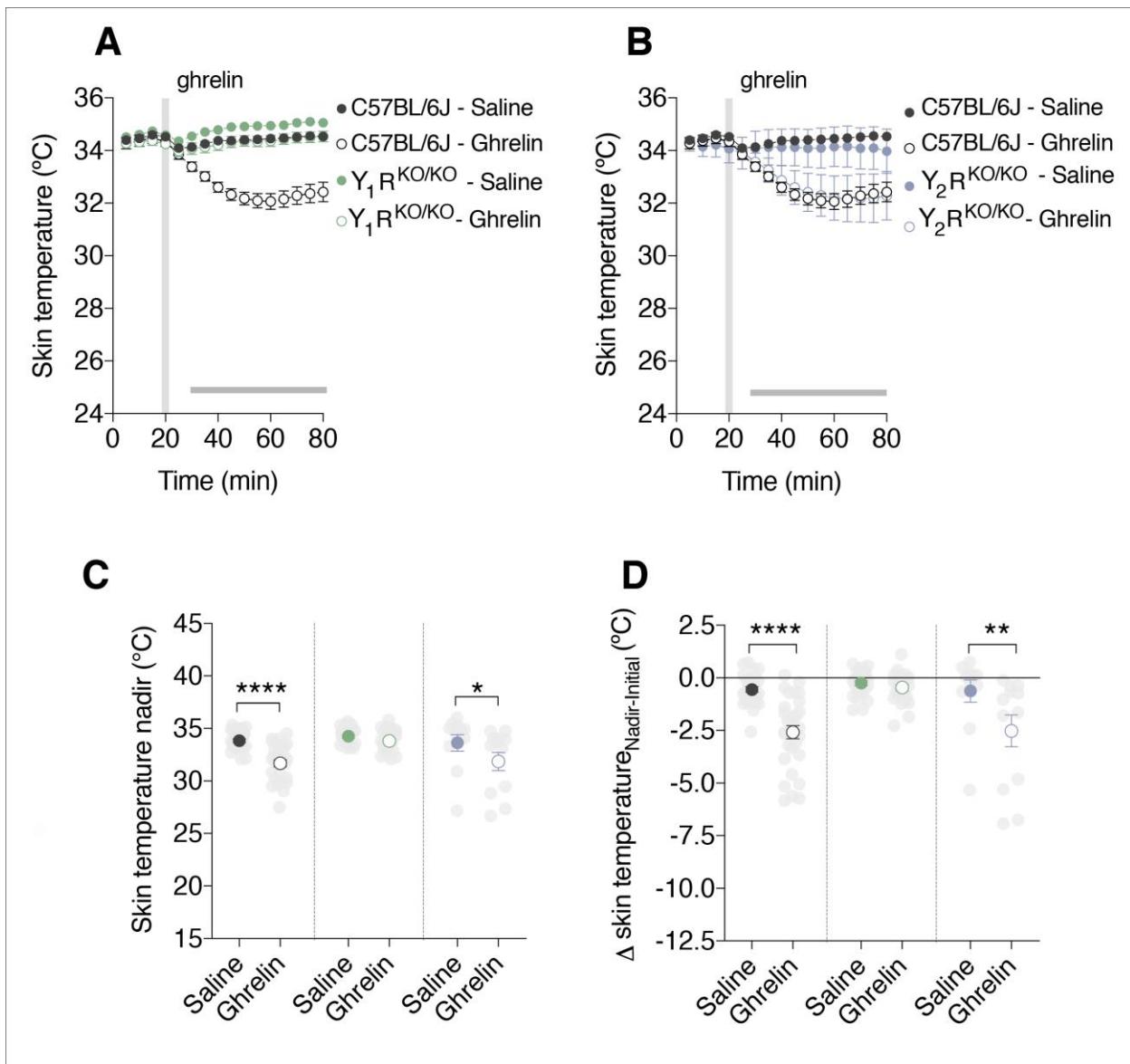
Figure 18. Y₁R possibly mediates the decrease in skin temperature upon exogenous ghrelin injections in neonatal mice. A Skin temperature measurements (baseline, 20 min) and after saline or ghrelin injections in 5-min bins in C57BL/6J, Y_1R^{KO} and Y_2R^{KO} pups; C57BL/6J - saline (n = 31), C57BL/6J - ghrelin (n = 30), Y_1R^{KO} - saline (n = 25), Y_1R^{KO} - ghrelin (n = 25), Y_2R^{KO} - saline (n = 11), Y_2R^{KO} - ghrelin (n = 12). **B** Skin temperature nadir (minimum skin temperature points detected); C57BL/6J - saline (n = 31), C57BL/6J - ghrelin (n = 30), Y_1R^{KO} - saline (n = 25), Y_1R^{KO} - ghrelin (n = 25), Y_2R^{KO} - saline (n = 11), Y_2R^{KO} - ghrelin (n = 12). **C** Delta skin temperature calculated by the difference between skin temperature nadir and initial skin temperature; C57BL/6J - saline (n = 31), C57BL/6J - ghrelin (n = 30), Y_1R^{KO} - saline (n = 25), Y₁R^{KO} - ghrelin (n = 25), Y_2R^{KO} - saline (n = 11), Y_2R^{KO} - ghrelin (n = 12). In **A-B**, lines represent mean ± SEM, horizontal grey bar represents time points in which p < 0.05. In **C-D** symbols show the mean ± SEM, grey points show the data point distribution. * represents p < 0.05; ** represents p < 0.01; *** represents p < 0.001. **** represents p < 0.0001.

PART III

In this part, discussion, conclusion and future perspectives will be described.

5. DISCUSSION

The results reported in this dissertation demonstrated the role of the Agrp neurons in the thermoregulation during early postnatal development in mice.

In our initial experiments, we found that isolating P10 mice from the nursing nest at room temperature increased Agrp neuron activation. Using fiber photometry, we found that Agrp neurons present rapid dynamics upon changes in floor temperature. Agrp neuronal activity increased when animals were exposed to ≈20°C and decreased upon exposure to ≈35°C. These rapid dynamics in Agrp neuronal activity suggest that thermosensorial signals modulate Agrp neuronal activity in young mice.

In our studies, we found that Agrp neuronal overactivation rapidly led to a reduction in skin temperature in P10 mice. A reduction in skin temperature suggests a suppression of BAT thermogenesis. In support of this idea, chemogenetic activation of Agrp neurons also reduces BAT temperature and energy expenditure in adult mice (Burke et al., 2017; Ruan et al., 2014; Steculorum et al., 2016). Importantly, because neonatal rodents survive hypothermia for a longer period than adults (Leon, 1986), active suppression of thermogenesis resulting in lower body temperature may be an advantageous strategy for the survival of neonatal mice. In future studies, it would be important to test loss-of-function experiments. Based on our findings, we hypothesize that Agrp neuronal loss-of-function would increase thermogenesis in neonates.

Furthermore, we also observed that *Agrp*^{VgatKO} pups decreased skin temperature upon Agrp chemogenetic activation, suggesting that GABA released by Agrp neurons does not modulate thermoregulation in mouse pups. In contrast, we found that P10 mice lacking NPY did not decrease skin temperature upon Agrp activation. NPY is known to be involved in the control of BAT thermogenesis in adult mice (Felies et al., 2004; Szreder et al., 1994). ICV injections of NPY reduced BAT thermogenesis whereas knockdown of NPY expression increased thermogenic activity (Chao et al., 2011; Egawa et al., 1991). Our findings suggest that NPY is already involved in the control of BAT thermogenesis and skin temperature in neonatal mice. However, in our studies, we utilized a whole-body knockout model for NPY, and we could not identify whether NPY is released specifically by the Agrp neurons. It is possible the effects seen in our studies are mediated by NPY released from non-Agrp ARC neurons or other brain areas. For instance, during

development in rats NPY is already found in the dorsomedial hypothalamus (DMH), paraventricular nucleus of the hypothalamus (PVH), lateral hypothalamus (LH) and perifornical area (Singer et al., 2000). Thus, we cannot rule out the possibility that other brain regions could be modulating the suppression in BAT thermogenesis in response to Agrp neuron activation in P10 mice. Future experiments employing specific deletion of NPY only in the ARC need to be performed.

In mice, NPY binds to different Y receptors to mediate its actions. Evaluating the role of the different Y in receptors in thermoregulation, our studies showed that neonatal mice lacking Y_1R presented higher skin temperature and possibly higher thermogenic activity compared to control littermates. In line with our results, it was shown in rodents that inhibition of Y_1R knock-down (downregulation of its gene) generates hyperthermia in rodents (Dark and Pelz, 2008; Lopez-Valpuesta et al., 1996; Pelz and Dark, 2007). Consistent with the idea that Y_1R can affect thermogenesis, Shi et al. demonstrated that NPY derived from ARC is critical for the control of sympathetic outflow and BAT function (Shi et al., 2013). These actions exerted by NPY are Y_1R-dependent. NPY released by ARC binds to PVN Y_1Rs in tyrosine-hydroxylase-expressing neurons, resulting in a functional inhibition of BAT thermogenesis (Shi et al., 2013). It is possible that this pathway is involved to reduce BAT thermogenesis in neonatal mice. Although this mechanism seems to be Y_1R-dependent, experiments assessing the role of other Y receptors such as the Y_5R in thermoregulation should be also addressed. Y_1R and Y_5R are commonly co-expressed in the same neurons and both are important for several metabolic functions. The understanding of the importance of the different Y receptors in thermoregulation will provide further comprehension of the downstream targets of Agrp neurons involved in thermoregulation.

Furthermore, we found that pups lacking Y_2R rapidly decreased skin temperature, suggesting that Y_2R may also affect thermoregulation in neonatal mice. Warm-sensing neurons in preoptic area (POA) express Y_2Rs and G protein-coupled receptor 83 (GPR83) an orphan receptor that shares similarities with Y_2R (Bartfai and Conti, 2012). Downregulation of the expression of this orphan receptor in POA by shRNAs reduces core temperature (Dubins et al., 2012). Interestingly, since there are similarities between the Y_2R and GPR83, it is possible that downregulation of Y_2R may lead to the same

effects. Overall, we found that Y_2R in P10 mice seems to be important for animals to maintain body temperature. Future experiments are necessary to investigate the proper contribution of this receptor in thermoregulation during development.

Finally, we demonstrated that ghrelin can decrease skin temperature in P10 mice. We further found that P10 mice lacking Y_1R did not decrease skin temperature upon exogenous ghrelin injections. These results support our previous findings that suggested that Y_1R is important for the control of skin temperature and BAT thermogenesis in neonatal mice. Previous studies have shown that P10 mice already express GhSR in the ARC and exogenous ghrelin injections activate Agrp neurons in mice at these ages (Steculorum et al., 2015). Altogether, our findings indicate that ghrelin is already functional at early age and plays a role in thermogenesis presumably via Agrp neuronal activation (Steculorum et al., 2015).

6. CONCLUSION

In this dissertation, we found that Agrp neurons modulate thermoregulation in mice during early postnatal development (**Figure 19**). Upon activation, Agrp neurons reduce skin temperature via NPY signaling. Ghrelin, a stomach-derived hormone that activates Agrp neurons, also reduced skin temperature, an effect that may be dependent on Y_1R signaling.
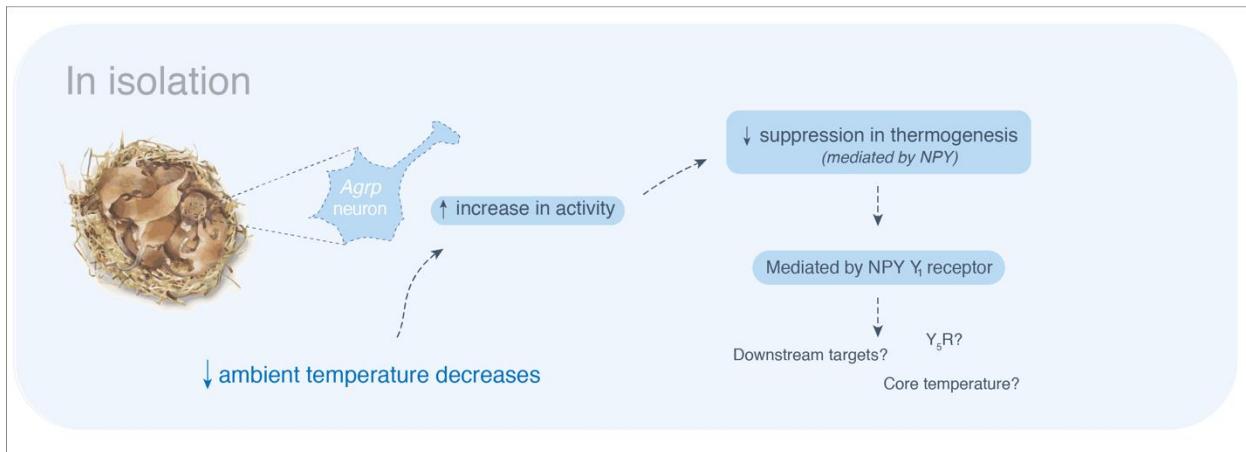
Figure 19. Isolation from dam and siblings activates the Agrp neurons and upon activation, Agrp neurons can suppress thermogenesis via NPY and Y_1 receptor.

7. FUTURE PERSPECTIVES

In future experiments, we would explore the following lines of inquiry:

- perform loss-of-function models to better comprehend additional details of the action of the Agrp neurons in thermoregulation;

- characterize the dynamics of the Agrp neurons changing floor temperature from 35 to $\approx 20°C$;

- characterize the thermoregulatory behavior of neonatal Y_5R^{KO};

- understand which Agrp neuronal downstream targets modulate the reduction of skin temperature;

- evaluate whether Agrp neurons also promote a decrease in core body temperature implanting a temperature transponder in the peritoneal region in neonatal mice and correlate with skin temperature.

REFERENCES

Andrews, Z.B., Liu, Z.W., Walllingford, N., Erion, D.M., Borok, E., Friedman, J.M., Tschop, M.H., Shanabrough, M., Cline, G., Shulman, G.I._, et al._ (2008). UCP2 mediates ghrelin's action on NPY/AgRP neurons by lowering free radicals. Nature _454_, 846-851.

Aponte, Y., Atasoy, D., and Sternson, S.M. (2011). AGRP neurons are sufficient to orchestrate feeding behavior rapidly and without training. Nat Neurosci _14_, 351-355.

Arenkiel, B.R., Klein, M.E., Davison, I.G., Katz, L.C., and Ehlers, M.D. (2008). Genetic control of neuronal activity in mice conditionally expressing TRPV1. Nat Methods _5_, 299-302.

Armbruster, B.N., Li, X., Pausch, M.H., Herlitze, S., and Roth, B.L. (2007). Evolving the lock to fit the key to create a family of G protein-coupled receptors potently activated by an inert ligand. Proc Natl Acad Sci U S A _104_, 5163-5168.

Barros, V.N., Mundim, M., Galindo, L.T., Bittencourt, S., Porcionatto, M., and Mello, L.E. (2015). The pattern of c-Fos expression and its refractory period in the brain of rats and monkeys. Front Cell Neurosci _9_, 72.

Bartfai, T., and Conti, B. (2012). Molecules affecting hypothalamic control of core body temperature in response to calorie intake. Front Genet _3_, 184.

Blumberg, M.S., and Alberts, J.R. (1990). Ultrasonic vocalizations by rat pups in the cold: an acoustic by-product of laryngeal braking? Behav Neurosci _104_, 808-817.

Blumberg, M.S., Efimova, I.V., and Alberts, J.R. (1992). Ultrasonic vocalizations by rat pups: the primary importance of ambient temperature and the thermal significance of contact comfort. Dev Psychobiol _25_, 229-250.

Burke, L.K., Darwish, T., Cavanaugh, A.R., Virtue, S., Roth, E., Morro, J., Liu, S.M., Xia, J., Dalley, J.W., Burling, K._, et al._ (2017). mTORC1 in AGRP neurons integrates exteroceptive and interoceptive food-related cues in the modulation of adaptive energy expenditure in mice. Elife _6_.

Cannon, B., and Nedergaard, J. (2004). Brown adipose tissue: function and physiological significance. Physiol Rev _84_, 277-359.

Cansell, C., Denis, R.G., Joly-Amado, A., Castel, J., and Luquet, S. (2012). Arcuate AgRP neurons and the regulation of energy balance. Front Endocrinol (Lausanne) _3_, 169.

Caterina, M.J., Schumacher, M.A., Tominaga, M., Rosen, T.A., Levine, J.D., and Julius, D. (1997). The capsaicin receptor: a heat-activated ion channel in the pain pathway. Nature _389_, 816-824.

Cavalcanti-de-Albuquerque, J.P., Bober, J., Zimmer, M.R., and Dietrich, M.O. (2019). Regulation of substrate utilization and adiposity by Agrp neurons. Nat Commun *10*, 311.

Chao, P.-T., Yang, L., Aja, S., Moran, Timothy H., and Bi, S. (2011). Knockdown of NPY Expression in the Dorsomedial Hypothalamus Promotes Development of Brown Adipocytes and Prevents Diet-Induced Obesity. Cell Metabolism *13*, 573-583.

Chen, S.-R., Chen, H., Zhou, J.-J., Pradhan, G., Sun, Y., Pan, H.-L., and Li, D.-P. (2017). Ghrelin receptors mediate ghrelin-induced excitation of agouti-related protein/neuropeptide Y but not pro-opiomelanocortin neurons. Journal of Neurochemistry *142*, 512-520.

Clark, J.T., Kalra, P.S., Crowley, W.R., and Kalra, S.P. (1984). Neuropeptide Y and human pancreatic polypeptide stimulate feeding behavior in rats. Endocrinology *115*, 427-429.

Cone, R.D. (2005). Anatomy and regulation of the central melanocortin system. Nat Neurosci *8*, 571-578.

Conklin, B.R., Hsiao, E.C., Claeysen, S., Dumuis, A., Srinivasan, S., Forsayeth, J.R., Guettier, J.M., Chang, W.C., Pei, Y., McCarthy, K.D.*, et al.* (2008). Engineering GPCR signaling pathways with RASSLs. Nat Methods *5*, 673-678.

Cowley, M.A., Smith, R.G., Diano, S., Tschop, M., Pronchuk, N., Grove, K.L., Strasburger, C.J., Bidlingmaier, M., Esterman, M., Heiman, M.L.*, et al.* (2003). The distribution and mechanism of action of ghrelin in the CNS demonstrates a novel hypothalamic circuit regulating energy homeostasis. Neuron *37*, 649-661.

Dana, H., Sun, Y., Mohar, B., Hulse, B., Hasseman, J.P., Tsegaye, G., Tsang, A., Wong, A., Patel, R., Macklin, J.J.*, et al.* (2018). High-performance GFP-based calcium indicators for imaging activity in neuronal populations and microcompartments. bioRxiv, 434589.

Dark, J., and Pelz, K.M. (2008). NPY Y1 receptor antagonist prevents NPY-induced torpor-like hypothermia in cold-acclimated Siberian hamsters. Am J Physiol Regul Integr Comp Physiol *294*, R236-245.

Date, Y., Kojima, M., Hosoda, H., Sawaguchi, A., Mondal, M.S., Suganuma, T., Matsukura, S., Kangawa, K., and Nakazato, M. (2000). Ghrelin, a novel growth hormone-releasing acylated peptide, is synthesized in a distinct endocrine cell type in the gastrointestinal tracts of rats and humans. Endocrinology *141*, 4255-4261.

Dietrich, M.O., Zimmer, M.R., Bober, J., and Horvath, T.L. (2015). Hypothalamic Agrp neurons drive stereotypic behaviors beyond feeding. Cell *160*, 1222-1232.

Dubins, J.S., Sanchez-Alavez, M., Zhukov, V., Sanchez-Gonzalez, A., Moroncini, G., Carvajal-Gonzalez, S., Hadcock, J.R., Bartfai, T., and Conti, B. (2012). Downregulation

of GPR83 in the hypothalamic preoptic area reduces core body temperature and elevates circulating levels of adiponectin. Metabolism *61*, 1486-1493.

Egawa, M., Yoshimatsu, H., and Bray, G.A. (1991). Neuropeptide Y suppresses sympathetic activity to interscapular brown adipose tissue in rats. Am J Physiol *260*, R328-334.

Felies, M., von Horsten, S., Pabst, R., and Nave, H. (2004). Neuropeptide Y stabilizes body temperature and prevents hypotension in endotoxaemic rats. J Physiol *561*, 245-252.

Gilbert, C., McCafferty, D., Le Maho, Y., Martrette, J.M., Giroud, S., Blanc, S., and Ancel, A. (2010). One for all and all for one: the energetic benefits of huddling in endotherms. Biol Rev Camb Philos Soc *85*, 545-569.

Gropp, E., Shanabrough, M., Borok, E., Xu, A.W., Janoschek, R., Buch, T., Plum, L., Balthasar, N., Hampel, B., Waisman, A.*, et al.* (2005). Agouti-related peptide-expressing neurons are mandatory for feeding. Nat Neurosci *8*, 1289-1291.

Guler, A.D., Rainwater, A., Parker, J.G., Jones, G.L., Argilli, E., Arenkiel, B.R., Ehlers, M.D., Bonci, A., Zweifel, L.S., and Palmiter, R.D. (2012). Transient activation of specific neurons in mice by selective expression of the capsaicin receptor. Nat Commun *3*, 746.

Hahn, T.M., Breininger, J.F., Baskin, D.G., and Schwartz, M.W. (1998). Coexpression of Agrp and NPY in fasting-activated hypothalamic neurons. Nat Neurosci *1*, 271-272.

Hayashida, T., Nakahara, K., Mondal, M.S., Date, Y., Nakazato, M., Kojima, M., Kangawa, K., and Murakami, N. (2002). Ghrelin in neonatal rats: distribution in stomach and its possible role. J Endocrinol *173*, 239-245.

Horvath, T.L., Bechmann, I., Naftolin, F., Kalra, S.P., and Leranth, C. (1997). Heterogeneity in the neuropeptide Y-containing neurons of the rat arcuate nucleus: GABAergic and non-GABAergic subpopulations. Brain Res *756*, 283-286.

Joly-Amado, A., Denis, R.G., Castel, J., Lacombe, A., Cansell, C., Rouch, C., Kassis, N., Dairou, J., Cani, P.D., Ventura-Clapier, R.*, et al.* (2012). Hypothalamic AgRP-neurons control peripheral substrate utilization and nutrient partitioning. EMBO J *31*, 4276-4288.

Kamegai, J., Tamura, H., Shimizu, T., Ishii, S., Sugihara, H., and Wakabayashi, I. (2001). Chronic central infusion of ghrelin increases hypothalamic neuropeptide Y and Agouti-related protein mRNA levels and body weight in rats. Diabetes *50*, 2438-2443.

Kassis, S., Olasmaa, M., Terenius, L., and Fishman, P.H. (1987). Neuropeptide Y inhibits cardiac adenylate cyclase through a pertussis toxin-sensitive G protein. J Biol Chem *262*, 3429-3431.

Kawate, R., Talan, M.I., and Engel, B.T. (1994). Sympathetic nervous activity to brown adipose tissue increases in cold-tolerant mice. Physiol Behav *55*, 921-925.

Krashes, M.J., Koda, S., Ye, C., Rogan, S.C., Adams, A.C., Cusher, D.S., Maratos-Flier, E., Roth, B.L., and Lowell, B.B. (2011). Rapid, reversible activation of AgRP neurons drives feeding behavior in mice. J Clin Invest *121*, 1424-1428.

Krashes, M.J., Shah, B.P., Koda, S., and Lowell, B.B. (2013). Rapid versus delayed stimulation of feeding by the endogenously released AgRP neuron mediators GABA, NPY, and AgRP. Cell Metab *18*, 588-595.

Lagerspetz, K.Y.H. (1966). Postnatal development of thermoregulation in laboratory mice. Helgoländer wissenschaftliche Meeresuntersuchungen *14*, 559-571.

Larsen, P.J., Tang-Christensen, M., Stidsen, C.E., Madsen, K., Smith, M.S., and Cameron, J.L. (1999). Activation of central neuropeptide Y Y1 receptors potently stimulates food intake in male rhesus monkeys. J Clin Endocrinol Metab *84*, 3781-3791.]

Leon, M. (1986). Development of thermoregulation, Vol 8 (Boston, MA: Springer).

Leon, M., Croskerry, P.G., and Smith, G.K. (1978). Thermal control of mother-young contact in rats. Physiol Behav *21*, 79O-811.

Lin, S., Boey, D., and Herzog, H. (2004). NPY and Y receptors: lessons from transgenic and knockout models. Neuropeptides *38*, 189-200.

Loh, K., Herzog, H., and Shi, Y.C. (2015). Regulation of energy homeostasis by the NPY system. Trends Endocrinol Metab *26*, 125-135.

Lopez-Valpuesta, F.J., Nyce, J.W., and Myers, R.D. (1996). NPY-Y1 receptor antisense injected centrally in rats causes hyperthermia and feeding. Neuroreport *7*, 2781-2784.

Luquet, S., Perez, F.A., Hnasko, T.S., and Palmiter, R.D. (2005). NPY/AgRP neurons are essential for feeding in adult mice but can be ablated in neonates. Science *310*, 683-685.

Meyer, C.W., Ootsuka, Y., and Romanovsky, A.A. (2017). Body Temperature Measurements for Metabolic Phenotyping in Mice. Front Physiol *8*, 520.

Meywirth, A., Redlin, U., Steinlechner, S., Heldmaier, G., and Reiter, R.J. (1991). Role of the sympathetic innervation in the cold-induced activation of 5'-deiodinase in brown adipose tissue of the Djungarian hamster. Can J Physiol Pharmacol *69*, 1896-1900.

Miner, J.L., Della-Fera, M.A., Paterson, J.A., and Baile, C.A. (1989). Lateral cerebroventricular injection of neuropeptide Y stimulates feeding in sheep. Am J Physiol *257*, R383-387.

Mizuno, T.M., and Mobbs, C.V. (1999). Hypothalamic agouti-related protein messenger ribonucleic acid is inhibited by leptin and stimulated by fasting. Endocrinology *140*, 814-817.

Morgan, J.I., and Curran, T. (1989). Stimulus-transcription coupling in neurons: role of cellular immediate-early genes. Trends Neurosci *12*, 459-462.

Morton, G.J., and Schwartz, M.W. (2001). The NPY/AgRP neuron and energy homeostasis. Int J Obes Relat Metab Disord *25 Suppl 5*, S56-62.

Nakazato, M., Murakami, N., Date, Y., Kojima, M., Matsuo, H., Kangawa, K., and Matsukura, S. (2001). A role for ghrelin in the central regulation of feeding. Nature *409*, 194-198.

Nedergaard, J., and Cannon, B. (2018). Brown adipose tissue as a heat-producing thermoeffector. Handb Clin Neurol *156*, 137-152.

Pelz, K.M., and Dark, J. (2007). ICV NPY Y1 receptor agonist but not Y5 agonist induces torpor-like hypothermia in cold-acclimated Siberian hamsters. Am J Physiol Regul Integr Comp Physiol *292*, R2299-2311.

Rinne, U.K. (1966). Ultrastructure of the median eminence of the rat. Z Zellforsch Mikrosk Anat *74*, 98-122.

Romanovsky, A.A. (2018). The thermoregulation system and how it works. Handb Clin Neurol *156*, 3-43.

Rossi, M., Kim, M.S., Morgan, D.G., Small, C.J., Edwards, C.M., Sunter, D., Abusnana, S., Goldstone, A.P., Russell, S.H., Stanley, S.A.*, et al.* (1998). A C-terminal fragment of Agouti-related protein increases feeding and antagonizes the effect of alpha-melanocyte stimulating hormone in vivo. Endocrinology *139*, 4428-4431.

Roth, B.L. (2016). DREADDs for Neuroscientists. Neuron *89*, 683-694.

Ruan, H.B., Dietrich, M.O., Liu, Z.W., Zimmer, M.R., Li, M.D., Singh, J.P., Zhang, K., Yin, R., Wu, J., Horvath, T.L.*, et al.* (2014). O-GlcNAc transferase enables AgRP neurons to suppress browning of white fat. Cell *159*, 306-317.

Sanz, E., Yang, L., Su, T., Morris, D.R., McKnight, G.S., and Amieux, P.S. (2009). Cell-type-specific isolation of ribosome-associated mRNA from complex tissues. Proc Natl Acad Sci U S A *106*, 13939-13944.

Sheng, M., and Greenberg, M.E. (1990). The regulation and function of c-fos and other immediate early genes in the nervous system. Neuron *4*, 477-485.

Shi, Y.C., Lau, J., Lin, Z., Zhang, H., Zhai, L., Sperk, G., Heilbronn, R., Mietzsch, M., Weger, S., Huang, X.F.*, et al.* (2013). Arcuate NPY controls sympathetic output and BAT function via a relay of tyrosine hydroxylase neurons in the PVN. Cell Metab *17*, 236-248.

Singer, L.K., Kuper, J., Brogan, R.S., Smith, M.S., and Grove, K.L. (2000). Novel expression of hypothalamic neuropeptide Y during postnatal development in the rat. Neuroreport *11*, 1075-1080.

Sobrino Crespo, C., Perianes Cachero, A., Puebla Jimenez, L., Barrios, V., and Arilla Ferreiro, E. (2014). Peptides and food intake. Front Endocrinol (Lausanne) *5*, 58.

Song, A.J., and Palmiter, R.D. (2018). Detecting and Avoiding Problems When Using the Cre–lox System. Trends in Genetics *34*, 333-340.

Stanley, B.G., Kyrkouli, S.E., Lampert, S., and Leibowitz, S.F. (1986). Neuropeptide Y chronically injected into the hypothalamus: a powerful neurochemical inducer of hyperphagia and obesity. Peptides *7*, 1189-1192.

Steculorum, S.M., Collden, G., Coupe, B., Croizier, S., Lockie, S., Andrews, Z.B., Jarosch, F., Klussmann, S., and Bouret, S.G. (2015). Neonatal ghrelin programs development of hypothalamic feeding circuits. J Clin Invest *125*, 846-858.

Steculorum, S.M., Ruud, J., Karakasilioti, I., Backes, H., Engstrom Ruud, L., Timper, K., Hess, M.E., Tsaousidou, E., Mauer, J., Vogt, M.C.*, et al.* (2016). AgRP Neurons Control Systemic Insulin Sensitivity via Myostatin Expression in Brown Adipose Tissue. Cell *165*, 125-138.

Szreder, Z.a., Hori, T., and Kaizuka, Y. (1994). Thermoregulatory effect of intracerebral injections of neuropeptide Y in rats at different environmental temperatures. General Pharmacology: The Vascular System *25*, 85-91.

Tan, C.L., and Knight, Z.A. (2018). Regulation of Body Temperature by the Nervous System. Neuron *98*, 31-48.

Tong, Q., Ye, C.P., Jones, J.E., Elmquist, J.K., and Lowell, B.B. (2008). Synaptic release of GABA by AgRP neurons is required for normal regulation of energy balance. Nat Neurosci *11*, 998-1000.

Tschop, M., Smiley, D.L., and Heiman, M.L. (2000). Ghrelin induces adiposity in rodents. Nature *407*, 908-913.

Urban, D.J., and Roth, B.L. (2015). DREADDs (Designer Receptors Exclusively Activated by Designer Drugs): Chemogenetic Tools with Therapeutic Utility. Annual Review of Pharmacology and Toxicology *55*, 399-417.

Vinter, J., Hull, D., and Elphick, M.C. (1982). Onset of thermogenesis in response to cold in newborn mice. Biol Neonate *42*, 145-151.

Wang, Q., Liu, C., Uchida, A., Chuang, J.-C., Walker, A., Liu, T., Osborne-Lawrence, S., Mason, B.L., Mosher, C., Berglund, E.D.*, et al.* (2014). Arcuate AgRP neurons mediate orexigenic and glucoregulatory actions of ghrelin. Molecular Metabolism *3*, 64-72.

Wren, A.M., Small, C.J., Abbott, C.R., Dhillo, W.S., Seal, L.J., Cohen, M.A., Batterham, R.L., Taheri, S., Stanley, S.A., Ghatei, M.A.*, et al.* (2001). Ghrelin causes hyperphagia and obesity in rats. Diabetes *50*, 2540-2547.

Wu, Q., Boyle, M.P., and Palmiter, R.D. (2009). Loss of GABAergic signaling by AgRP neurons to the parabrachial nucleus leads to starvation. Cell *137*, 1225-1234.

Yasuda, T., Masaki, T., Kakuma, T., and Yoshimatsu, H. (2004). Hypothalamic melanocortin system regulates sympathetic nerve activity in brown adipose tissue. Exp Biol Med (Maywood) *229*, 235-239.

Zimmer, M.R., Fonseca, A.H.O., Iyilikci, O., Pra, R.D., and Dietrich, M.O. (2019). Functional Ontogeny of Hypothalamic Agrp Neurons in Neonatal Mouse Behaviors. Cell.

ANNEXES

Here I will present the article that I co-authored that is not part of the main body of this dissertation.

Annex 1.

Functional ontogeny of hypothalamic Agrp neurons in neonatal mouse behaviors.
Article published on *Cell.*

Cell

Functional Ontogeny of Hypothalamic Agrp Neurons in Neonatal Mouse Behaviors

Graphical Abstract

Highlights

- Isolation from the nest activates Agrp neurons in neonatal mice

- Care and warmth, but not milk, blunts activation of Agrp neurons

- Neonatal Agrp neurons modulate isolation-induced ultrasonic vocalizations

- Agrp neurons increase milk ingestion in 15- but not in 10-day-old mice
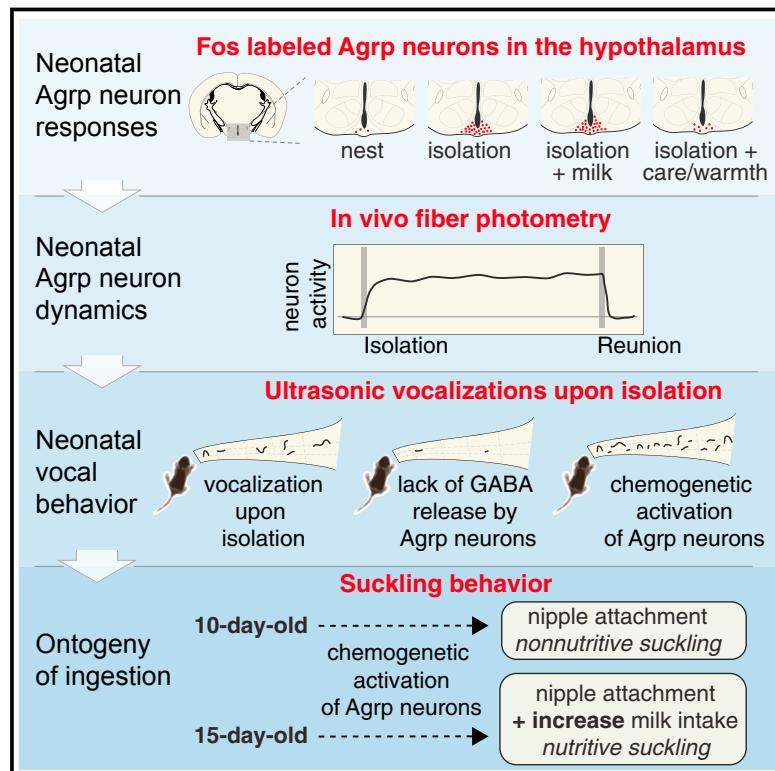
Authors

Marcelo R. Zimmer,
Antonio H.O. Fonseca, Onur Iyilikci,
Rafael Dai Pra, Marcelo O. Dietrich

Correspondence

marcelo.dietrich@yale.edu

In Brief

Hypothalamic Agrp neurons play a role in offspring-to-caregiver bonding independent of their role in food ingestion.

CellPress

Functional Ontogeny of Hypothalamic Agrp Neurons in Neonatal Mouse Behaviors

Marcelo R. Zimmer,[1,3] Antonio H.O. Fonseca,[1,4] Onur Iyilikci,[1] Rafael Dai Pra,[1,3] and Marcelo O. Dietrich[1,2,3,5,*]

[1]Program in Integrative Cell Signaling and Neurobiology of Metabolism, Department of Comparative Medicine, Yale University School of Medicine, New Haven, CT 06520, USA
[2]Department of Neuroscience, Yale University School of Medicine, New Haven, CT 06520, USA
[3]Graduate Program in Biological Sciences-Biochemistry, Universidade Federal do Rio Grande do Sul, Porto Alegre, RS 90035, Brazil
[4]Graduate Program in Microelectronics, Universidade Federal do Rio Grande do Sul, Porto Alegre, RS 15064, Brazil
[5]Lead Contact
*Correspondence: marcelo.dietrich@yale.edu
https://doi.org/10.1016/j.cell.2019.04.026

SUMMARY

Hypothalamic Agrp neurons regulate food ingestion in adult mice. Whether these neurons are functional before animals start to ingest food is unknown. Here, we studied the functional ontogeny of Agrp neurons during breastfeeding using postnatal day 10 mice. In contrast to adult mice, we show that isolation from the nursing nest, not milk deprivation or ingestion, activated Agrp neurons. Non-nutritive suckling and warm temperatures blunted this effect. Using _in vivo_ fiber photometry, neonatal Agrp neurons showed a rapid increase in activity upon isolation from the nest, an effect rapidly diminished following reunion with littermates. Neonates unable to release GABA from Agrp neurons expressed blunted emission of isolation-induced ultrasonic vocalizations. Chemogenetic overactivation of these neurons further increased emission of these ultrasonic vocalizations, but not milk ingestion. We uncovered important functional properties of hypothalamic Agrp neurons during mouse development, suggesting these neurons facilitate offspring-to-caregiver bonding.

INTRODUCTION

Agouti-related peptide (Agrp) neurons in the arcuate nucleus of the hypothalamus serve as a central coordinator to regulate food intake. Ablation of these neurons leads to aphagia in adult mice (Gropp et al., 2005; Luquet et al., 2005), but not in neonates, suggesting that Agrp neurons do not contribute to ingestive behaviors early in development. In support of this view, Agrp neurons show delayed development in rodents (Nilsson et al., 2005; Padilla et al., 2010), when the final maturation of Agrp neuronal circuitry coincides with weaning (Grove and Smith, 2003). However, impairing development of Agrp neurons during the first postnatal week in mice has persistent consequences to metabolism and behavior (Dietrich et al., 2012; Joly-Amado

et al., 2012), suggesting an unidentified function for Agrp neurons during early development.

Here, we assessed the functional ontogeny of Agrp neurons in early postnatal development of mice at postnatal day 10 (P10) and during the weaning period during postnatal days 15–21 (P15–P21).

RESULTS

Isolation from the Nursing Nest, Not Nutrient Intake, Activates Agrp Neurons in Neonates

In adult mice, nutrient deprivation activates Agrp neurons (Hahn et al., 1998; Takahashi and Cone, 2005). So, we investigated the extent to which Agrp neurons respond to a lack of nutrients in neonatal mice. To test this, we isolated P10 mice from the nest for 90 min or 8 h to prevent nutrient intake via milk ingestion (Figure 1A). A 90-min time from onset of separation maximizes Fos expression (Barros et al., 2015). Both periods of isolation increased Agrp neuronal activity, as indicated by the increased number of Fos positive Agrp neurons upon isolation (nest: $3.14 \pm 0.96\%$, n = 9; isolation/90 min: $31.19 \pm 1.89\%$, n = 10; isolation/8 h: $46.19 \pm 2.04\%$, n = 3; $F_{2,\ 19} = 128.6$, p < 10^{-11}, one-way ANOVA; Figures 1B–1D).

Because 90 min significantly increased Fos positive Agrp neurons, we tested whether this period of isolation also stimulated milk intake. We measured milk intake by calculating the change in body weight in animals that remained in the nest for 90 min compared to animals isolated for 90 min followed by re-introduction to the nest for an additional 90-min period (Figure 1E). In this protocol, we did not observe significant differences in the body-weight changes between the two experimental conditions (nest: 62.1 ± 15.4 mg, n = 12; reunion: 76.2 ± 14.4 mg, n = 12; $t_{22} = 0.65$, p = 0.51, unpaired _t_ test; Figure 1F). Thus, activation of Agrp neurons after 90 min of isolation from the nest in P10 mice is not significant to increase milk intake. Moreover, the increased activation of Agrp neurons does not seem to arise from a generalized stress response, as corticosterone levels did not increase after isolation (nest: 9.96 ± 1.85 ng/mL, n = 7; isolation: 12.40 ± 1.85 ng/mL, n = 11; $t_{16} = 0.88$, p = 0.39, unpaired t test; Figure 1G), and testing pups in the presence of a predator odor for 90 min did not alter Fos labeling in Agrp neurons (nest: $1.19 \pm 0.92\%$, n = 2; isolation: $23.82 \pm 4.78\%$,
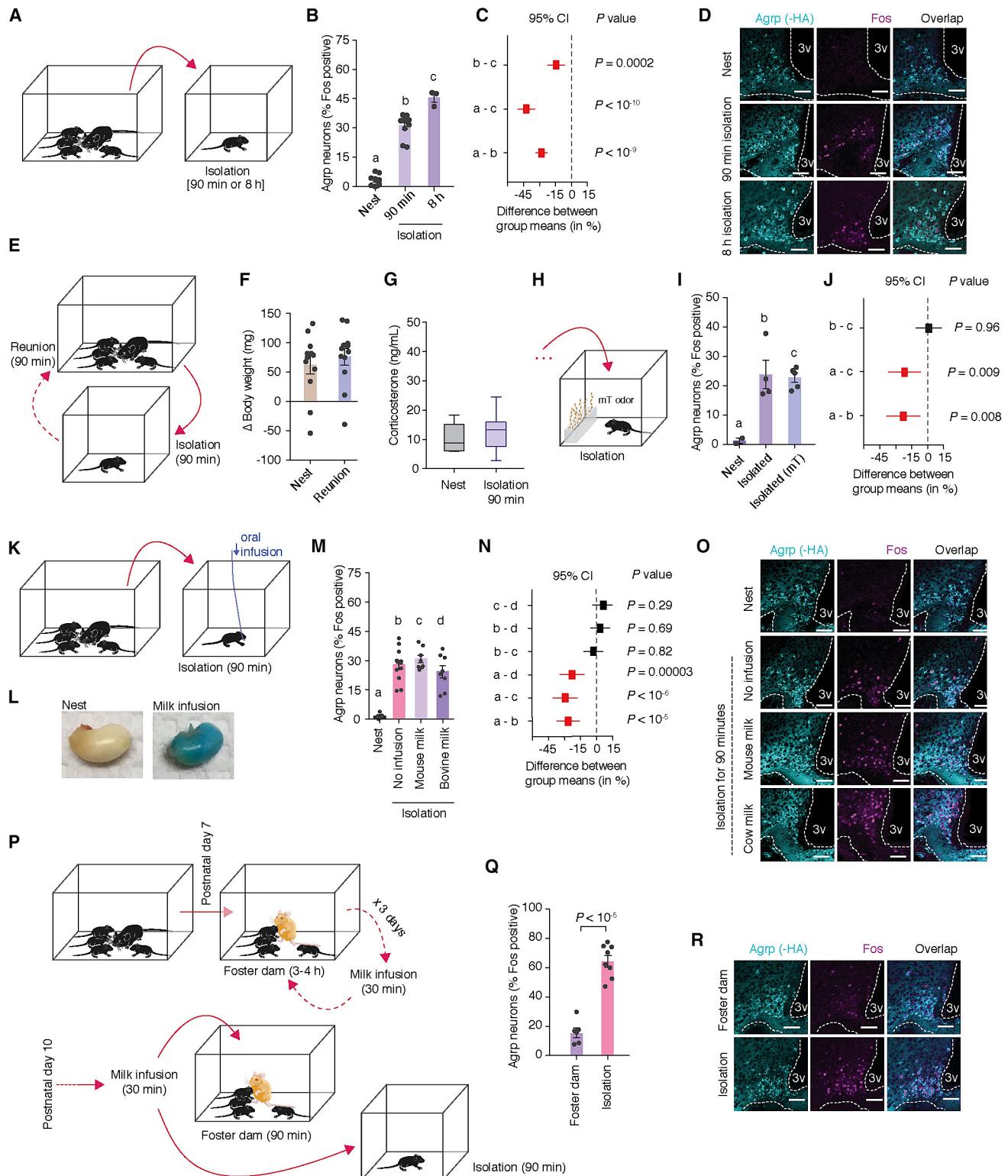
Figure 1. Fos Labels Agrp Neuron Activation in P10 Mice upon Social Isolation

(A) P10 mice were socially isolated for 90 min or 8 h.

(B) Agrp neurons positive for Fos immunoreactivity (nest, n = 9; isolation/90 min, n = 10; isolation/8 h, n = 3, one-way ANOVA, p < 10^{-11}).

(legend continued on next page)

n = 4; isolation and predator odor: 22.71 ± 1.59%, n = 5; $F_{2, 8}$ = 9.73, p = 0.007, one-way ANOVA; Figures 1H–1J).

To evaluate whether the activation of Agrp neurons upon isolation from nest is due to caloric deprivation, we isolated P10 mice while orally infusing bovine or mouse derived milk (Figure 1K). We confirmed milk ingestion by adding a colored dye to the milk to verify its presence in the stomach (Figure 1L). Surprisingly, our results showed no significant difference between the activation of Agrp neurons between the groups that received an oral infusion of milk and the control group that received a passive oral probe with no milk infusion (nest: 1.51 ± 0.65%, n = 5; isolation and no infusion: 27.88 ± 2.39%, n = 12; isolation and mouse milk: 30.73 ± 1.93%, n = 8; isolation and bovine milk: 24.24 ± 3.14%, n = 8; $F_{3, 29}$ = 19.38, p < 10^{-6}, one-way ANOVA; Figures 1M–1O).

Next, we tested the hypothesis that Agrp neuron activity in P10 mice increases upon separation in anticipation of future nutrient deprivation. To this end, we investigated the extent to which isolation from the nest activates Agrp neurons when dissociating milk intake and the nest. P7 mice were housed with a foster non-lactating dam and were manually fed milk by an investigator (Figure 1P). All neonates quickly developed locomotor activity toward the investigator at feeding onset, which suggests a learned association that the milk source was outside the home nest. We then assessed activation of Agrp neurons at P10 at either isolation or return to the home cage with the foster dam for a period of 90 min after all pups were previously fed with equal volumes of milk. Similar to our previous experiments, isolation from the home nest strongly increased the number of Fos positive Agrp neurons compared to mice that returned to the home cage (foster dam: 15.59 ± 3.26%, n = 6; isolation: 64.39 ± 3.94%, n = 8; t_{12} = 9.06, p < 10^{-5}, unpaired t test; Figures 1Q and 1R). Taken together, these results suggest that activation of Agrp neurons in P10 mice following isolation from the nest does not require milk

deprivation or anticipation of milk deprivation, which stands in contrast to adult mice.

Non-nutritive Suckling and Thermal Support Blunt Agrp Neuron Activation in Neonates

Our next goal was to evaluate the relative importance of different components of the nest environment and mother-infant interaction that contribute to Agrp neuron activation in P10 mice after isolation from the nest. In the nursing nest, pups receive care from the dam. An important feature of maternal care is neonatal attachment to the mother's nipple and suckling. So, we investigated the extent to which suckling alters the activation of Agrp neurons. We fostered P10 mice with non-lactating dams, non-lactating dams with protruded nipples, and lactating dams (Figure 2A). In all cases, foster dams promptly retrieved the pups and placed them in the nest. All foster dams displayed maternal behaviors, such as grooming and licking and arched-back "nursing" of pups, as expected. Interestingly, all foster dams blunted the activation of Agrp neurons in P10 mice compared to isolated pups (nest: 2.10 ± 0.21%, n = 6; isolation: 26.47 ± 1.57%, n = 6; non-lactating foster dam: 16.59 ± 1.64%, n = 7; non-lactating foster dam with protruded nipples: 8.66 ± 1.26%, n = 6; lactating foster dam: 10.29 ± 0.65%, n = 4; $F_{4, 24}$ = 50.29, p < 10^{-10}, one-way ANOVA; Figures 2B and 2C). Attachment of pups to the foster dam's nipples further decreased the number of Fos-labeled Agrp neurons compared to pups placed with a foster dam with non-protruded nipples to prevent nipple attachment (Figures 2B and 2C). The effect of nipple attachment was irrespective of milk availability, as the expression of Fos in pups showed a similar magnitude when placed with lactating and non-lactating foster dams with protruded nipples (Figures 2B and 2C). Overall, activation of Agrp neurons in P10 mice is blunted by non-nutritive suckling, an important component of maternal care, and is not further reduced by availability of milk in the dam's nipples.

(C) Tukey-Kramer's multiple comparisons test of the difference between means (95% confidence intervals from B), representing effect sizes.

(D) Representative images of immunohistochemistry for HA (cyan, labels Agrp neurons in $Agrp^{Rpl22-HA}$ mice), Fos (magenta), and overlap. Scale bars represent 50 μm.

(E) Effect of isolation (90 min) on milk intake upon reunion with the dam and litter for an additional 90 min.

(F) Delta body weight as a measure of milk intake during 90 min in P10 mice (control, n = 12; reunion, n = 12, unpaired t test, p = 0.51).

(G) Plasma corticosterone levels in P10 mice after 90-min isolation (control, n = 7; reunion, n = 11, unpaired t test, p = 0.39). Boxplot represents median, $1^{st}/3^{rd}$ quartiles, and min and max values.

(H) Effect of exposure to predator odor (mT) during 90-min isolation in P10 mice.

(I) Quantification of Agrp neurons positive for Fos (nest, n = 2; isolation, n = 4; isolation/mT, n = 5, one-way ANOVA, p = 0.007).

(J) Tukey-Kramer's multiple comparisons test of the difference between means (95% confidence intervals from I), representing effect sizes.

(K) Effect of milk infusion (mouse or bovine) in the activation of Agrp neurons in isolated P10 mice.

(L) Infused milk was labeled with a blue dye to confirm ingestion. Post-mortem images of the stomach of P10 mice.

(M) Quantification of Agrp neurons positive for Fos (nest, n = 5; isolation with no infusion, n = 12; isolation with infusion of mouse milk, n = 8; isolation with infusion of cow milk, n = 8, one-way ANOVA, p < 10^{-6}).

(N) Tukey-Kramer's multiple comparisons test of the difference between means (95% confidence intervals from M), representing effect sizes.

(O) Representative images of immunohistochemistry for HA (cyan, labeling Agrp neurons in $Agrp^{Rpl22-HA}$ mice), Fos (magenta), and overlap. Scale bars represent 50 μm.

(P) Effect of artificial rearing mice on Fos upon isolation. P7 mice were fostered with a non-lactating dam, while hand-fed every 3–4 h for 3 days. At P10, all mice were hand-fed and separated in two groups: reunited with the foster dam or isolated for 90 min.

(Q) Quantification of Agrp neurons positive for Fos (foster dam, n = 6; isolation, n = 8, unpaired t test, p < 10^{-5}).

(R) Representative images of immunohistochemistry for HA (cyan, labeling Agrp neurons in $Agrp^{Rpl22-HA}$ mice), Fos (magenta), and overlap. Scale bars represent 50 μm.

In (B), (F), (I), (M), and (Q), bars indicate mean ± SEM. Circles represent individual values. In (C), (J) and (N), symbols represent mean ± SEM; red denotes statistically significant differences.
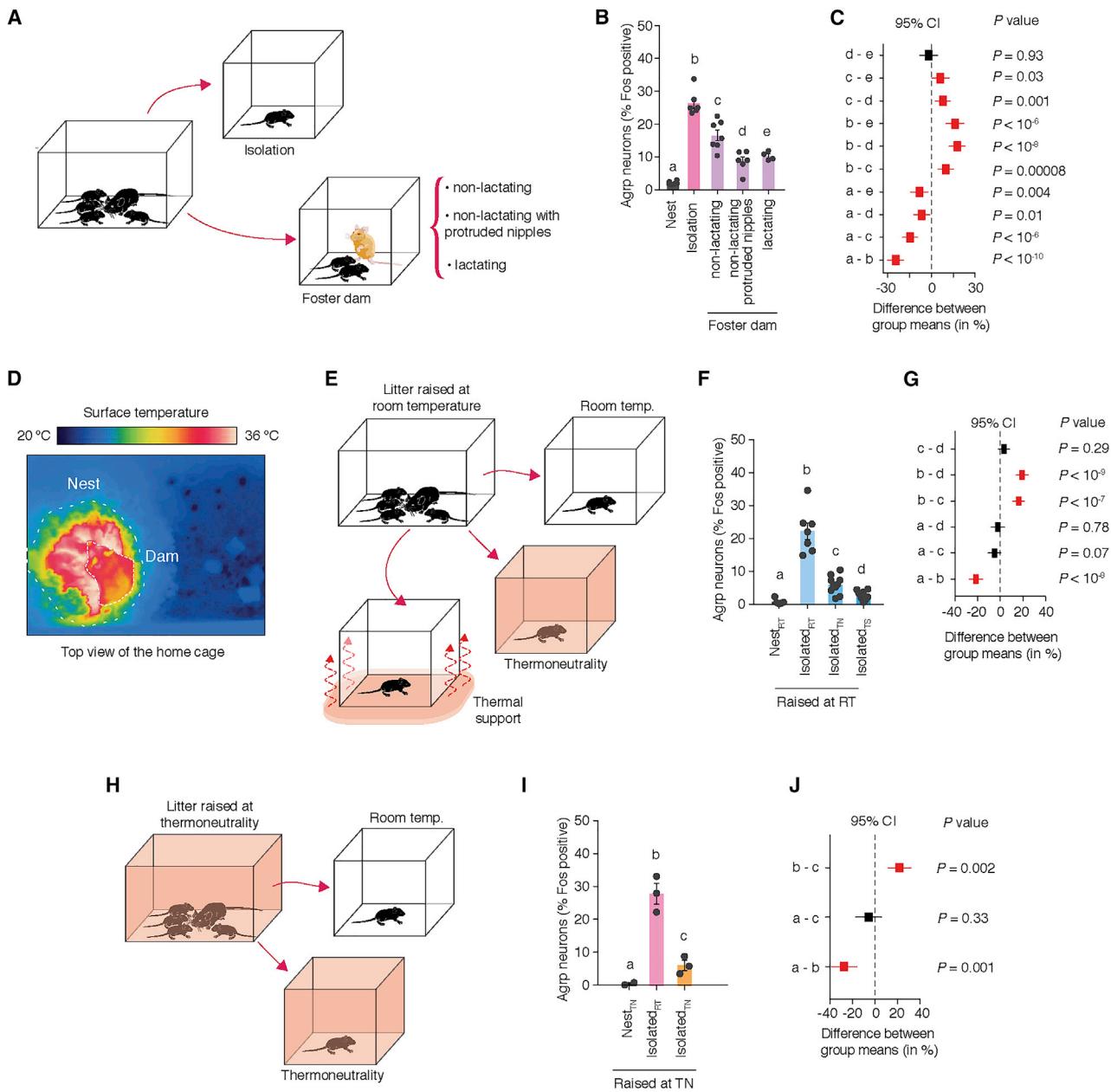
Figure 2. Warm Temperatures Blunt Activation of Agrp Neurons in P10 Mice

(A) Study design: P10 mice were either fostered with non-lactating dams, with non-lactating dams with protruded nipples, or with lactating dams for 90 min. A control group was not manipulated (nest) and a second group was isolated (isolation).

(B) Quantification of Agrp neurons positive for Fos (nest, n = 6; isolation, n = 6; non-lactating foster dam, n = 7; non-lactating foster dam with protruded nipples, n = 6; lactating foster dam, n = 4, one-way ANOVA, p < 10^{-10}).

(C) Tukey-Kramer's multiple comparisons test of the difference between means (95% confidence intervals from B), representing effect sizes.

(D) Thermo-photography of the nursing nest. Lactating dam is on the top of P10 offspring. Nest temperature is approximately 34°C–36°C.

(E) Offspring raised at room temperature (RT) were isolated either at room temperature, at thermoneutrality (TN, in a climate chamber set to 35°C) or at room temperature with a thermal support (TS) irradiating heat from underneath the cage (≈35°C).

(F) Quantification of Agrp neurons positive for Fos (nest and room temperature, n = 5; isolation and room temperature, n = 7; isolation and thermoneutrality, n = 10; isolation and thermal support, n = 8, one-way ANOVA, p = 10^{-10}).

(G) Tukey-Kramer's multiple comparisons test of the difference between means (95% confidence intervals from F) representing effect sizes.

(H) Offspring raised at thermoneutrality (climate chamber at 35°C) were isolated for 90 min at room temperature or thermoneutrality.

(legend continued on next page)

The nursing nest provides critical thermal insulation, which reduces heat loss from neonates that have not fully developed homeostatic mechanisms for thermoregulation. Dams contribute to thermal insulation by building a nest and skin-to-skin contact with pups (Figure 2D). To test the effects of thermal insulation on the activation of Agrp neurons, we isolated P10 mice at room temperature or at a thermoneutral temperature ($\approx 35°C$; Figure 2E). Because temperature exchanges in the nest occur by skin-to-skin contact, we included an additional control group, in which we provided thermal support by irradiating heat ($\approx 35°C$) from underneath (Figure 2E). 90 min of isolation at thermoneutrality or with thermal support strongly suppressed activation of Agrp neurons in P10 mice as assayed by Fos labeling compared with pups isolated at room temperature (nest: $0.77 \pm 0.39\%$, n = 5; isolation and room temperature: $22.19 \pm 2.53\%$, n = 7; isolation and thermoneutrality: $5.90 \pm 0.86\%$, n = 10; isolation and thermal support: $2.75 \pm 0.51\%$, n = 8; $F_{3, 26} = 47.31$, p = 10^{-10}, one-way ANOVA; Figures 2F and 2G). Thus, Agrp neurons in P10 mice respond to the withdrawal of thermal insulation when isolated from the nursing nest. This factor holds primary importance for the responses of these neurons to isolation.

Next, we tested the extent to which the response of Agrp neurons in P10 mice to the withdrawal of thermal insulation was dependent on prior experience with drops in ambient temperature. To prevent mice from experiencing ambient temperatures lower than nest temperatures, we repeated the experiments in animals born and raised in a thermoneutral environment (Figure 2H). P10 mice raised at thermoneutrality showed increased Fos-labeled Agrp neurons when isolated at room temperature but not at thermoneutrality (nest and thermoneutrality: $0.62 \pm 0.33\%$, n = 2; isolation and room temperature: $27.94 \pm 3.13\%$, n = 3; isolation and thermoneutrality: $6.16 \pm 1.54\%$, n = 3; $F_{2, 5} = 37.91$, p = 0.001, one-way ANOVA; Figures 2I and 2J). Thus, the response of Agrp neurons to withdrawal of thermal insulation in P10 mice does not require previous experiences with drops in ambient temperature.

Neonatal Agrp Neurons Undergo Rapid Activity Changes
In the previous experiments, we could not elucidate the temporal dynamics of physiological activation of Agrp neurons. For example, Agrp neurons after isolation (Figure 3A) could slowly increase their activity similar to a homeostat (Figure 3B). Alternatively, these neurons could rapidly respond to isolation (Figure 3C) similar to an alarm and reflexive system. A third alternative suggests that Agrp neurons could show delayed activation (Figure 3D), suggesting a thresholding mechanism triggers these neurons in neonates.

To better understand the natural activity dynamics of Agrp neurons early in postnatal development, we injected an adeno-associated virus encoding jGCaMP7s in a Cre-dependent manner in newborn $Agrp^{Cre/Cre}$ mice (Figures 3E–G) (Dana et al., 2018). We then used fiber photometry to measure calcium transients originating from Agrp neurons upon isolation-reunion in P13–14 pups (Figure 3A). We found that pup isolation from the nest increased activity of Agrp neurons that occurred within seconds (Figures 3H and 3I) and persisted throughout the isolation period (10 min). After this initial separation, reunion of the isolated animal with the litter immediately decreased the activity of Agrp neurons (Figures 3H and 3I). The suppression of Agrp neuronal activity was robust and rapid, normalizing the detected signal to pre-isolation levels in less than 30 s (Figures 3H and 3I). All animals tested showed this response to isolation-reunion, suggesting a general model in which Agrp neurons in neonates rapidly respond to disruptions in the nest conditions (Figure 3C).

Neonatal Agrp Neurons Modulate the Emission of Ultrasonic Vocalizations
In most neonatal mammals, including mice, disruptions in the nest condition lead to infant vocalization (Hofer, 1994). In mice and rats, neonates emit ultrasonic vocalizations (USVs) when separated from the dam (Noirot, 1966, 1968; Zippelius and Schleidt, 1956) (Figures 4A and 4B). We investigated whether activation of Agrp neurons in neonates upon isolation from the nest could modulate emission of USVs.

First, we confirmed that isolation from the nest induced vocal behavior in P10 mice (Figure 4A). We then investigated whether isolation at thermoneutrality would influence USVs, since these conditions blunt activation of Agrp neurons upon isolation (Figure 2). Analysis of vocal behavior showed a rapid increase in USV emission upon isolation from the nest (Figures 4B–4E), an effect that blunted at thermoneutrality (nest, n = 3; isolated and room temperature, n = 16; isolated and thermoneutrality, n = 4; $F_{2,20} = 18.08$, p < 10^{-4}, one-way ANOVA; Figures 4C–4E). Thus, vocal behavior dynamics in neonatal mice follow the dynamics of Agrp neuron activation upon isolation in these experimental conditions.

To test the extent to which Agrp neurons contribute to vocal behavior of P10 mice upon isolation, we tested animals lacking the transmitters released by Agrp neurons (NPY and GABA) (Hahn et al., 1998; Horvath et al., 1997). We recorded the emission of USVs in Npy^{KO} and $Agrp^{Vgat-KO}$ mice and their littermate controls following 10 minutes isolation in P10 mice. Animals lacking NPY exhibited a similar number of USVs after isolation compared to controls (control: 343.4 ± 56.8 USVs, n = 12; $Npy^{KO/+}$: 384.5 ± 69.3 USVs, n = 17; $Npy^{KO/KO}$: 348.0 ± 91.7 USVs, n = 7; p = 0.74, Kruskal-Wallis [KW] test; Figure 4F). In contrast, $Agrp^{Vgat-KO}$ mice had a significant decrease in emission of USVs upon isolation (control: 321.0 ± 50.4 USVs, n = 10; $Agrp^{Vgat-KO}$: 57.7 ± 14.6 USVs, n = 14; $U = 2$, p < 10^{-5}, Mann-Whitney test; Figures 4G and 4H).

We further analyzed the spectro-temporal characteristics of 3,427 USVs from control mice and 786 USVs from $Agrp^{Vgat-KO}$ mice. We characterized individual USVs by changes in

(I) Quantification of Agrp neurons positive for Fos (nest and thermoneutrality, n = 2; isolation and room temperature, n = 3; isolation and thermoneutrality, n = 3; one-way ANOVA, p = 0.001).

(J) Tukey-Kramer's multiple comparisons test of the difference between means (95% confidence intervals from I), representing effect sizes.

In (B), (F), and (I), bars represent mean ± SEM; round symbols represent individual values. In (C), (G), and (J), symbols represent mean ± SEM; red denotes statistically significant differences.
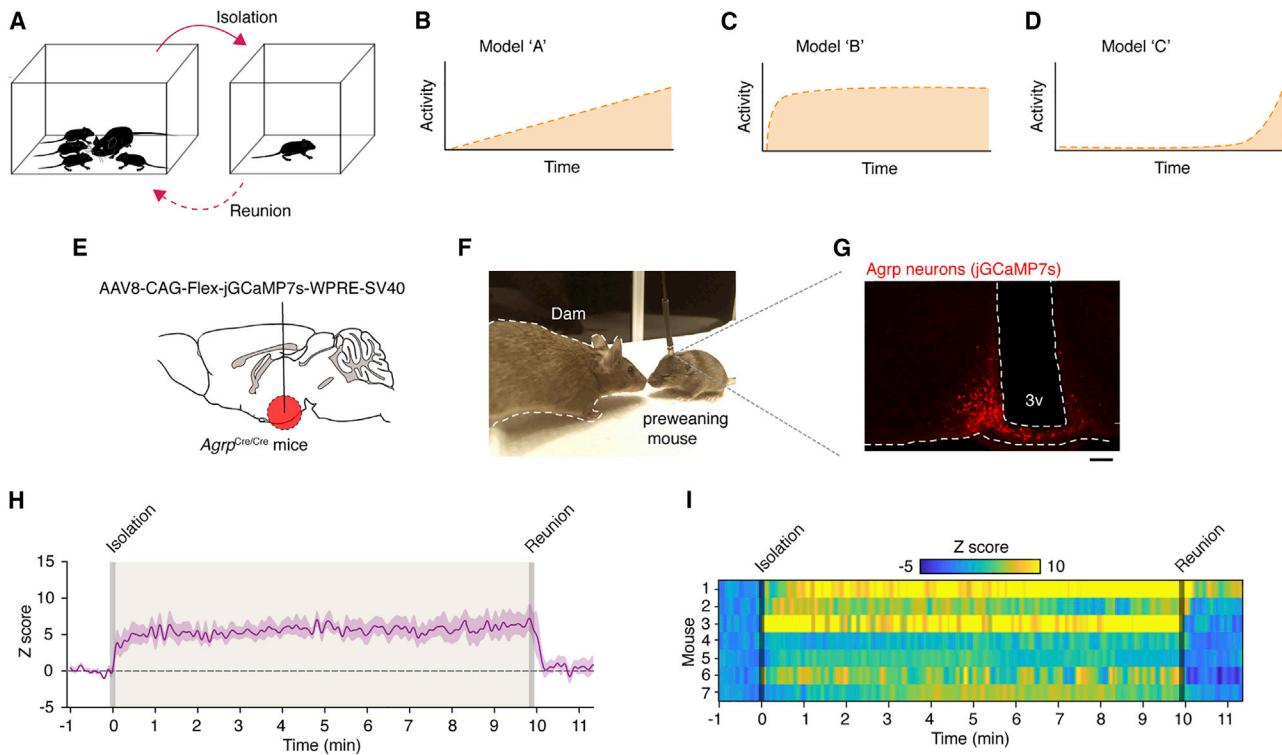
Figure 3. Rapid Dynamics of Agrp Neuronal Activity in Mice during Early Development

(A) Experimental model of isolation and reunion in neonates, which activates Agrp neurons after 90 min. Three theoretical models of activity changes of these neurons are illustrated in (B)–(D).

(B) Model A: activity of Agrp neurons gradually increases during the 90-min isolation.

(C) Model B: activity of Agrp neurons rapidly increases upon isolation.

(D) Model C: activity of Agrp neurons increases in isolation after a delay.

(E) In newborn $Agrp^{Cre/Cre}$ mice, an adeno-associated virus was injected in the arcuate nucleus of the hypothalamus to express jGCaMP7s in Agrp neurons (AAV-CAG-Flex-jGCaMP7s).

(F) Preweaning mouse connected to an optic fiber and its dam.

(G) Expression of jGCaMP7s in Agrp neurons of a P14 mouse.

(H) Z score of Agrp neuronal activity in P13–14 mice. Baseline was recorded for 1 min and then pups were isolated for 10 min. Subsequently, pups were reunited with the litter. Plot represents mean ± SEM (n = 7 animals).

(I) Heat plot representing individual responses to isolation and reunion.

spectro-temporal characteristics, such as duration, frequency, and bandwidth. Compared to control mice, USVs from $Agrp^{Vgat-KO}$ mice decreased in duration of 9.5 ms (control: 37.84 ± 0.45 ms; $Agrp^{Vgat-KO}$: 28.31 ± 0.84 ms; $D = 0.176$, p = 10^{-15}, Kolmogorov-Smirnov [KS] test; Figure 4I), in mean frequency of 1.9 kHz (control: 82.20 ± 0.28 kHz; $Agrp^{Vgat-KO}$: 80.24 ± 0.55 kHz; $D = 0.10$, p = 10^{-15}, KS test; Figure 4J), and in bandwidth of 5.6 kHz (control: 22.86 ± 0.35 kHz; $Agrp^{Vgat-KO}$: 17.20 ± 0.67 kHz; $D = 0.17$, p = 10^{-15}, KS test; Figure 4K). We also found an overall decrease in the number of vocalizations across most USV categories (Figures 4L–4X) (Grimsley et al., 2011). However, we observed an increase in the incidence of "short" vocalizations, when analyzing the relative frequency of USV categories (Figure 4Y). This syllable represents the simplest form of vocalization by neonatal mice based on spectro-temporal characteristics (Figures 4L–4V). Thus, lacking GABA release from Agrp neurons, P10 $Agrp^{Vgat-KO}$ mice led to fewer and simpler USVs compared to control animals.

Taken together, these findings indicate Agrp neurons are critically positioned to modulate the emission of USVs in neonatal mice.

Chemogenetic Activation of Agrp Neurons Increases USV Emission

We further tested whether chemogenetic activation of Agrp neurons could modulate emission of USV in isolated P10 pups using $Agrp^{Trpv1}$ mice (Dietrich et al., 2015; Ruan et al., 2014; Arenkiel et al., 2008; Güler et al., 2012) (Figure 5A; Figure S1). Subcutaneous injection of capsaicin (10 mg/kg) in $Agrp^{Trpv1}$ mice robustly activated Agrp neurons in young pups (Figure 5B; n = 5 mice per group; $U = 0$, p = 0.004, Mann-Whitney test). Chemogenetic activation of Agrp neurons using the $Agrp^{Trpv1}$ animal model induced a 61% increase in USV emission in P10 mice (control: 686.7 ± 50.22 USVs, n = 32; $Agrp^{Trpv1}$: 1040.0 ± 66.56 USVs, n = 24; $t_{51} = 4.318$, p < 0.0001; 2-tailed unpaired t test; Figures 5C–5E).
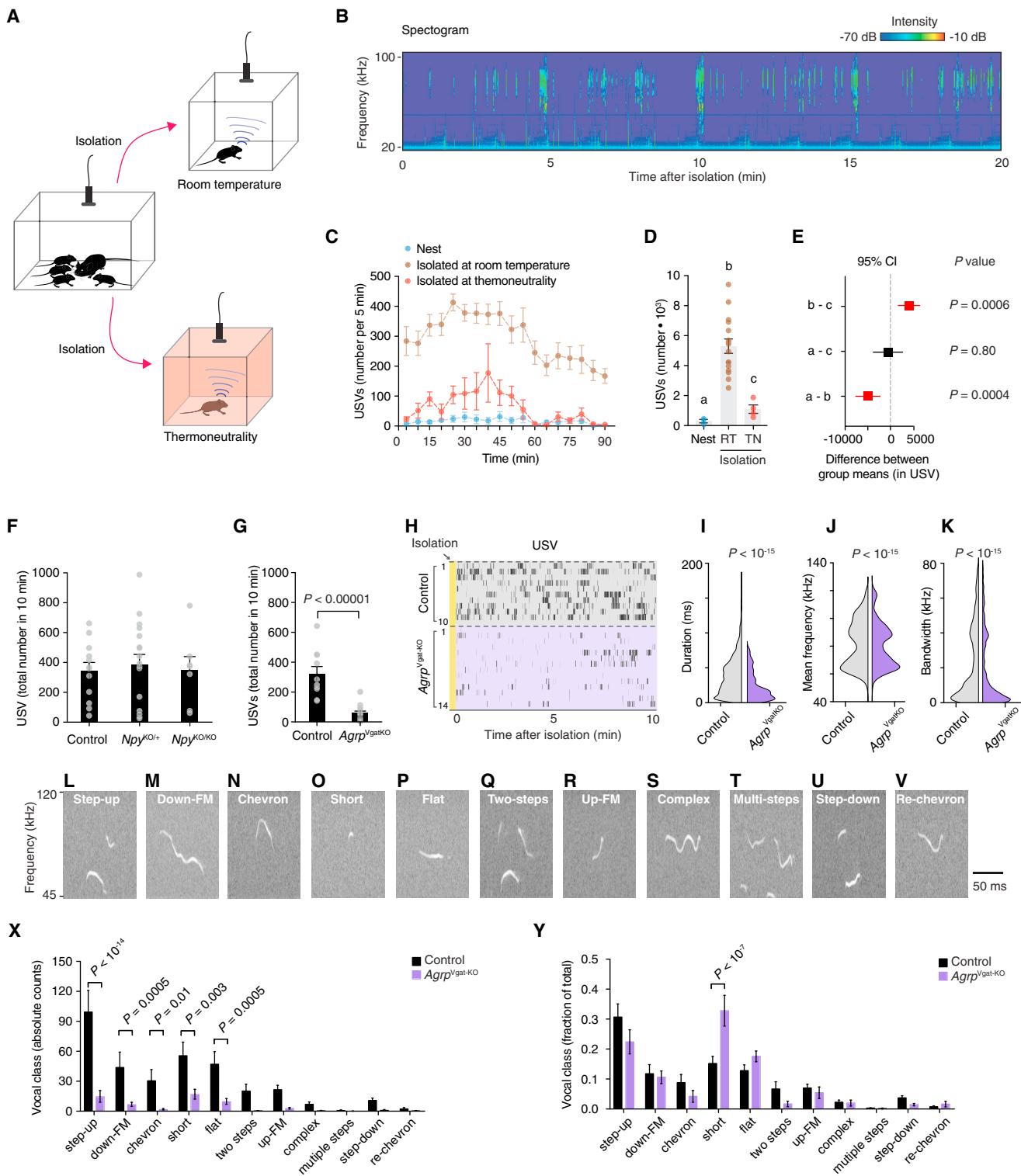
Figure 4. Agrp Neurons in P10 Mice Modulate Emission of Ultrasonic Vocalizations via GABA Release

(A) Experimental model of isolation in P10 mice at room temperature (RT) or at thermoneutral conditions (thermoneutrality; climate chamber set at 35°C).

(B) Representative spectrogram of ultrasonic vocalizations (USVs) in P10 mice recorded in isolation.

(C) Number of USVs in five-minute bins during isolation at room temperature or thermoneutrality and control group recorded in the nest.

(legend continued on next page)

We also analyzed the spectro-temporal characteristics of a total of 21,019 USVs from control mice and 24,976 vocalizations from $Agrp^{Trpv1}$ mice. Upon activation of Agrp neurons, the USV duration decreased by 4 ms (control: 51.42 ± 0.23 ms; $Agrp^{Trpv1}$: 47.09 ± 0.19 ms; $D = 0.077$, p = 10^{-15}, KS test; Figure 5F), the mean frequency increased by 3 kHz (control: 77.50 ± 0.08 kHz; $Agrp^{Trpv1}$: 80.96 ± 0.07 kHz; $D = 0.12$, p = 10^{-15}, KS test; Figure 5G), and the bandwidth increased by 2 kHz (control: 27.31 ± 0.13 kHz; $Agrp^{Trpv1}$: 29.84 ± 0.12 kHz; $D = 0.07$, p = 10^{-15}, KS test; Figure 5H). The selected categories of USVs induced by activation of Agrp neurons (Figure 5I) showed a higher complexity compared to those suppressed in $Agrp^{Vgat-KO}$ mice (Figure 4).

Interestingly, when we analyzed the relative frequency of USV categories, we found a selective increase in the frequency of "chevrons" upon chemogenetic activation of Agrp neurons (Figures 5J and 4N). To further corroborate these findings, we used a second software tool MUPET to classify vocalizations based on their shape (Van Segbroeck et al., 2017). We found six clusters of vocalizations that showed a more than 2.5-fold increase upon activation of Agrp neurons (Figures 5K and 5L). These clusters were very similar to each other, resembling our previous analysis (Figures 4G and 4H). We also found that activation of Agrp neurons suppressed vocalizations in cluster 39 (Figures 5K and 5M). The USVs in cluster 39 were simpler in shape, resembling vocalizations predominantly emitted by $Agrp^{Vgat-KO}$ pups (Figure 4). In contrast to mice lacking GABA release by Agrp neurons, chemogenetic activation of these neurons stimulated USV emission at a higher rate and with higher complexity. Together, these results strongly suggest a model in which neonatal Agrp neurons are rapidly activated upon isolation from the nest, which modulates USV emission, presumably to attract the dam.

Chemogenetic Activation of Agrp Neurons in Neonatal Mice Modulates the Behavior of Dams

Neonatal behavior is linked to maternal behavior, as the former can enhance and entrain the behavior of the latter. Based on our previous results, we expected that chemogenetic activation of Agrp neurons in the neonate would change the response of the dam toward the neonate. We devised a test to assess maternal responsiveness to P10 mice, the "maternal preference test" (Figure 5N). In this test, maternal responsiveness was measured as the time of dam-pup interaction. We found maternal exploratory behavior was strongly skewed toward $Agrp^{Trpv1}$ pups compared to controls (preference index - control: 44.96 ± 13.68 s, n = 25; $Agrp^{Trpv1}$: 125.1 ± 21.74 s, n = 25; $t_{24} = 2.69$; p = 0.01, 2-tailed paired t test; Figures 5O and 5P). These results support the model in which neonatal Agrp neurons modulate vocal behaviors signaling the dam should return to the nest.

Chemogenetic Activation of Neonatal Agrp Neurons Increases Odds for Nipple Attachment

In young pups, contact with the dam is critical for suckling behavior and ingestion of breast milk. Thus, we next devised behavior experiments to test whether activation of Agrp neurons in pups would drive behaviors toward the dam, including exploratory activity, suckling, and milk intake. We eliminated active participation by the dam as the driver of these behaviors by examining the behavior of P10 mice toward anesthetized dams (Figure 6A). In anesthetized dams, milk ejection decreases considerably (Lincoln et al., 1973), so suckling under these conditions is considered non-nutritive. Indeed, we did not observe the stretching reflex in pups that suckled during our experiments, which is a pathognomonic sign of milk ejection and ingestion (Vorherr et al., 1967).

Activation of Agrp neurons in P10 mice increased the total number of pups that attached to the dam's nipples (control: 9 out of 22; $Agrp^{Trpv1}$: 13 out of 15; p = 0.005, chi-square test; Figure 6B) and increased the distance traveled in the testing chamber (control: 0.75 ± 0.14 m, n = 22; $Agrp^{Trpv1}$: 1.20 ± 0.21 m, n = 15; $U = 94$, p = 0.027, Mann-Whitney test; Figures 6C and 6D). We then compared nipple attachment behavior of P10 mice, excluding animals that did not attach to the dam's nipples from post hoc analysis. Chemogenetic activation of Agrp neurons did not change the frequency (control: 3.11 ± 1.23; $Agrp^{Trpv1}$: 3.61 ± 0.83; $U = 51$, p = 0.63, Mann-Whitney test; Figure 6E), latency (control: 279.9 ± 57.4 s; $Agrp^{Trpv1}$: 485.4 ± 86.2 s; $U = 35$, p = 0.12, Mann-Whitney test; Figure 6F), or the duration of nipple attachment (control: 719.4 ± 128.0 s; $Agrp^{Trpv1}$: 529.8 ± 99.86 s; $U = 39$, p = 0.20, Mann-Whitney test; Figure 6G). Thus, while chemogenetic activation of Agrp neurons in P10 mice increased the probability of attaching to the dam's nipples, it did not change the observable microstructure of nipple attachment behavior.

(D) Total number of USVs during recording from (C) (nest, n = 3; isolation and room temperature, n = 16, isolation and thermoneutrality, n = 4; one-way ANOVA, p < 10^{-4}).

(E) Tukey-Kramer's multiple comparisons test of the difference between means (95% confidence intervals from D), representing effect sizes.

(F) The total number of vocalizations upon isolation (10 min) in $Npy^{+/+}$ (n = 12), $Npy^{KO/+}$ (n = 17), and $Npy^{KO/KO}$ (n = 7) P10 mice; Kruskall-Wallis test, p = 0.74.

(G) Similar to (F) but using P10 mice knockout for $Vgat$ specifically in Agrp neurons ($Agrp^{Vgat-KO}$) and their littermate controls (control, n = 10; $Agrp^{Vgat-KO}$, n = 14; Mann-Whitney test, p < 10^{-5}).

(H) Raster plots; ticks represent USVs. Each row represents an animal.

(I–K) Violin plots representing the distribution of USV characteristics in control (n = 3,427 USVs) and $Agrp^{Vgat-KO}$ mice (n = 786 USVs) in (I) duration, (J) mean frequency of the main component, and (K) the bandwidth; p values calculated using the Kolmogorov-Smirnov test.

(L–V) Types of USVs labeled in this study. Each panel represents the spectrogram of one type of vocal call as followed: (L) Step-up, (M) Down-frequency modulation, (N) Chevron, (O) Short, (P) Flat, (Q) Two-steps, (R) Up-frequency modulation, (S) Complex, (T) Multi-steps, (U) Step-down and (V) Reverse chevron.

(X) Distribution of absolute counts of each vocal call type.

(Y) Similar to (X) but vocal types normalized to total counts. In (X) and (Y), multiple t tests with p values corrected for multiple comparisons using the Holm-Sidak method.

In (C), symbols represent mean ± SEM. In (D), (F), (G), (X), and (Y), bars represent mean ± SEM. In (E), symbols represent mean ± 95% CI. In (I)–(K), data distribution is plotted. In (D), (F), and (G), symbols represent individual data. Statistically significant p values are displayed in the panels.
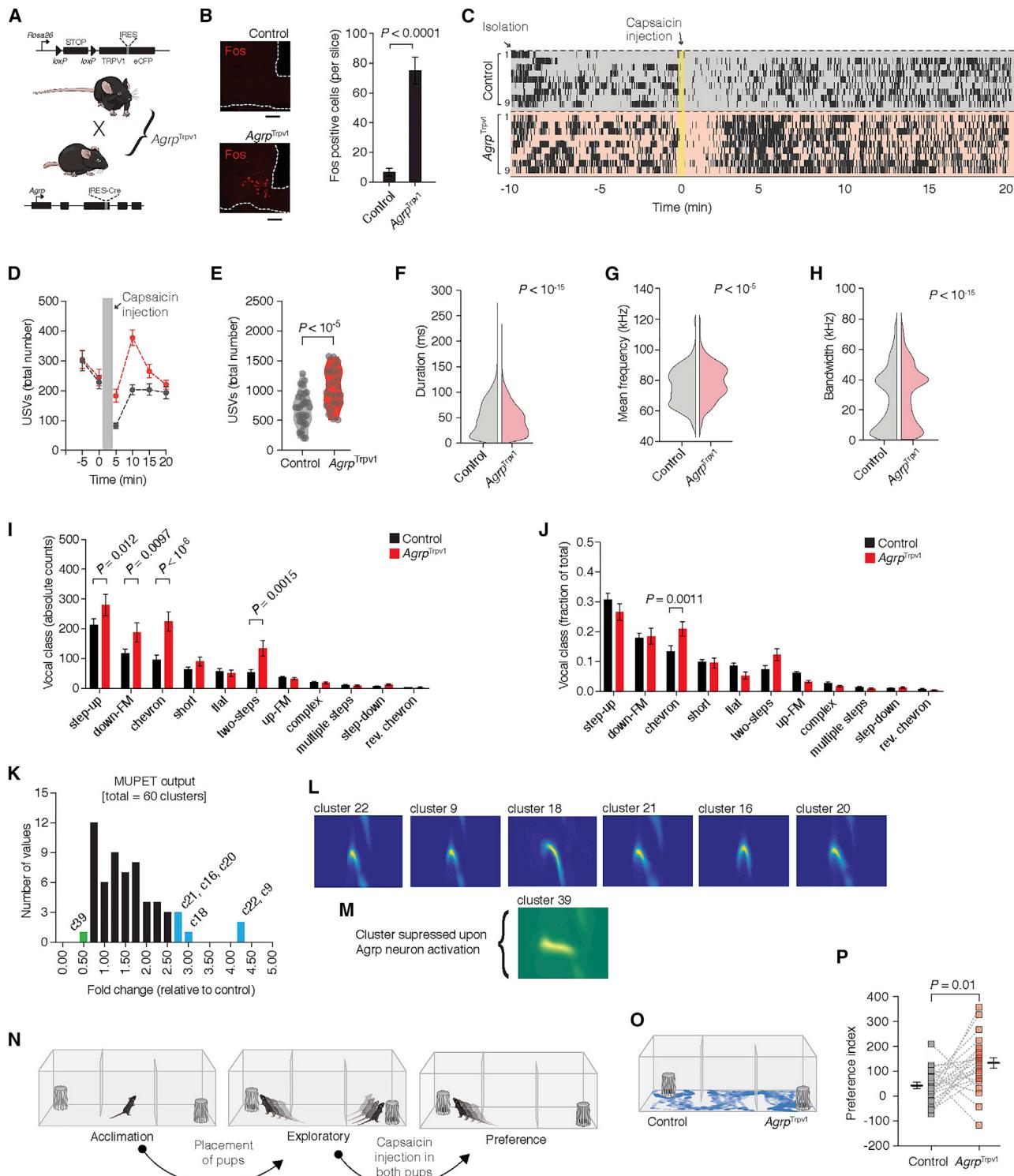
Figure 5. Activation of Agrp Neurons in P10 Mice Increases USV Emission and Alters the Dam's Behavior

(A) Generation of $Agrp^{Trpv1}$ mice.

(B) Fos in the arcuate nucleus of P15 $Agrp^{Trpv1}$ mice upon injection of capsaicin (10 mg/kg, s.c.; n = 5 mice per group). Scale bar corresponds to 50 μm. Bars and symbols represent mean ± SEM.

(C) Raster plots show USV in isolated P10 controls (n = 32) and $Agrp^{Trpv1}$ mice (n = 24). A tick represents a USV.

(D) Related to (C), number of USVs (in 5-min bins).

Next, we investigated the influence of the environmental temperature on nipple attachment behavior (Figure 6H). Thermal support from underneath the testing chamber completely suppressed nipple attachment behavior in P10 control mice (0 out of 11 pups tested attached), while 4 out of 10 pups with activated Agrp neurons attached to the dam's nipples (p = 0.019, chi-square test; Figure 6I). Interestingly, the arousal response of P10 mice upon activation of Agrp neurons was intact, as measured by the distance traveled during the test (control: 0.30 ± 0.07 m, n = 11; $Agrp^{Trpv1}$: 1.03 ± 0.19 m, n = 10; U = 13, p = 0.002, Mann-Whitney test; Figures 6J and 6K). When we analyzed the different components of nipple attachment behavior of the four P10 mice that successfully attached, we found the frequency of attachments was largely suppressed with mice only attaching once during the test (Figure 6L). The latency to attach (386.5 ± 49.62 s; Figure 6M) was similar to the other experimental conditions (Figures 6F and 6S). The duration animals remained attached to the nipples (787.9 ± 48.20 s; Figure 6N) was within the range of our other experiments (Figures 6G and 6T). We conclude providing warmth did not blunt the arousal response after activating Agrp neurons but did suppress nipple attachment behavior of P10 mice. Taken together, our behavioral experiments further support the importance of a thermal stimulus in neonates to modulate the functional properties of Agrp neurons.

We then assessed whether a lactating anaesthetized dam would alter attachment by P10 mice. Oxytocin triggers the milk ejection reflex following nipple stimulation by the pups during suckling (Lincoln and Paisley, 1982). To facilitate milk ejection, we injected a group of anesthetized dams with oxytocin immediately before testing each pup (Figure 6O) (Singh and Hofer, 1978; Vorherr et al., 1967). Similar to non-lactating dams, activation of Agrp neurons in P10 mice increased the number of mice that attached to the dam's nipples (control: 8 out of 18; $Agrp^{Trpv1}$: 13 out of 15; p = 0.012, chi-square test; Figure 6P). The total distance traveled during the test was not different between groups (control: 0.87 ± 0.22 m, n = 18; $Agrp^{Trpv1}$: 1.13 ± 0.28 m, n = 15; U = 100.5, p = 0.21, Mann-Whitney test; Figure 6Q). When comparing the behavior of animals that attached to the dam's nipples, we did not find statistical differences in the frequency (control: 5.25 ± 0.99, n = 8; $Agrp^{Trpv1}$: 8.38 ± 1.52, n = 13;

U = 34, p = 0.20, Mann-Whitney test; Figure 6R) or duration of attachments (control: 515.7 ± 78.68 s, n = 8; $Agrp^{Trpv1}$: 502.6 ± 91.98 s, n = 13; U = 50, p = 0.91, Mann-Whitney test; Figure 6T), but we found a decrease in the latency of attachment (control: 501.9 ± 68.91 s, n = 8; $Agrp^{Trpv1}$: 335.2 ± 55.52 s, n = 13; U = 21, p = 0.02, Mann-Whitney test; Figure 6S). Since dams were lactating, we also measured body-weight changes in the pups as a measure of milk intake. Interestingly, upon activation of Agrp neurons, P10 mice ingested a lower amount of milk than controls during the test (control: 91.2 ± 19.9 mg; $Agrp^{Trpv1}$: 43.7 ± 10.0 mg; pups that did not attach: −10.0 ± 2.9 mg, n = 12; $F_{2,30}$ = 19.35, p < 10^{-5}, one-way ANOVA; Figures 6U and 6V). These results suggest that activated Agrp neurons increase dam-seeking behavior but not necessarily increase ingestion of milk.

Chemogenetic Activation of Agrp Neurons Increases Ingestive Behaviors in P15 Mice

Mice rapidly transition from breastfeeding to independent feeding during weaning period. At approximately P15, mice begin experimenting with food sources but still rely on breast-feeding for nutrition (Hammond et al., 1996). We next examined the behavior of P15 mice toward the dam to investigate the ontogeny of Agrp neuron function. All tested P15 mice attached to the nipples of the anesthetized dam regardless of chemogenetic activation of Agrp neurons (n = 19 mice per group; Figure 7A). Activating Agrp neurons did not significantly change the distance traveled in the testing chamber (control: 2.03 ± 0.34 m; $Agrp^{Trpv1}$: 2.20 ± 0.22 m; U = 145, p = 0.31, Mann-Whitney test; Figure 7B). In contrast to P10 mice, chemogenetic activation of Agrp neurons in P15 mice showed a striking increase in the number of attachments to the dam's nipples compared to control (control: 3.68 ± 1.02; $Agrp^{Trpv1}$: 11.74 ± 1.80; U = 72.5, p = 0.001; Mann-Whitney test; Figures 7C and 7D). We observed no statistical difference in the latency of the first attachment (control: 226.6 ± 50.8 s; $Agrp^{Trpv1}$: 123.0 ± 16.92 s; U = 116, p = 0.06; Mann-Whitney test; Figure 7E) or the total duration of nipple attachment (control: 711.6 ± 85.2 s; $Agrp^{Trpv1}$: 798.9 ± 79.02 s; U = 143, p = 0.28; Mann-Whitney test; Figure 7F).

Since P15 mice displayed numerous nipple attachments (Figure 7D), we could track and quantify the number of nipples

(E) Related to (C) and (D), total number of USVs in the 20 min after activating Agrp neurons in isolated pups (control, n = 32; $Agrp^{Trpv1}$, n = 24; p value calculated using a 2-tailed unpaired t test).

(F–H) Violin plots representing the distribution of USV characteristics in control (n = 22,168 USVs) and $Agrp^{Trpv1}$ mice (n = 24,971 USVs) in (F) duration, (G) mean frequency of the main component of the USV, and (H) the bandwidth; p values calculated using the Kolmogorov-Smirnov test.

(I) Distribution of absolute counts of each vocal call type.

(J) Similar to (I), but vocal types normalized to total counts. In (I) and (J), multiple t tests with p values corrected for multiple comparisons using the Holm-Sidak method.

(K) Distribution of the fold change (number of USVs from $Agrp^{Trpv1}$ mice related to number of USVs from control mice) in each of the 60 output clusters analyzed by MUPET (see STAR Methods). Shown in blue are 6 clusters highly enriched in USVs from $Agrp^{Trpv1}$ mice. Shown in green is 1 cluster enriched in USVs from controls.

(L) Related to (K), images represent the 6 clusters enriched in USVs from $Agrp^{Trpv1}$ mice.

(M) Related to (K), image represents the cluster enriched in USVs from control mice.

(N) Maternal preference test (MPT).

(O) Representative tracking (in blue) of a dam in the preference stage.

(P) Preference index (in seconds) during MPT (n = 25 pairs; p value calculated using a 2-tailed paired t test).

In (D), symbols represent mean ± SEM. In (B), (I), and (J), bars represent mean ± SEM. In (F)–(H), data distribution is plotted. In (E) and (P), symbols represent individual data. In (P), black lines indicate mean ± SEM. See also Figure S1.
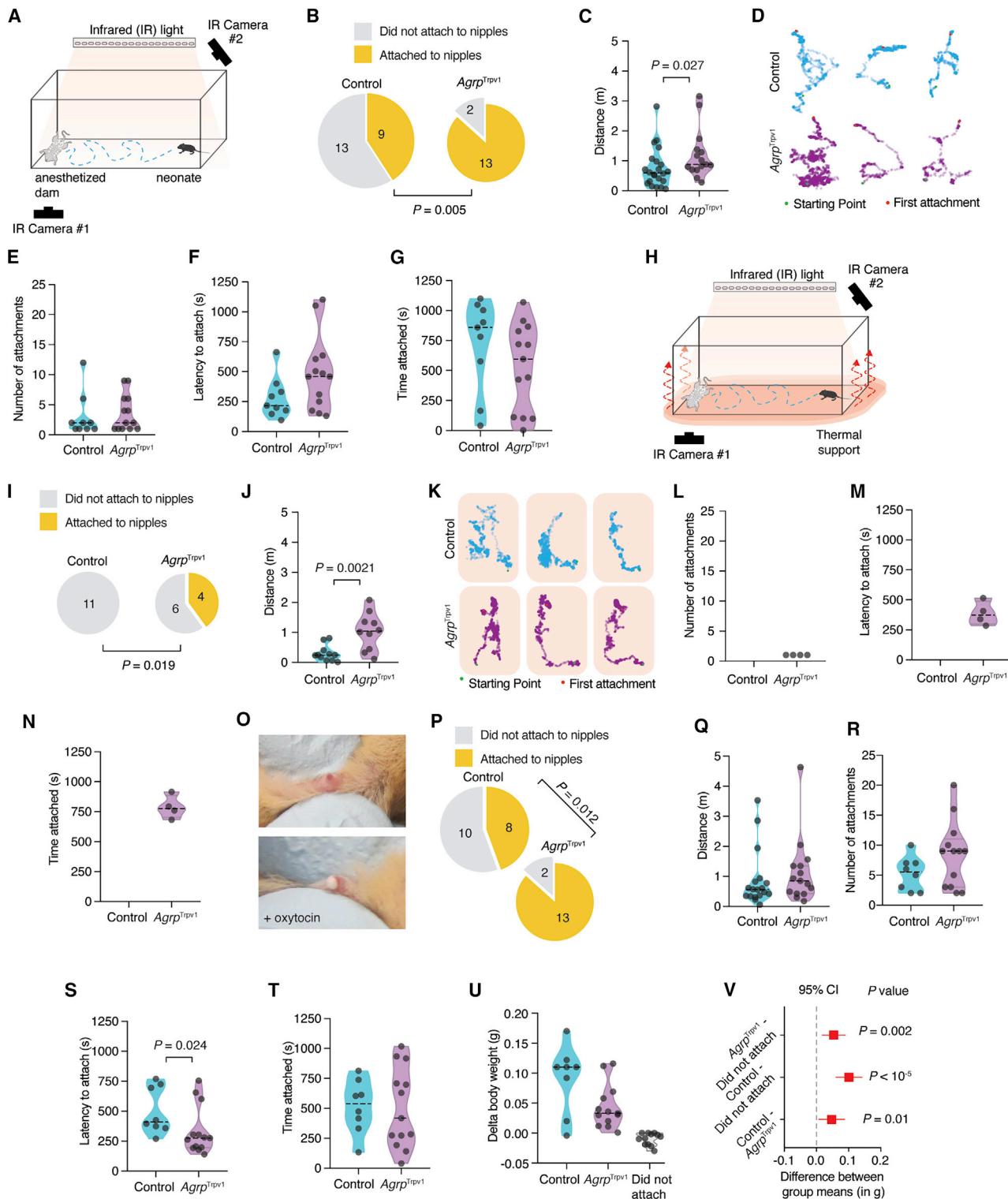
Figure 6. Agrp Neuron Activation and Suckling Behavior in P10 Mice

(A) Chamber to assay suckling behavior in mice.

(B–G) Quantification of suckling behavior in P10 mice tested with an anesthetized, non-lactating dam. In (B), proportion of mice displaying nipple attachment. In (C), total distance traveled. In (D), tracking of locomotor activity (bottom: starting point; top: anesthetized dam). In (E)–(G), data only considering mice that attached to nipples. In (E), number of nipple attachments. In (F), latency to the first attachment. In (G), total time attached to nipples.

(legend continued on next page)

explored to measure nipple-shifting behavior (Figure 7G) (Cramer et al., 1980). Chemogenetic activation of Agrp neurons in P15 mice increased the total number of different nipples explored during the test (control: 2.68 ± 0.57 nipples; $Agrp^{Trpv1}$: 5.21 ± 0.62 nipples; U = 92.5, p = 0.007; Mann-Whitney test; Figure 7H). In these experiments, mice did not show a nipple preference (n = 38 mice; p = 0.42, one-way ANOVA; Figures 7I and 7J), which is a phenomenon observed in other species (Erwin et al., 1975; Hudson et al., 2009; Tomaszycki et al., 1998).

We repeated the above experiments using anesthetized dams injected with oxytocin during a 10-min test. In control mice, 50% of P15 mice attached to the dam's nipples (4 out of 8 mice), while 91% of $Agrp^{Trpv1}$ mice displayed the same behavior (11 out of 12 mice; p = 0.035, chi-square test; Figure 7K). Activating Agrp neurons did not significantly change the distance traveled in the testing chamber (control: 1.13 ± 0.26 m; $Agrp^{Trpv1}$: 1.56 ± 0.21 m; U = 31, p = 0.20, Mann-Whitney test; Figure 7L) but strongly increased the number of nipple attachments (control: 2.00 ± 0.70; $Agrp^{Trpv1}$: 9.90 ± 1.82; U = 2.5, p = 0.007, Mann-Whitney test; Figure 7M). The latency to the first nipple attachment (control: 162.0 ± 33.1 s; $Agrp^{Trpv1}$: 119.9 ± 27.1 s; U = 14, p = 0.34, Mann-Whitney test; Figure 7N) and the total duration of nipple attachment (control: 332.2 ± 11.9 s; $Agrp^{Trpv1}$: 388.0 ± 34.7 s; U = 20, p = 0.85, Mann-Whitney test; Figure 7O) were not changed upon chemogenetic activation of Agrp neurons. In contrast to P10 mice, chemogenetic activation of Agrp neurons in P15 mice did significantly increase milk intake in mice that attached to the nipples of lactating dams (control: 17.2 ± 26.1 mg; $Agrp^{Trpv1}$: 109.5 ± 38.7 mg; U = 7, p = 0.02, Mann-Whitney test; Figure 7P).

We also tested the extent to which activation of Agrp neurons induces ingestion of solid food during the weaning period. We did not observe changes in food intake in P15 mice, but we observed increased food intake in P18 and P21 mice upon chemogenetic activation of Agrp neurons (Figure 7Q). Similarly, we only found changes in body weight during the feeding test in P21 mice (Figure 7R). Together, this set of behavioral experiments suggest that Agrp neurons in P10 mice are not proximally involved in milk intake or signaling milk ingestion. We propose that these functional properties of Agrp neurons rapidly change (or appear) as mice approach weaning age.

DISCUSSION

Overall, our results reveal functional properties of Agrp neurons in neonatal mice. These insights demonstrate developmental differences that emerge during ontogeny, so studying any complex system may remain incomplete without assessing its developmental properties (Tinbergen, 1963).

Our experiments unexpectedly revealed that Agrp neurons are functional during the first 2 postnatal weeks in mice despite their immature characteristics (Nilsson et al., 2005; Padilla et al., 2010). We showed that Agrp neurons in P10 mice did not respond to milk intake and their activation did not directly increase milk intake. Conversely, non-nutritive suckling and thermal insulation were key factors modulating the activity of Agrp neurons. These results are compatible with the physiology of breastfeeding in neonatal mammals. During breastfeeding, mice, like most other mammals, do not receive continuous milk ejection. Milk ejection remains under control of a neuroendocrine reflex (Cross and Harris, 1952) and occurs at random intervals, as demonstrated in rats (Lincoln et al., 1973). In spite of milk ejection patterns, neonatal rats stay attached to the dam's nipple for at least 12 h a day in the first days of life (Lincoln et al., 1973). In fact, homeostatic sensing of milk deprivation to modulate nutritive suckling behavior only develops later as shown in laboratory rodents (Ellis et al., 1984; Hall and Rosenblatt, 1978; Kenny et al., 1979). Thus, these studies strongly imply that nipple attachment serves as a stimulus for more than milk ejection. In fact, neonatal rodents develop filial huddling to dams triggered by thermotactile stimulation rather than provision of milk (Alberts, 2007; Alberts and May, 1984). Similar to rodents, neonatal monkeys prefer a cloth mother that provides thermal and tactile stimuli to a wired mother with a nursing bottle (Harlow, 1958), establishing that maternal comfort has a superior importance compared to milk intake in driving neonatal affectional responses. We posit that Agrp neurons of neonates drive this milk-independent encoding of the offspring-to-caregiver bond.

In our studies, thermal insulation was the primary factor modulating the activation of Agrp neurons in neonates following isolation from the nest. Notably, experiencing previous thermal challenges was not significant to activate neonatal Agrp neurons following isolation from the nest, which suggests an "innate" property of Agrp neurons. Intriguingly, foster dams also provide thermal insulation for the neonates, but they do not suppress activation of Agrp neurons after isolation from

---

(H) Suckling behavior using thermal support (≈35°C).

(I–N) Quantification of suckling behavior in P10 mice tested with an anesthetized, non-lactating dam (as displayed in H). In (I), proportion of mice that attached to the nipples. In (J), total distance traveled. In (K), tracking of locomotor activity (bottom: starting point; top: anesthetized dam). In (L), number of nipple attachments. In (M), latency to the first attachment. In (N), total time attached to nipples.

(O) Milk letdown prior to and after oxytocin injection in anesthetized dams.

(P–T) Quantification of suckling behavior in P10 mice tested with an anesthetized, lactating dam. In (P), proportion of P10 mice that attached to the nipples. In (Q), total distance traveled. In (R)–(T), data only reflect pups that attached to nipples. In (R), number of nipple attachments. In (S), latency to the first attachment. In (T), the total time attached to nipples.

(U) Delta body weight after suckling assay (control, n = 8; $Agrp^{Trpv1}$, n = 13; pups that did not attach, n = 12; one-way ANOVA, p < 10^{-5}).

(V) Tukey-Kramer's multiple comparisons test of the difference between means (95% confidence intervals from U), representing effect sizes.

In (B), (I), and (P), statistical analysis was performed using the chi-square test (2-tailed). In yellow, proportion of mice that attached to the dam's nipples are shown. In gray, mice that did not attach are shown.

In (C), (E)–(G), (J), (L)–(N), and (Q)–(U), violin plots represent the distribution of the data. Symbols represent individual values. Statistical analysis was performed using Mann-Whitney test, with the exception of (U). p values are provided in the panels when statistically significant.

Figure 7. Ontogeny of Ingestive Behaviors in Mice

(A–J) Suckling behavior in P15 mice using anesthetized non-lactating dams during a 20-min test. (A) All pups attached to the dam's nipples during the test. (B) Total distance traveled. (C) Raster plot, ticks indicate nipple attachment. (D) Number of nipple attachments. (E) Latency to the first nipple attachment. (F) Total time attached to nipples. (G) Representative tracking data of nipple attachment. (H) Number of nipples explored. (I) Illustration of the location and number of nipples in the dam and (J) nipple preference as measured by the number of nipple attachments per nipple row in P15 mice (n = 38; both control and $Agrp^{Trpv1}$ mice were included).

(K–O) Suckling behavior in P15 mice using anesthetized lactating dams during a 10-min test. (K) Proportion of P15 mice that attached to the nipples of lactating dams. In (L), total distance traveled during the test. In (M)–(O), only showing mice that attached to nipples. In (M), the number of nipple attachments is shown. In (N), latency to the first attachment is shown. In (O), total time attached to nipples is shown.

(P) Delta body weight after the suckling assay (control, n = 4; $Agrp^{Trpv1}$ n = 11).

(Q) Chow intake during 30 min after activation of Agrp neurons in mice at 15, 18, and 21 days of age.

(R) Delta body weight in the same animals as in (Q).

In (A) and (K), statistical analysis performed using the chi-square test (2-tailed). In yellow, proportion of mice that attached to the dam's nipples. In gray, mice that did not attach. In (B), (D)–(F), (H), and (L)–(P), violin plots represent the distribution of the data. Symbols represent individual values. Statistical analysis performed using Mann-Whitney test. In (Q) and (R), differences tested using unpaired t test with Welch's correction (unequal SDs) are shown. p values provided in the panels when statistically significant. Bars and symbols (in J, Q, and R) represent mean ± SEM.

the nest to the same degree as thermal support. This observation suggests that neonates integrate several sensory signatures coupled to the nest environment, such as sensory cues from the dam, siblings, home-nest odors, or from all these sources, to create and build expectations of the external world. We unexpectedly propose that activity of Agrp neurons partially encodes this information. Future studies should address the exact nature of this information and the combination of sensory modalities needed to modulate the activity of neonatal Agrp neurons.

Our results provide further evidence to the proposal that Agrp neurons serve as motivational drivers in the mammalian brain. In adult mice, Agrp neurons may encode negative valence (Betley et al., 2015). Under this proposal, these neurons when active would generate an unpleasant state of hunger leading the adult mouse to engage in behaviors to eat and suppress this state (Betley et al., 2015). Our results support this functional property of Agrp neurons in encoding an overall negative state beginning in early development. Clearly, isolation from the nursing nest serves as a negative stimulus for the neonate, which triggers a rapid activation of Agrp neurons and emission of vocalizations. Conversely, reunion then serves as a positive stimulus for the isolated neonate, which immediately suppresses the activity of Agrp neurons. By studying the functional ontogeny of Agrp neurons, our results support a model by which Agrp neurons generate a motivational drive to suppress an overall negative state.

In our studies, we could not find increases in corticosterone levels upon isolation or an enhanced activation of Agrp neurons (as labeled by Fos) in the presence of predator odor. Despite these negative results, we cannot rule out the possibility that Agrp neurons early in life are responsive to general stressors.

Upon parental separation, some infant mammals and birds respond with protest, despair, and emit sounds to attract them (Hofer, 1994). Our results demonstrated that neonatal Agrp neurons are a critical component of the circuit modulating vocal behavioral response in mice. These findings provide further insight into the underlying neural pathways subserving neonatal vocal behavior (Curry et al., 2013; Mosienko et al., 2015; Winslow et al., 2000). Investigating downstream circuits linking Agrp neurons to brain regions involved in the emission of USVs (Arriaga and Jarvis, 2013; Arriaga et al., 2012) will reveal how the neonatal brain encodes sensory information and internal state-dependent variables to generate behavioral responses (Boulanger-Bertolus et al., 2017; Hofer, 1996).

Our results have a broad impact to understand the functional ontogeny of hypothalamic neurons and the importance of the neonatal period in brain and behavior development. Additionally, these studies establish a mechanistic substrate underlying infant-caregiver interaction, which suggests an initial population of neurons underlying the long-sought nature of this social bond in mammals (Harlow, 1958; Lewis et al., 2007).

STAR★METHODS

Detailed methods are provided in the online version of this paper and include the following:

- KEY RESOURCES TABLE
- CONTACT FOR REAGENT AND RESOURCE SHARING
- EXPERIMENTAL MODELS AND SUBJECT DETAILS
- METHOD DETAILS
  - Drugs
  - Immunohistochemistry
  - Isolation from the nest (Figures 1A–1D):
  - Milk intake in the nursing nest (Figures 1E and 1F):
  - Measurement of corticosterone levels (Figure 1G):
  - Isolation from the nest in the presence of a predator odor (Figures 1H–1J):
  - Isolation from the nest with milk infusion (Figures 1K–1O):
  - Mouse milk collection
  - Artificial feeding protocol (Figures 1P–1R):
  - Assessment of maternal components with foster dams (Figures 2A–2C):
  - Isolation from the nest with thermal support (Figures 2D–2G):
  - Isolation from the nest in pups raised at thermoneutrality (Figures 2H–2J):
  - Fiber photometry (Figure 3):
  - Recording of ultrasonic vocalizations (Figures 4 and 5):
  - Maternal preference test (Figures 5N–5P):
  - Analysis of ultrasonic vocalizations
  - Mouse pup behavior toward the anesthetized dam (Figures 6A–6G and 7A–7J):
  - Mouse pup behavior toward the anesthetized dams injected with oxytocin (Figures 6P–6V and 7K–7P):
  - Independent feeding (Figures 7Q and 7R):
- QUANTIFICATION AND STATISTICAL ANALYSIS

AUTHOR CONTRIBUTIONS

M.R.Z. performed the experiments, designed the studies, analyzed the data, and helped write the manuscript. A.H.O.F. developed a tool for ultrasonic vocalization analysis in neonates and analyzed the data. R.D.P. performed part of the Fos and behavior experiments. O.I. performed the fiber photometry experiment. M.O.D. supervised the work, designed the studies, analyzed the data, and wrote the manuscript.

DECLARATION OF INTERESTS

The authors declare no competing interests.

REFERENCES

Alberts, J.R. (2007). Huddling by rat pups: ontogeny of individual and group behavior. Dev. Psychobiol. *49*, 22–32.

Alberts, J.R., and May, B. (1984). Nonnutritive, thermotactile induction of filial huddling in rat pups. Dev. Psychobiol. *17*, 161–181.

Arenkiel, B.R., Klein, M.E., Davison, I.G., Katz, L.C., and Ehlers, M.D. (2008). Genetic control of neuronal activity in mice conditionally expressing TRPV1. Nat. Methods *5*, 299–302.

Arriaga, G., and Jarvis, E.D. (2013). Mouse vocal communication system: are ultrasounds learned or innate? Brain Lang. *124*, 96–116.

Arriaga, G., Zhou, E.P., and Jarvis, E.D. (2012). Of mice, birds, and men: the mouse ultrasonic song system has some features similar to humans and song-learning birds. PLoS ONE *7*, e46610.

Barros, V.N., Mundim, M., Galindo, L.T., Bittencourt, S., Porcionatto, M., and Mello, L.E. (2015). The pattern of c-Fos expression and its refractory period in the brain of rats and monkeys. Front. Cell. Neurosci. *9*, 72.

Betley, J.N., Xu, S., Cao, Z.F.H., Gong, R., Magnus, C.J., Yu, Y., and Sternson, S.M. (2015). Neurons for hunger and thirst transmit a negative-valence teaching signal. Nature *521*, 180–185.

Boulanger-Bertolus, J., Rincón-Cortés, M., Sullivan, R.M., and Mouly, A.M. (2017). Understanding pup affective state through ethologically significant ultrasonic vocalization frequency. Sci. Rep. *7*, 13483.

Cramer, C.P., Blass, E.M., and Hall, W.G. (1980). The ontogeny of nipple-shifting behavior in albino rats: mechanisms of control and possible significance. Dev. Psychobiol. *13*, 165–180.

Cross, B.A., and Harris, G.W. (1952). The role of the neurohypophysis in the milk-ejection reflex. J. Endocrinol. *8*, 148–161.

Curry, T., Egeto, P., Wang, H., Podnos, A., Wasserman, D., and Yeomans, J. (2013). Dopamine receptor D2 deficiency reduces mouse pup ultrasonic vocalizations and maternal responsiveness. Genes Brain Behav. *12*, 397–404.

Dana, H., Sun, Y., Mohar, B., Hulse, B., Hasseman, J.P., Tsegaye, G., Tsang, A., Wong, A., Patel, R., Macklin, J.J., et al. (2018). High-performance GFP-based calcium indicators for imaging activity in neuronal populations and microcompartments. bioRxiv. https://doi.org/10.1101/434589.

Dietrich, M.O., Bober, J., Ferreira, J.G., Tellez, L.A., Mineur, Y.S., Souza, D.O., Gao, X.B., Picciotto, M.R., Araújo, I., Liu, Z.W., and Horvath, T.L. (2012). AgRP neurons regulate development of dopamine neuronal plasticity and nonfood-associated behaviors. Nat. Neurosci. *15*, 1108–1110.

Dietrich, M.O., Zimmer, M.R., Bober, J., and Horvath, T.L. (2015). Hypothalamic Agrp neurons drive stereotypic behaviors beyond feeding. Cell *160*, 1222–1232.

Ellis, S., Axt, K., and Epstein, A.N. (1984). The arousal of ingestive behaviors by chemical injection into the brain of the suckling rat. J. Neurosci. *4*, 945–955.

Erwin, J., Anderson, B., and Bunger, D. (1975). Nursing behavior of infant pigtail monkeys (Macaca nemestrina): preferences for nipples. Percept. Mot. Skills *40*, 592–594.

Girish, V., and Vijayalakshmi, A. (2004). Affordable image analysis using NIH Image/ImageJ. Indian J. Cancer *41*, 47.

Görs, S., Kucia, M., Langhammer, M., Junghans, P., and Metges, C.C. (2009). Technical note: Milk composition in mice–methodological aspects and effects of mouse strain and lactation day. J. Dairy Sci. *92*, 632–637.

Grimsley, J.M., Monaghan, J.J., and Wenstrup, J.J. (2011). Development of social vocalizations in mice. PLoS ONE *6*, e17460.

Gropp, E., Shanabrough, M., Borok, E., Xu, A.W., Janoschek, R., Buch, T., Plum, L., Balthasar, N., Hampel, B., Waisman, A., et al. (2005). Agouti-related peptide-expressing neurons are mandatory for feeding. Nat. Neurosci. *8*, 1289–1291.

Grove, K.L., and Smith, M.S. (2003). Ontogeny of the hypothalamic neuropeptide Y system. Physiol. Behav. *79*, 47–63.

Güler, A.D., Rainwater, A., Parker, J.G., Jones, G.L., Argilli, E., Arenkiel, B.R., Ehlers, M.D., Bonci, A., Zweifel, L.S., and Palmiter, R.D. (2012). Transient activation of specific neurons in mice by selective expression of the capsaicin receptor. Nat. Commun. *3*, 746.

Hahn, T.M., Breininger, J.F., Baskin, D.G., and Schwartz, M.W. (1998). Coexpression of Agrp and NPY in fasting-activated hypothalamic neurons. Nat. Neurosci. *1*, 271–272.

Hall, W.G., and Rosenblatt, J.S. (1978). Development of nutritional control of food intake in suckling rat pups. Behav. Biol. *24*, 413–427.

Hammond, K.A., Lloyd, K.C., and Diamond, J. (1996). Is mammary output capacity limiting to lactational performance in mice? J. Exp. Biol. *199*, 337–349.

Harlow, H.F. (1958). The nature of love. Am. Psychol. *13*, 673–685.

Hofer, M.A. (1994). Hidden regulators in attachment, separation, and loss. Monogr. Soc. Res. Child Dev. *59*, 192–207.

Hofer, M.A. (1996). Multiple regulators of ultrasonic vocalization in the infant rat. Psychoneuroendocrinology *21*, 203–217.

Horvath, T.L., Bechmann, I., Naftolin, F., Kalra, S.P., and Leranth, C. (1997). Heterogeneity in the neuropeptide Y-containing neurons of the rat arcuate nucleus: GABAergic and non-GABAergic subpopulations. Brain Res. *756*, 283–286.

Hudson, R., Raihani, G., González, D., Bautista, A., and Distel, H. (2009). Nipple preference and contests in suckling kittens of the domestic cat are unrelated to presumed nipple quality. Dev. Psychobiol. *51*, 322–332.

Joly-Amado, A., Denis, R.G., Castel, J., Lacombe, A., Cansell, C., Rouch, C., Kassis, N., Dairou, J., Cani, P.D., Ventura-Clapier, R., et al. (2012). Hypothalamic AgRP-neurons control peripheral substrate utilization and nutrient partitioning. EMBO J. *31*, 4276–4288.

Kenny, J.T., Stoloff, M.L., Bruno, J.P., and Blass, E.M. (1979). Ontogeny of preference for nutritive over nonnutritive suckling in albino rats. J. Comp. Physiol. Psychol. *93*, 752–759.

Lewis, T., Amini, F., and Lannon, R. (2007). A General Theory of Love (Knopf Doubleday Publishing Group).

Lincoln, D.W., and Paisley, A.C. (1982). Neuroendocrine control of milk ejection. J. Reprod. Fertil. *65*, 571–586.

Lincoln, D.W., Hill, A., and Wakerley, J.B. (1973). The milk-ejection reflex of the rat: an intermittent function not abolished by surgical levels of anaesthesia. J. Endocrinol. *57*, 459–476.

Luquet, S., Perez, F.A., Hnasko, T.S., and Palmiter, R.D. (2005). NPY/AgRP neurons are essential for feeding in adult mice but can be ablated in neonates. Science *310*, 683–685.

Mosienko, V., Beis, D., Alenina, N., and Wöhr, M. (2015). Reduced isolation-induced pup ultrasonic communication in mouse pups lacking brain serotonin. Mol. Autism *6*, 13.

Nilsson, I., Johansen, J.E., Schalling, M., Hökfelt, T., and Fetissov, S.O. (2005). Maturation of the hypothalamic arcuate agouti-related protein system during postnatal development in the mouse. Brain Res. Dev. Brain Res. *155*, 147–154.

Noirot, E. (1966). Ultra-sounds in young rodents. I. Changes with age in albino mice. Anim. Behav. *14*, 459–462.

Noirot, E. (1968). Ultrasounds in young rodents. II. Changes with age in albino rats. Anim. Behav. *16*, 129–134.

Padilla, S.L., Carmody, J.S., and Zeltser, L.M. (2010). Pomc-expressing progenitors give rise to antagonistic neuronal populations in hypothalamic feeding circuits. Nat. Med. *16*, 403–405.

Ruan, H.B., Dietrich, M.O., Liu, Z.W., Zimmer, M.R., Li, M.D., Singh, J.P., Zhang, K., Yin, R., Wu, J., Horvath, T.L., and Yang, X. (2014). O-GlcNAc transferase enables AgRP neurons to suppress browning of white fat. Cell *159*, 306–317.

Schindelin, J., Arganda-Carreras, I., Frise, E., Kaynig, V., Longair, M., Pietzsch, T., Preibisch, S., Rueden, C., Saalfeld, S., Schmid, B., et al. (2012). Fiji: an open-source platform for biological-image analysis. Nat. Methods *9*, 676–682.

Singh, P.J., and Hofer, M.A. (1978). Oxytocin reinstates maternal olfactory cues for nipple orientation and attachment in rat pups. Physiol. Behav. *20*, 385–389.

Takahashi, K.A., and Cone, R.D. (2005). Fasting induces a large, leptin-dependent increase in the intrinsic action potential frequency of orexigenic arcuate nucleus neuropeptide Y/Agouti-related protein neurons. Endocrinology *146*, 1043–1047.

Tinbergen, N. (1963). On aims and methods of Ethology. Z. Tierpsychol. *20*, 410–433.

Tomaszycki, M., Cline, C., Griffin, B., Maestripieri, D., and Hopkins, W.D. (1998). Maternal cradling and infant nipple preferences in rhesus monkeys (Macaca mulatta). Dev. Psychobiol. *32*, 305–312.

Van Segbroeck, M., Knoll, A.T., Levitt, P., and Narayanan, S. (2017). MUPET-Mouse Ultrasonic Profile ExTraction: A Signal Processing Tool for Rapid and Unsupervised Analysis of Ultrasonic Vocalizations. Neuron *94*, 465–485.

Vorherr, H., Kleeman, C.R., and Lehman, E. (1967). Oxytocin-induced stretch reaction in suckling mice and rats: a semiquantitative bio-assay for oxytocin. Endocrinology *81*, 711–715.

Winslow, J.T., Hearn, E.F., Ferguson, J., Young, L.J., Matzuk, M.M., and Insel, T.R. (2000). Infant vocalization, adult aggression, and fear behavior of an oxytocin null mutant mouse. Horm. Behav. *37*, 145–155.

Zippelius, H.-M., and Schleidt, W.M. (1956). Ultraschall-Laute bei jungen Mäusen. Naturwissenschaften *43*, 502.

STAR★METHODS

KEY RESOURCES TABLE

REAGENT or RESOURCE	SOURCE	IDENTIFIER
Antibodies		
Rabbit polyclonal anti-c-Fos	Santa Cruz Biotechnologies	Cat# sc-52-G; RRID: AB_2629503
Rabbit monoclonal anti-c-Fos (9F6)	Cell Signaling Technology	Cat# 2250; RRID: AB_2247211
Mouse polyclonal anti-HA	BioLegend	Cat# 901503; RRID: AB_2565005
Donkey anti-mouse IgG (H+L), Alexa Fluor 488	Thermo Fisher Scientific	Cat# A-21202; RRID: AB_141607
Donkey anti-rabbit IgG (H+L), Alexa Fluor 594	Thermo Fisher Scientific	Cat# A-21207; RRID: AB_141637
Donkey anti-rabbit IgG (H+L), Alexa Fluor 647	Thermo Fisher Scientific	Cat# A-31573; RRID: AB_2536183
Bacterial and Virus Strains		
AAV8-CAG-Flex-jGCaMP7s-WPRE-SV40	Janelia Research Campus	Addgene, 104495
Biological Samples		
N/A		
Chemicals, Peptides, and Recombinant Proteins		
Capsaicin	Sigma-Aldrich	Cat# M2028-1G
Oxytocin	Sigma-Aldrich	Cat# O4375-250IU
Critical Commercial Assays		
Corticosterone ELISA kit	Enzo Life Sciences	ADI-900-097
Deposited Data		
N/A		
Experimental Models: Cell Lines		
N/A		
Experimental Models: Organisms/Strains		
Mouse: $Agrp^{Cre}$, Agrptm1(cre)Lowl/J	The Jackson Laboratory	JAX: 012899
Mouse: $R26^{LSL-Trpv1}$, B6;129P2-Gt(ROSA)26Sortm1(Trpv1,ECFP)Mde/J	The Jackson Laboratory	JAX: 008513
Mouse: $Trpv1^{KO}$, B6.129X1-Trpv1tm1Jul/J	The Jackson Laboratory	JAX: 003770
Mouse: $Rpl22^{LSL-HA}$, B6N.129-Rpl22tm11Psam/J	The Jackson Laboratory	JAX: 011029
Mouse: Npy^{KO}, 129S-Npy^{tm1Rpa}/J	The Jackson Laboratory	JAX: 004545
Mouse: $Vgat^{Flox/Flox}$, $Slc32a1^{tm1Lowl}$	The Jackson Laboratory	JAX: 012897
Oligonucleotides		
Trpv1 knockout Wild type (5′-TGGCTCATATTTGCCTTCAG-3′)	Yale Keck Oligonucleotide Synthesis	Custom preparation
Trpv1 knockout Common (5′-CAGCCCTAGGAGTTGATGGA-3′)	Yale Keck Oligonucleotide Synthesis	Custom preparation
Trpv1 knockout Mutant (5′-TAAAGCGCATGCTCCAGACT-3′)	Yale Keck Oligonucleotide Synthesis	Custom preparation
Ectopic Trpv1 allele F (5′-TCCCAAAGTCGCTCTGAGTT-3′)	Yale Keck Oligonucleotide Synthesis	Custom preparation
Ectopic Trpv1 ectopic (5′-TGGCTTGCAGTTAGGGTCTC-3′)	Yale Keck Oligonucleotide Synthesis	Custom preparation
Recombinant DNA		
N/A		
Software and Algorithms		
ImageJ/Fiji	Girish and Vijayalakshmi, 2004; Schindelin et al., 2012	https://imagej.nih.gov/ij/, RRID:SCR_002285
MUPET	Van Segbroeck et al., 2017	https://sail.usc.edu/mupet

(Continued on next page)

Continued

REAGENT or RESOURCE	SOURCE	IDENTIFIER
Any-Maze	Stoelting Co	http://www.anymaze.co.uk/index.htm, RRID:SCR_014289
GraphPad Prism 8.0	GraphPad	https://www.graphpad.com/scientific-software/prism/,RRID:SCR_002798
Sound Recording Software Avisoft-RECORDER	Avisoft	https://www.avisoft.com/recorder.htm, RRID:SCR_014436
MATLAB 2016a	MathWorks	https://www.mathworks.com/products/matlab.html,RRID:SCR_001622
Other		
Micro-Renathane® Tubing	Braintree Scientific, Inc	MRE-033
Promethion CAB-8 Temperature Control Cabinet	Sables Systems International	N/A
UltraSoundGate 416 USGH	Avisoft Bioacoustics	34163
UltraSoundGate Condenser Microphone CM 16	Avisoft Bioacoustics	40011
2.5 μL Microliter Syringe Model 62 RN	Hamilton Company	7632-01
32 gauge, Small Hub RN Needle, 15 mm, 15°	Hamilton Company	7803-04
Optic Cannulae	Doric	MFC-400/430-0.48-RM2-FLT
Optic Fibers	Doric	MFP-400/460/1100_FCM-CM2
Attenuator Fiberoptic Patchcode	Doric	MFP-400/430/LWMJ-0.48_FCM-FCM_T0.05
Fluorescence MiniCube	Doric	FMC4_AE(405)_E(460-490)_F(500-550)
LED Driver	Doric	RVP_2CH_1A
405 nm LED	Doric	CLED_405
465 nm LED	Doric	CLED_465
Fiber Photometry Processor	Tucker-Davis Technology	RZ5P
Half & Half cow's milk	Organic Valley	UPC# 0 93966 00033 7

CONTACT FOR REAGENT AND RESOURCE SHARING

Further information and requests for reagents should be direct to and will be fulfilled by the Lead Contact, Marcelo Dietrich (marcelo.dietrich@yale.edu).

EXPERIMENTAL MODELS AND SUBJECT DETAILS

All preweaning mice used in the experiments were 10-21 days old from both genders. Dams used were 2 – 6 months old. In this study, we used the following mouse lines from The Jackson Laboratories: *Agrptm1(cre)Lowl/J* (*Agrp*[Cre]) (JAX: 012899)*;* B6;129P2-*Gt(ROSA)26Sortm1(Trpv1,ECFP)Mde/J* (*R26*[LSL-Trpv1]) (JAX: 008513); B6.129X1-*Trpv1tm1Jul/J* (*Trpv1*[KO]) (JAX: 003770); B6N.129-*Rpl22tm11Psam/J* (*Rpl22*[LSL-HA]) (JAX: 011029); 129S-*Npy*[tm1Rpa]/J (*Npy*[KO]) (JAX: 004545); and *Slc32a1*[tm1Lowl] *(or Vgat*[Flox/Flox]) (JAX: 012897).

Agrp[Trpv1] mice were: *AgrpCre*[Tm/+]*::Trpv1*^{−/−}*::R26-LSL-Trpv1*[Gt/+]; control animals were *Trpv1*^{−/−}*:R26-LSL-Trpv1*[Gt/+] mice in-jected with capsaicin. *Agrp*[Cre] and *R26*[LSL-Trpv1] mice were backcrossed to *Trpv1*[KO] mice to avoid the peripheral actions of capsaicin when injected systemically to activate Agrp neurons (Arenkiel et al., 2008; Dietrich et al., 2015; Güler et al., 2012; Ruan et al., 2014). We have thoroughly characterized *Agrp*[Trpv1] mice previously (Dietrich et al., 2015). *Agrp*[HA] mice were generated by crossing *Agrp*[Cre] to *Rpl22*[LSL-HA] mice. Analysis of ectopic expression of Cre was performed by using a specific set of primers against the excised con-ditional allele, as characterized before (Dietrich et al., 2015); mice with ectopic expression of the excised allele were not used in the studies. *Agrp*[Vgat-KO] mice were generated by crossing *Agrp*[Cre] to *Vgat*[Flox/Flox] mice to finally generate *Agrp*[Cre/+]*:: Vgat*[Flox/Flox]. Controls were Cre negative littermates. All mice were kept in temperature- and humidity-controlled rooms, in a 12/12 hr light/dark cycle, with lights on from 7:00 AM–7:00 PM. Food (Teklad 2018S, Envigo) and water were provided *ad libitum* unless otherwise stated. All pro-cedures were approved by IACUC (Yale University).

METHOD DETAILS

Drugs
capsaicin (10 mg/kg, s.c. or i.p.; 3.33% Tween-80 in PBS; from Sigma) and oxytocin (5mg/kg, 15 IU/mg dissolved in PBS; from Sigma).

Immunohistochemistry
Mice were deeply anesthetized and perfused with freshly prepared fixative (paraformaldehyde 4%, in PBS 1x [pH = 7.4]). Brains were post-fixed overnight in fixative and sectioned on a vibratome. Coronal brain sections (50 μm) were washed several times in PBS 1x (pH = 7.4) and pre-incubated with Triton X-100 (0.3% in PBS 1x) for 30 min. Sections were then incubated in a blocking solution (Triton 0.3%, Donkey Serum 10%, Glycine 0.3M in PBS 1x) for one hour. Sections were then incubated with rabbit polyclonal anti-Fos (1:200; sc-52, Santa Cruz Biotechnologies) or rabbit monoclonal anti-Fos (1:1000; #2250; Cell Signaling Technology) and mouse polyclonal anti-HA (1:1000; 901503, Biolegend) for 16 hr. After, sections were extensively washed in 0.3% Triton in PBS and incubated with secondary fluorescent Alexa antibodies (1:500). Sections were mounted and visualized by a Leica TCS SP5 Spectral Confocal Microscope (Center for Cellular e Molecular Imaging, Yale University). During the entire procedure, investigators were blinded to the experimental groups. The ImageJ analysis program (version 1.51h, NIH, USA) (Girish and Vijayalakshmi, 2004; Schindelin et al., 2012) was utilized to count the number of –HA positive ($Agrp^{HA}$ neurons) and Fos-positive neurons manually.

Isolation from the nest (Figures 1A–1D):
At postnatal day 10 (P10), neonates ($Agrp^{HA}$) were divided into three conditions: (1) kept with the biological mother and littermates (nest); (2) isolated for 90 minutes and (3) isolated for 8 hours. Isolated animals were single-housed and placed in a clean chamber with fresh bedding. Pups were sacrificed and expression of Fos was evaluated. Samples were prepared for immunohistochemistry as described above. $Agrp^{HA}$ pups were used in these studies to allow identification of Agrp neurons. All samples were prepared and counted blinded for the experimental groups.

Milk intake in the nursing nest (Figures 1E and 1F):
when ten days of age (P10), pups were divided into two groups: kept with the biological mother or isolated for 90 minutes. Isolated pups were reintroduced to the biological mother for another 90 minutes after isolation. Body weight was measured prior and after 90 minutes. To ensure that animals within each group had similar milk availability, they were tested using an equal number of animals. Upon reintroduction of the isolated pups to the home cage, pups that stayed with the dam were removed to avoid competition. These experiments were not blinded.

Measurement of corticosterone levels (Figure 1G):
At postnatal day 10, neonates were divided into two groups: kept with the biological mother or isolated for 90 minutes. After testing, neonates were deeply anesthetized, and blood samples were collected through cardiac puncture. A total of 150 μl of blood was collected. Blood samples were left at room temperate for one hour and centrifuged at 5000 rpm for 20 minutes. Plasma was collected and stored at −80°C. Corticosterone level was measured using an enzyme immunoassay (ELISA) kit (Enzo Life Sciences, Farmingdale, NY, USA) according to the manufacturer's instructions.

Isolation from the nest in the presence of a predator odor (Figures 1H–1J):
At postnatal day 10 (P10), pups ($Agrp^{HA}$) were divided into three conditions: (1) kept with the biological mother and littermates (nest); (2) isolated for 90 minutes and (3) isolated for 90 minutes in the presence of a synthetic predator odor (2,4,5-Trimethylthiazole (mT), Sigma-Aldrich). Isolated animals were single-housed and placed in a clean chamber with fresh bedding. Ten microliters of mT odor were pipetted onto a small square nesting material (2 × 2 cm). To avoid contact with the odor, the chamber was divided by a wire mesh resulting in two small compartments, allowing the pups to smell the odor.

Isolation from the nest with milk infusion (Figures 1K–1O):
The procedure of milk infusion consisted in the insertion of a polyurethane-based catheter tubing (Micro-Renathane® Tubing, MRE-033, Braintree Scientific, Inc.) attached to a pump. To avoid an invasive procedure, the inserted tube end was heated and bent to create a small U shape at its end tip. After insertion into the mouth, the tube was attached to the fur on the outside of the cheek using a small drop of crazy glue to hold it in place. The whole procedure did not require anesthesia and last less than 30 s. A total of 200 μl of milk was infused during the 90 minutes (15 μl ejections, every 5-15 minutes). The following types of milk were used: (1) commercial Half & Half cow's milk (Organic Valley, Ultra Pasteurized Grade A); an (2) mouse milk collected from lactating dams. To confirm that milk was infused, a tasteless blue dye (Erioglaucine disodium salt, Sigma-Aldrich, Cat. 861146) was added (< 1 mg/mL) to the milk prior infusion. The stomach was excised to confirm the blue color indicating milk ingestion.

Mouse milk collection

The milk collection was performed on lactating dams with litters between the ages of P8-P12. Dams were separated from their litter for 6 hours prior collection to ensure adequate milk production. Dams were lightly anesthetized with isoflurane and oxytocin (5 mg/kg, i.p) was administered to promote milk release. Milk was expressed from the nipples using pressure from the thumb and forefinger to gently massage and squeeze the mammary tissue in an upward motion until a visible bead of milk begins to form at the base of the teat. Then, milk was collected using a 20 μl calibrated pipette, pipetted into a 1.5 mL Eppendorf tube and stored at −20°C until the day of the test. The duration of the milk collection lasts less than 10 minutes.

Artificial feeding protocol (Figures 1P–1R):

when seven days old, neonates were separated from the biological dam and kept with a non-lactating foster dam. Every 3-4 hours, the neonates were separated from the foster dam and milk was provided for ∼30 minutes by the experimenter using a surrogate nipple attached to a tip in a 100 μL pipette. The volume of intake in each session varied between 80 μl to 150 μl of milk. Because of the limitation in getting mouse milk, we performed the artificial feeding using a more caloric formula of cow milk (Heavy Whipping Cream, Organic Valley) that resembles the nutrition facts of a mouse milk (Görs et al., 2009). At postnatal day 10, milk was provided for 30 minutes and immediately after neonates were separated into two groups: kept with the non-lactating foster dam and littermates (nest) or isolated for 90 minutes. All other procedures for Fos counting were as described above.

Assessment of maternal components with foster dams (Figures 2A–2C):

At postnatal day 10, neonates were separated from the biological dam and placed in the cage of a foster dam. Foster dams in different lactation conditions were used: (1) non-lactating foster dam; (2) non-lactating foster dam with protruded nipples; (3) lactating foster dam. Dam rodents have the nipples still distended without milk release permitting suckling for two weeks after weaning if the female is not pregnant again. Lactating foster dams were chosen in a similar postnatal day of lactation, and their offspring was removed immediately before placing the alien/unfamiliar neonates. Neonates were divided into five groups: (1) kept with the biological dam and littermates (nest); (2) kept with a non-lactating foster dam; (3) kept with a non-lactating foster dam with protruded nipple; (4) kept with lactating foster dam with protruded nipple and (5) isolated for 90 minutes. All other procedures for Fos counting were as described above.

Isolation from the nest with thermal support (Figures 2D–2G):

When ten-day-old, neonates were separated from the biological dam, and thermal support was provided using two different conditions. In the first condition, neonates were placed in a humidity and temperature-controlled climate chamber (70%–80% of humidity, 35°C, Sables Systems). In the second condition, a thermal support device set at 35°C was placed underneath the chamber in which the neonates were separated. We confirmed appropriated thermal conditions by monitoring the temperature throughout testing using calibrated thermometers. Neonates were divided into four groups: (1) kept with the biological dam and littermates (nest); (2) isolated for 90 minutes at thermoneutrality; (3) isolated for 90 minutes in the thermal support device; and (4) isolated for 90 minutes without thermal support (room temperature). All other procedures for Fos counting were as described above.

Isolation from the nest in pups raised at thermoneutrality (Figures 2H–2J):

The lactating dam was placed in a humidity and temperature-controlled climate chamber (70%–80% of humidity, 35°C, Sables Systems) two weeks before delivery to acclimate to the new environment. Temperature and humidity in the climate chamber were monitored twice a day until testing. At postnatal day 10, neonates were divided into three groups: (1) kept with the biological dam and littermates (nest); (2) isolated for 90 minutes at room temperature; and (3) isolated for 90 minutes at thermoneutrality. All other procedures for Fos counting were as described above.

Fiber photometry (Figure 3):

$Agrp^{Cre/Cre}$ mouse neonates (P0-P1) were cryo-anesthetized. Neonates were placed on ice, using aluminum foil as a barrier to prevent direct contact with the ice. After 8 minutes, neonates were removed from the ice and placed onto a chilled rat/mouse neonatal frame (Stoelting Co., Wood Dale, IL). A Cre-dependent adeno-associated virus (AAV) encoding the calcium sensor jGCaMP7s (AAV8-CAG-Flex-jGCaMP7s-SV40, Penn Vector Core) was injected unilaterally at a volume of 300 nL using following coordinates from lambda: AP = +.98 ML, lateral = −0.3mm, DV = −4.1mm. On postnatal day 12, a fiber optic cannula (NA = 0.48, core diameter = 400 μm from Doric Lenses) was placed over the arcuate nucleus using following coordinates from bregma: AP = −1.38 mm, lateral = −0.3mm, DV = −5.8 mm. One to two days after placing the fiber optic cannula, experimental mice were placed in a Plexiglas cage (10 cm x 8 cm x 6 cm) with 4 siblings and bedding from home cage. After 5 minutes of baseline fiber photometry recordings (see below), mice connected to the fiber photometry system were moved to an identical adjacent Plexiglas cage for a period of ten minutes of isolation. Subsequently, experimental mice were return to the cage with the siblings for 5 minutes. The fiber photometry system consisted of two different sets of LEDs: 405 nm LED sinusoidally modulated at 211 Hz and a 460 nm LED sinusoidally modulated at 333 Hz. Both light streams were merged into an optical fiber patch using a minicube (Doric Systems). The fiber optic patch was connected to the cannula on the mouse pup. Fluorescence emitted by jGCaMP7s in response to light excitation was collected with same fiber patch cord and focused into a photodetector (Newport). The signal collected at the photodetector was

collected in a digital fiber photometry processor (RZ5P, Tucker-Davis Technologies). Signal was processed and pre-analyzed using the Synapse Software Suite (Tucker-Davis Technologies). The data were exported to MATLAB for post-processing. First, the isosbestic channel (405 nm excitation) was fitted to the calcium-dependent channel (460 nm excitation, denoted as F) using first order polynomial fitting (F_0 denotes the fitted isosbestic). The calcium fluorescence activity was calculated as: $(F - F_0)/F_0$. The high-frequency components of the fluorescence activity were then filtered out by a low pass filter at 0.5 Hz. We then down sampled the signal by averaging it in non-overlapping windows of 0.1 s. The Z-score was calculated considering the minute before isolation as the baseline.

Recording of ultrasonic vocalizations (Figures 4 and 5):
P10 mice were separated from the dam and placed in a soundproof chamber. In the thermoneutrality experiment, pups were divided into two groups: (1) isolated for 90 minutes at room temperature or (2) isolated for 90 minutes at thermoneutrality (70%–80% of humidity, 35°C, Sables Systems). USVs were recorded for 90 minutes. In experiments with the Npy^{KO} and $Agrp^{Vgat-KO}$ mice, USVs were recorded for ten minutes immediately following separation from the dam in the soundproof chamber. In the experiment with $Agrp^{Trpv1}$ mice, this initial ten minutes was considered as a baseline before activation of Agrp neurons. Then, P10 mice were injected with capsaicin (10 mg/kg, s.c) and USVs were recorded for an additional twenty minutes. USVs were recorded using an UltraSoundGate Condenser Microphone CM 16 (Avisoft Bioacoustics, Berlin, Germany) placed 10 cm above the animals. The microphone was connected via an UltraSoundGate 416 USGH audio device and recorded with a sampling rate of 250,000 Hz by the software Avisoft RECORDER (version 4.2.16; Avisoft Bioacoustics).

Maternal preference test (Figures 5N–5P):
The maternal preference test was performed in a three-chamber apparatus (65 × 42 × 23 cm) and comprised of three stages: Stage 1 – acclimation: the dam was allowed to explore the apparatus without the presence of pups for ten minutes. Stage 2 – exploration: two P10 mice (control and $Agrp^{Trpv1}$, n = 25 pairs) were placed on each side of the apparatus inside of an inverted metal wire cup and the dam was allowed to explore the pups for ten minutes. Stage 3 - preference: dam was restricted to the center compartment, pups were injected with capsaicin (10 mg.kg, s.c) and placed in the cups and then the dam was allowed to explore all compartments for 20 minutes. Groups were randomly alternated between both sides to avoid preference for one side of the chamber. Time spent interacting with the pups was measured using Any-maze (Stoelting Co., Wood Dale, IL).

Analysis of ultrasonic vocalizations
Ultrasonic vocalizations (USV) were automatically extracted from the audio recordings by using spectral analysis through image processing. Each audio file was analyzed in segments of 1 minute long and then Short Fourier transformed with a Hamming windowing function (window = 256), NFFT = 1024 sampling points and an overlap between successive windows equal to half of the window size. These parameters generate a spectrogram with resolution of 0.5 ms and 244 Hz. The spectrograms were converted to grayscale images and the USVs were segmented on the spectrogram through a sequence of image processing techniques, which included the contrast enhancement of the image ($\gamma = 1$), the application of an adaptive threshold (sensitivity of 20%) followed by a series of morphological operations and identification of connected components. The segmented USV candidates were then analyzed by a local median filtering (LMF) to eliminate segmentation noise based on the contrast between an USV candidate and its background. The minimum contrast acceptable between an USV candidate and its background was automatically estimated based on a differential geometry analysis of the contrast of all the USV candidates detected in an audio recording. USVs less than 10 ms apart were considered as part of the same syllable. Next, all the USVs were classified in 11 distinct call types (Grimsley et al., 2011) by a Convolutional Neural Network, which had the AlexNet architecture as starting point. The network was trained for USV classification with over 14,000 samples of real USVs, which were then augmented in order to increase the variability of the samples, resulting in > 57,000 samples. The output consisted of a table summarizing the main features of the USVs detected. This table contains the start and end time of the USVs, as well as its mean, maximum and minimum frequency, mean intensity and other relevant spectral features such as the existence of harmonic components. Each vocalization received a label based on the most likely call type label attributed by the Convolutional Neural Network. The label of each USV is also available as a probability distribution function over all the call types. The software was custom developed in our laboratory and is available upon request. The details of the software will be published elsewhere.

Mouse pup behavior toward the anesthetized dam (Figures 6A–6G and 7A–7J):
Animals were recorded under infrared illumination and assessed for 20 minutes at postnatal day 10 (P10) and postnatal day 15 (P15). Each animal was tested at one age only. Before the experiment, the dam was anesthetized (100 mg/kg Ketamine + 10 mg/kg Xylazine). The maximum number of pups tested per dam was eight. Animals received an injection of capsaicin (10 mg/kg, s.c.) before the experiment. We used a custom built-chamber (20 × 15 cm built in opaque Plexiglas). The dam was placed at an angle of 45° on her back along the edge. Pups were placed on the other edge of the chamber, ~20 cm away from their dam. Parameters such as latency to attach to the dam's nipple, distance traveled, and the number of nipple attachments were assessed using Any-Maze (Stoelting Co., Wood Dale, IL). Experiments were performed blinded for the genotype.

Mouse pup behavior toward the anesthetized dams injected with oxytocin (Figures 6P–6V and 7K–7P):

In anesthetized dams, milk ejection is largely decreased, and dams are considered non-lactating (Lincoln et al., 1973). To circumvent this issue, we performed a similar experiment as described above but injected the anesthetized dams with oxytocin (5 mg/kg, i.p) immediately before each test. Nipples were manually expressed to confirm that there was milk ejection before the experiment. P10 mice received an injection of capsaicin (10 mg/kg, s.c) and were subsequently assessed for 20 minutes. In this assay, a second injection of oxytocin (5 mg/kg, i.p) was given at 10 minutes of test. P15 mice received an injection of capsaicin (10 mg/kg, s.c) and were subsequently assessed for 10 minutes. The duration of the testing period was shorter because P15 mice quickly attached to the dam's nipple in preliminary experiments. Parameters such as latency to attach to the dam's nipple, distance traveled, and the number of nipple attachments were analyzed using Any-Maze (Stoelting Co., Wood Dale, IL). Body weight was measured prior and after testing. Experiments were performed blinded for the genotype.

Independent feeding (Figures 7Q and 7R):

Mice were tested at postnatal days P15, P18, and P21. Naive animals were used for each postnatal age and mice were acclimated to the behavior room for one-hour before the experiment. Food was left inside the cage to prevent a state of deprivation. Animals were tested in a mouse cage filled with home bedding and two Petri dishes placed in opposite corners. After the acclimation period (1 hour), the experiment was performed. Animals were removed from the cage, received an injection of capsaicin (10 mg/kg, i.p.) and were returned to the cage. One Petri dish was empty; the other had a pellet of chow diet. Body weight and food intake were evaluated after 30 minutes. Experiments were performed blinded for the genotype.

QUANTIFICATION AND STATISTICAL ANALYSIS

MATLAB (2016a or above) and Prism 8.0 were used to analyze data and plot figures. All figures were edited in Adobe Illustrator CS6/CC. Illustrations were designed by Mind the Graph (MindtheGraph.com). Data were first subjected to a normality test using the D'Agostino & Pearson normality test or the Shapiro-Wilk normality test. When homogeneity was assumed, a parametric analysis of variance test was used. The Student's t test was used to compare two groups. Welch's correction was used when standard deviations were unequal between groups. ANOVA was used to compare multiple groups. Tukey-Kramer's multiple comparisons test was used to find post hoc differences among groups and calculate 95% confidence intervals to report effect size. When 95% confidence intervals were not calculated, then the Holm-Sidak's multiple comparisons test was used. When homogeneity was not assumed, the Kruskal-Wallis nonparametric ANOVA was selected for multiple statistical comparisons. The Mann-Whitney U test was used to determine significance between groups. Two sample Kolmogorov–Smirnov test was used to calculate the statistical differences between features of ultrasonic vocalizations. Chi-square test was used to find differences in the number of pups that attached to nipples in the behavior tests performed in neonates. One- or two-tail tests were used based on prior experimental hypothesis. Statistical data are provided in text and in the figures. In the text, values are provided as mean ± SEM $p < 0.05$ was considered statistically significant.
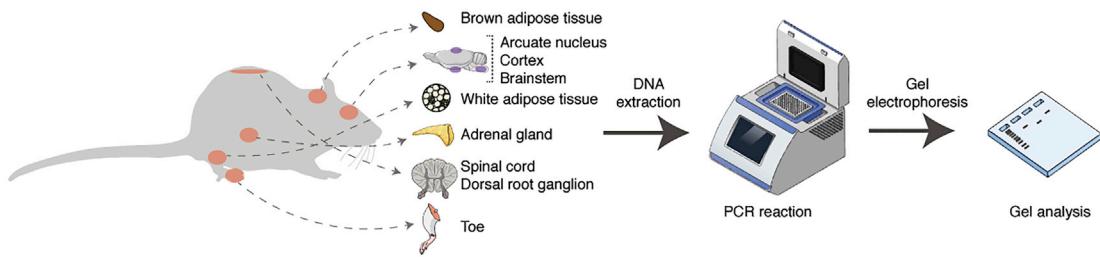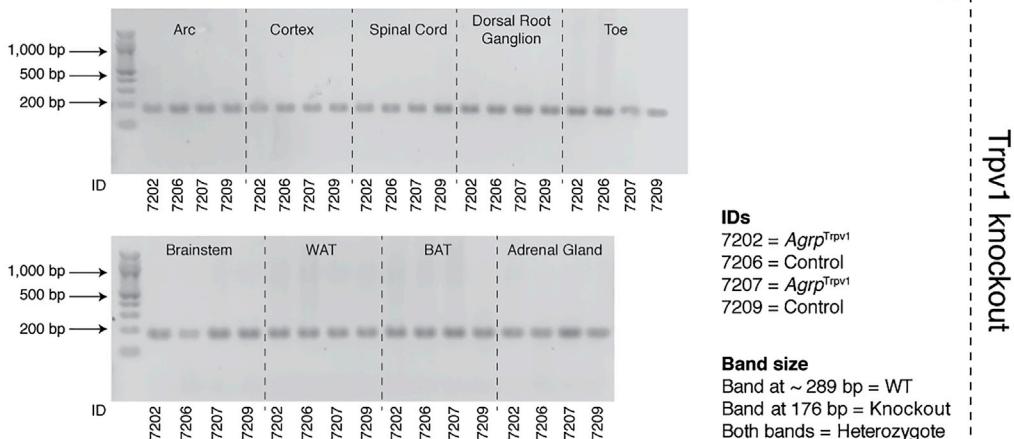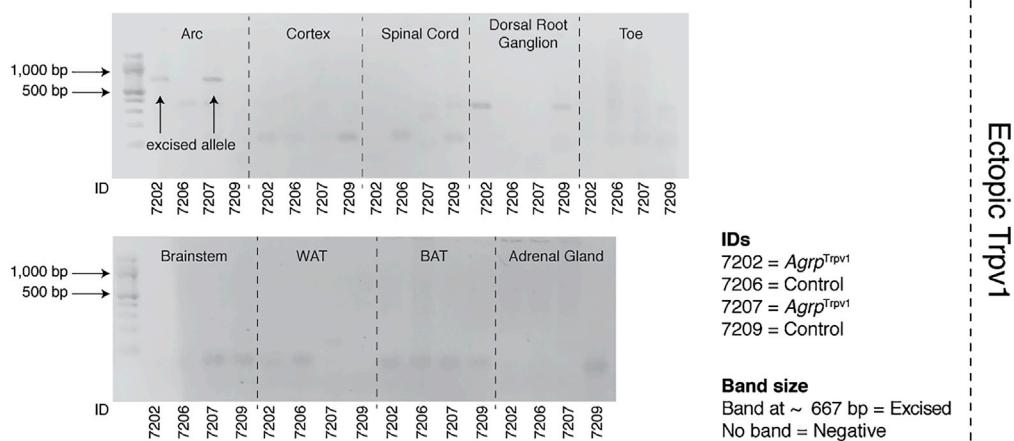
Figure S1. PCR-Based Analysis for Genotyping Agrp^{trpv1} and Control Mice, Related to Figure 5

(A) Illustrative diagram of the tissue collection and PCR-based analysis genotyping.

(B) Genomic DNA samples from P15 mice were extracted and amplified using primers for Trpv1 knockout allele. The lower band is the knockout allele for the Trpv1 gene.

(C) Genomic DNA samples from P15 mice were extracted and amplified using primers for ectopic Trpv1 allele. The upper band (667 bp) shows that the excised allele for Trpv1 is specifically expressed in the arcuate nucleus of the hypothalamus.